

## 19. CONTINENTAL RISE AND ABYSSAL PLAIN SEDIMENTATION IN THE SOUTHEAST PACIFIC BASIN — LEG 35 DEEP SEA DRILLING PROJECT

Brian E. Tucholke,<sup>1</sup> Charles D. Hollister,<sup>2</sup> Fred M. Weaver,<sup>3</sup> and Walter R. Vennum<sup>4</sup>

Somewhere hearts are happy,  
Somewhere children shout,  
But there'll be no joy in Mudville  
'Til the Miocene gives out.

—C. Craddock

### ABSTRACT

Four sites were drilled on the Bellingshausen Abyssal Plain and continental rise off Antarctica during Leg 35 of the Deep Sea Drilling Project. Site 322 penetrated 513 meters of lower Miocene (? Oligocene) to Holocene diatomaceous claystone, siltstone, and sandstone overlying basalt. A similar Neogene section at Site 323 caps 63 meters of upper Maestrichtian to (?) Oligocene brown nano claystone and Fe-claystone bottoming on basalt. Site 324 penetrated 218 meters of Pliocene-Pleistocene terrigenous clay with interbedded silt layers interpreted as contourites, and 718 meters of lower Miocene-Holocene diatomaceous claystone grading downward into coarse sandstone were drilled at Site 325.

The brown Fe-claystone at Site 323 and a similar, thin basal unit at Site 322 indicate pelagic deposition, largely from volcanogenic sources at rates  $<0.5$  cm/1000 yr, from the late Maestrichtian to the (?) Oligocene. Abundant nannoplankton in lower Paleocene claystone suggest depression of the CCD at this time, in contrast to a shallow CCD in most other areas of the world's oceans. Significant bottom-current activity was not initiated until the latest Oligocene or early Miocene, probably in response to formation of deep gaps in the Drake Passage area. An apparent 35-40 m.y. hiatus in sedimentation (middle Paleocene-Oligocene) at Site 323 may represent erosion by Miocene bottom currents. The subsequent sedimentary record is dominated by turbidites derived from Antarctica and exhibits frequent reworking by bottom currents at Sites 322, 323, and 325. Silt and clay contourites, deposited from contour currents flowing west along the continental rise, are found at Site 324.

The earliest firm evidence for Antarctic glaciation encountered on Leg 35 is ice-rafted debris in lower middle Miocene sediment at Site 325. Comparison of our drilling results with those of Legs 28 and 29 shows a clear latitudinal control on the earliest occurrence of ice rafting: late Oligocene to early Miocene at  $65^{\circ}$ - $70^{\circ}$ S ranging to late Miocene to Pliocene at  $55^{\circ}$ - $60^{\circ}$ S. The earliest ice-rafting is preceded in all cases by deposition of diatomaceous sediment which is taken to indicate the northward migration of the polar front zone.

Analysis of sedimentary textures, composition, and rates of accumulation in Leg 35 cores suggests increasing glaciation of West Antarctica through the Miocene, culminating in a glacial maximum with grounded shelf ice near the Miocene-Pliocene boundary. The timing of Pliocene-Pleistocene fluctuations in the glaciation of West Antarctica is not clearly defined in Leg 35 cores, but the ice sheet probably again reached extensive, but ungrounded, shelf-ice conditions several times during this period.

<sup>1</sup>Lamont-Doherty Geological Observatory of Columbia University, Palisades, N. Y.

<sup>2</sup>Woods Hole Oceanographic Institution, Woods Hole, Massachusetts.

<sup>3</sup>Sonoma State College, Rohnert Park, California.

<sup>4</sup>Florida State University, Tallahassee, Florida.

## INTRODUCTION

Several objectives were undertaken in sampling the sedimentary record of the Bellingshausen Basin on Leg 35 of the Deep Sea Drilling Project. It was hoped that compositional and textural data together with inferred rates of accumulation would help to determine: (a) the history of climatic events in Antarctica, specifically with regard to early development and fluctuations of the West Antarctic ice sheet, (b) the corresponding patterns of biogenic productivity in circum-Antarctic surface waters, (c) the initiation and development of the Antarctic Circumpolar Current, (d) the origin of the circumpolar countercurrent, and (e) the processes responsible for development of the Bellingshausen continental rise.

Two sites (322 and 323) drilled in the Bellingshausen Abyssal Plain penetrated to basaltic basement (Figure 1). These sites lie beneath the Antarctic Circumpolar Current, and data from these holes contribute to our understanding of the development of circum-Antarctic currents. The other two sites drilled on Leg 35 were located on the continental rise. Site 324 penetrated 200 meters of acoustically nonlaminated sediments on the lower rise before caving sand caused hole collapse. Site 325 penetrated 718 meters into the central continental rise, but the hole failed about 500 meters short of probable basaltic basement and 300 meters short of the strong, smooth reflector comprising acoustic basement. Coring results of all Leg 35 sites are summarized in Figure 2.

The purpose of this report is to describe the depositional environments and mechanisms of sedimentation in the Bellingshausen Basin, as inferred from the sediment recovered. Compositional and textural data are briefly reviewed, but readers are also referred to detailed analyses of sediment composition and inferred source areas by Peters and Hollister; Bogdanov et al.; and Gorbunova (all in this volume). The paucity of good paleontologic material has led to inevitable conflicts between ages determined from various microfossil groups, and the ages used here conform to those outlined in the biostratigraphic summary (this volume). Grain-size data discussed herein are from Bogdanov, Zhivago, Lisitzin, Serova, and Zharikova (this volume).

## SITE DESCRIPTIONS

### Site 322

Thirty-four meters of sediment and igneous rocks (6% recovery) were recovered from the 544 meters penetrated at this site. The sediment recovered is primarily clastic sands, silts, and clays, with occurrence of diatom oozes in the top half of the hole. The sedimentary section is divided into four lithologic units: (1) an upper unit of interbedded, unconsolidated sand, silt, clay, and diatom ooze; (2) an interval of consolidated claystone; (3) a unit containing some claystone but dominated by sandstones; and (4) a thin basal unit of pelagic brown claystone (Table 1 and Figure 2). The division of the first three units is somewhat artificial because it is based primarily on sediment consolidation; the low core recovery ratios in the second unit suggest that uncon-

solidated sands are much more abundant at this depth than is indicated by their sparse recovery.

The base of Unit 1 is arbitrarily placed at 295 meters, just above Core 3. Cores 1 and 2 recovered greenish-gray clayey sediment with interbedded quartz sands and silts and with common diatoms and sponge spicules of latest Miocene to Pliocene age (Figure 3). The quartz sand and sandy silt beds range from mere partings to several centimeters in thickness, but show no detectable internal structure. They exhibit fair to excellent size sorting and contain fragmented diatom tests and appreciable amounts of feldspar and heavy minerals (up to 10%). Quartzose rock fragments are generally rare. Grains range from mostly angular and subangular to subrounded. Ice-rafted sand in the clay of Sample 2, CC (upper Miocene) is the earliest observed occurrence of ice-rafted debris at this site.

Unit 2 (Cores 3-8; 295-466 m) is dominated by dark greenish-gray to greenish-black claystone and silty claystone of middle (?early) to late Miocene age. Cores 6-1 (438 m) and 8, CC (466 m) contain yellow-brown, crudely bedded, pelagic clays which are finely mottled and manganese stained. Quartz silt occurs locally as partings in the gray claystone but more commonly in intervals of complex, distorted laminae with admixed clay galls (disturbance is not due to coring). Feldspars and heavy minerals are usually present in quantities less than 10%, although rich heavy-mineral assemblages (up to 25%) do occur. Rock fragments become common in the lower part of the unit, whereas diatoms (mostly fragmentary) persist downward in significant quantities only to Core 4 at 354 meters (Figure 3). Mineral grains are mostly angular to subangular, and sorting is poor to very good. A few well-sorted, unconsolidated sands may owe their texture to washing during the coring process, and poor core recovery in this interval suggests the presence of significant additional quantities of unconsolidated sand.

The predominance of dark gray to gray-black sandstone in Unit 3 (Cores 9 through 11-4; 466 to 509 m) distinguishes this unit from the over- and underlying units. Unit 3 ranges in age from approximately early to middle Miocene. The lower contact on claystone is preserved at 54 cm in Core 11-4 (509 m). The sandstone beds vary from about 1 to 5 meters in thickness and for the most part are visually uniform (massive) to very weakly bedded (at about 30° to the horizontal). The sandstones are enriched in rock fragments, quartz, feldspars, and heavy minerals, and they exhibit poor to moderate size sorting with 5%-10% clay-size material. Trace amounts of magnetite, mica, hematite, pyrite, glauconite, and recrystallized silica also appear. Contacts with interbedded claystones are sharp and usually irregular. Slight size grading occurs in the basal 20 cm of the sandstone unit bottoming in Core 11-4, and the base of a similar unit in Core 10-1 (490 m) contains large, angular claystone clasts of lithology similar to the underlying claystone. Faint, near-vertical stripes appear in the sandstone at the bottom of Core 11-2 and top of Core 11-3. They contain beautifully developed, silt-size authigenic crystals identified as analcime.

The thin (4.26 m) basal unit of the sediment column is a dominantly pelagic claystone of (?)Oligocene to early Miocene age. It lies on basalt recovered in 11, CC

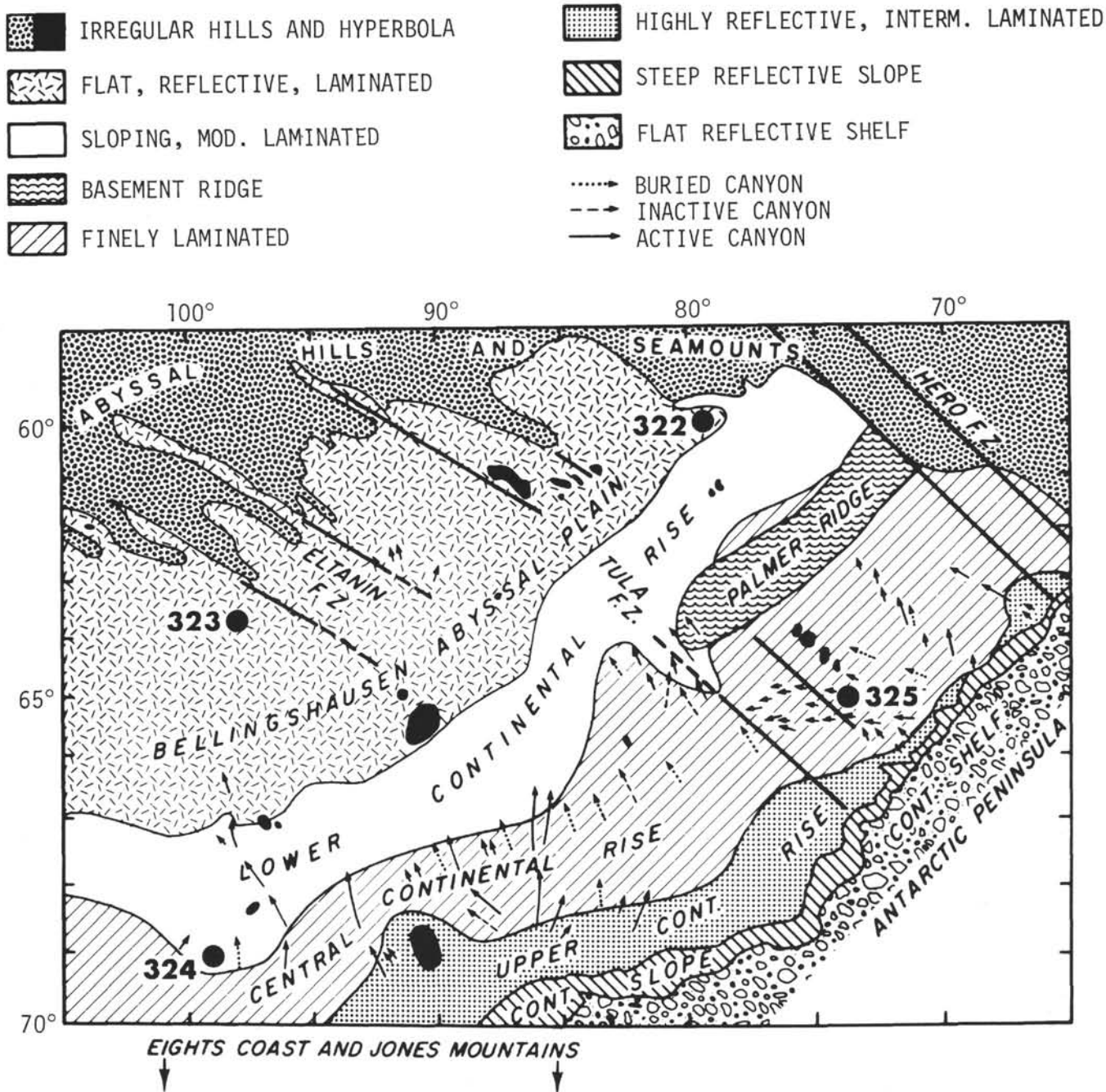


Figure 1. Location of Leg 35 drill sites.

(513.3 m), but the contact with basalt is not preserved. The uppermost claystone is dark gray, contains about 5% quartz, and is fissile (parting about 30° with the horizontal) with diffuse laminae and mottles. It grades rapidly (<1 m) downward through dark greenish and olive-gray to a moderate yellow-brown claystone with only traces of terrigenous detritus. The parting in the yellow-brown claystone is horizontal, and the sediment is mottled and manganese stained. Zeolites, palagonite, and amorphous iron oxides occur in quantities less than 5%, and the sediment is dominated by montmorillonite with significant quantities of chlorite and illite; otherwise, the sediment is lithologically similar to the basal pelagic claystone at Site 323.

Sedimentation rates at Site 322 are not well determined because of poor paleontologic control. Units 1 through 3 have accumulated at an average rate of about 3.3 cm/1000 yr, but variations between about 1 and 10 cm/1000 yr appear likely (Figure 4). The most rapid accumulation is indicated for upper Miocene through middle Pliocene sediments, with much slower rates in the lower to middle Miocene and in the Pleistocene. However, the average minimum rate for the upper 80 meters of sediment (2 cm/1000 yr) is still several times higher than the 0.4 to 0.5 cm/1000 yr rate determined for Brunhes age (Pleistocene) piston cores in this area (Goodell and Watkins, 1968). The pelagic clays of Unit 4 probably accumulated at very slow rates. If the clays

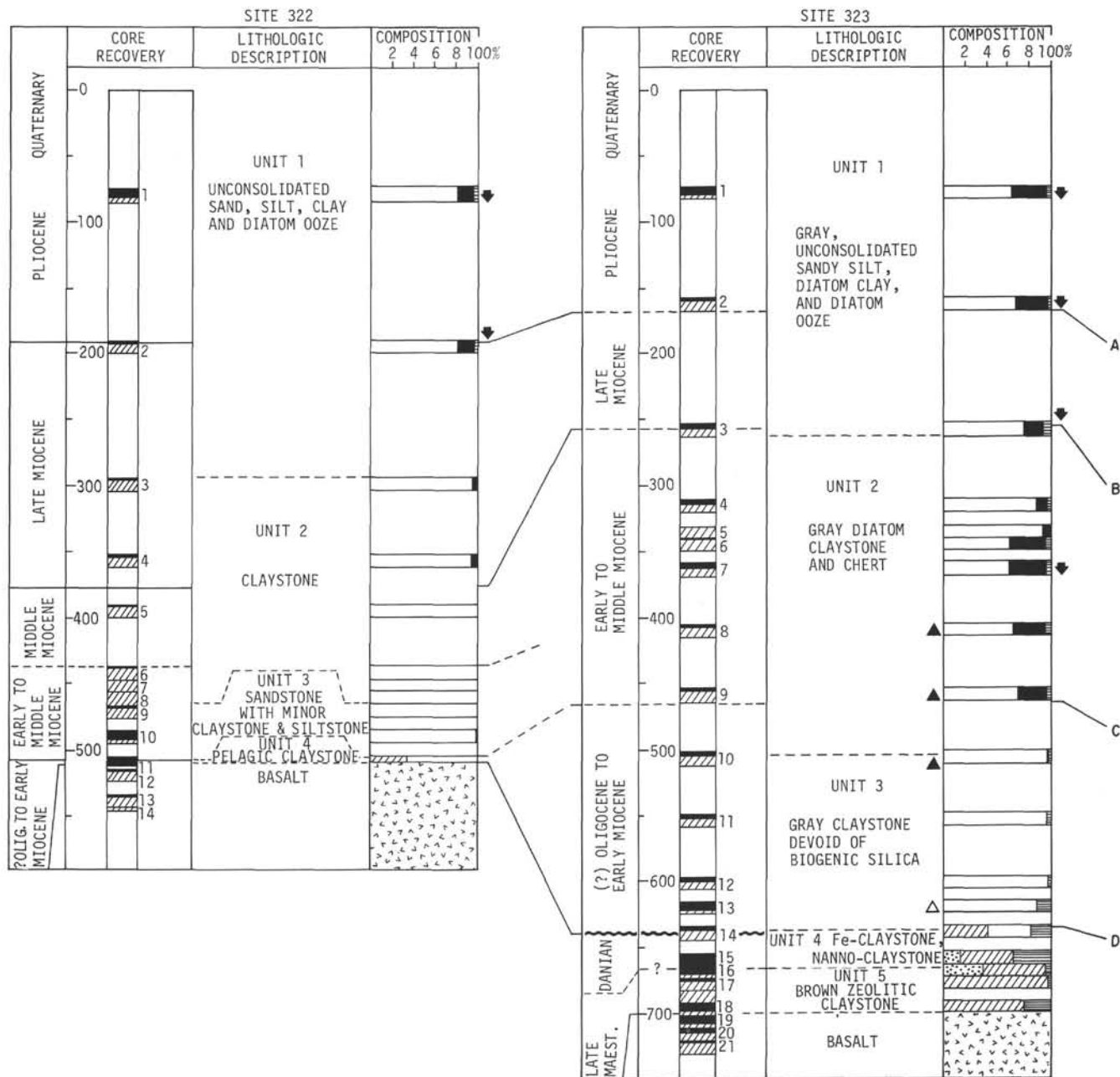


Figure 2. Summary of sites drilled on Leg 35.

just above the basalt contact are indeed as old as Oligocene, their accumulation rate could be as low as 0.5 cm/1000 yr; this rate is comparable to that of lithologically similar clays recovered at the bottom of Site 323.

**Site 323**

Sediments were penetrated to a depth of 701 meters at Site 323, and 66.5 meters of sediment (9.5%) were recovered (Figure 2). Sediments at this site are dominated by clays and claystones, but biogenic components are more common than at Site 322. Diatom clays and diatom oozes predominate in the upper 465 meters of the section; radiolarians are also restricted to

this interval but comprise less than 5% of the sediment. The base of the siliceous sediments is marked by the occurrence of silicified claystones (cherts) in Cores 8, 9, and 10 (408-512 m). Calcareous foraminifera and nanoplankton occur only near the bottom of the hole at 655 to 674 meters in Cores 15 and 16. The only megascopic evidence of ice-rafting encountered is in Core 7-2 (granite cobble) and Sample 7, CC (ice-rafted gravel in clay); this sediment is of middle Miocene age.

The sedimentary record is divided into five primary units based on sediment color, relative induration, and composition (Table 2). Contacts between the units were preserved in three places: (1) the contact between the siliceous and nonsiliceous claystones of Units 2 and 3

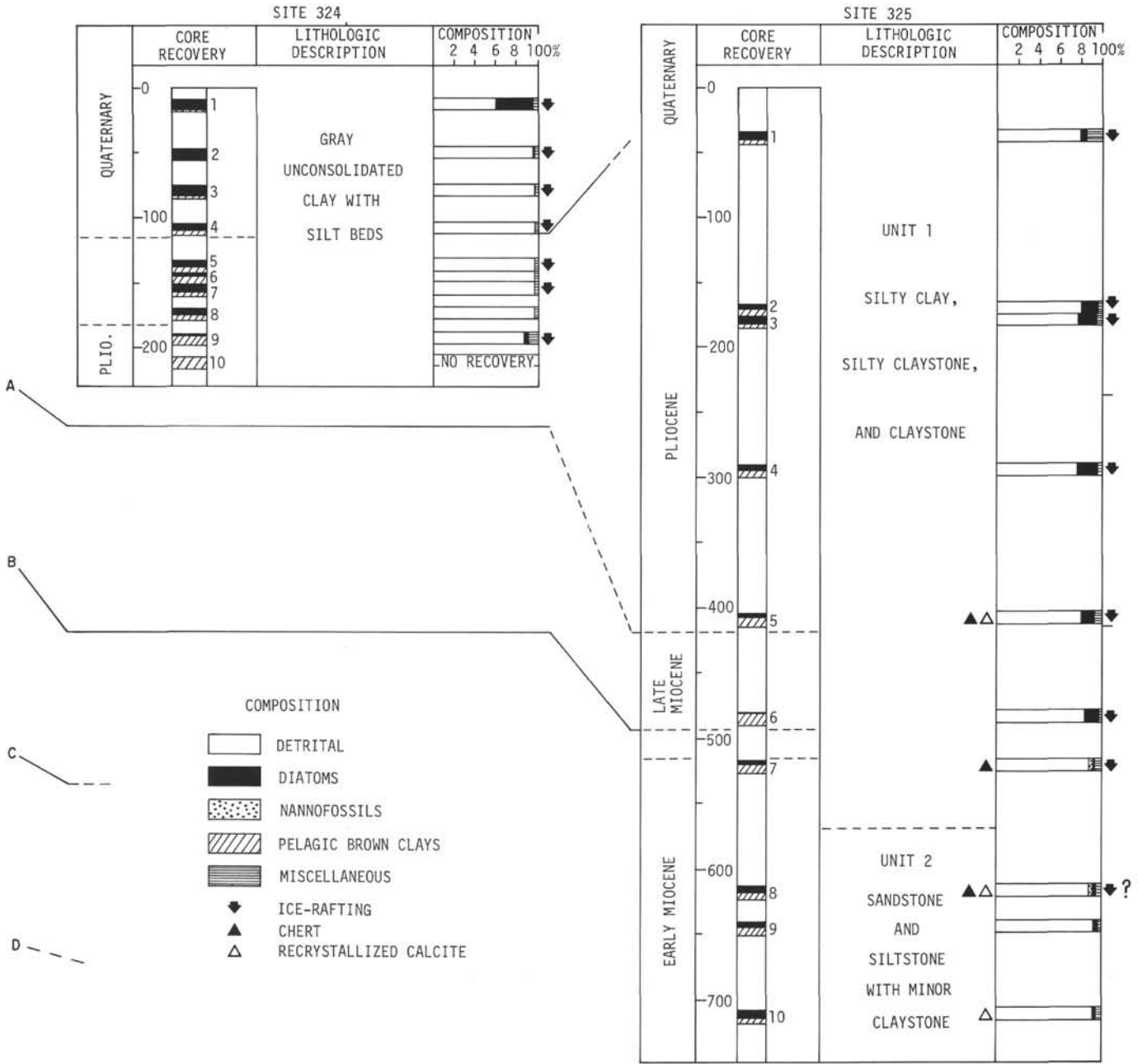


Figure 2. (Continued).

occurs in Core 10; it appears to be a gradational contact because discrete chert cobbles are encountered between nonsiliceous claystones down through Core 10-3. Although it is possible that the cherts in Core 10 were displaced from higher in the hole, this is considered unlikely because the cobbles are not excessively abraded as if worked downhole by the bit. Furthermore, sonic velocities determined on cherts in Cores 8 through 10 consistently decrease downhole (see Tucholke et al., this volume) in a manner compatible with a gradient of downward decreasing silicification. (2) The contact between Units 3 and 4 is a sharp mineralogical and color change in Core 14, from gray claystones to underlying, iron-bearing, brown claystones. (3) The contact

between Units 4 and 5 occurs at 666.5 meters in Core 16-2 and marks a sharp change from claystones rich in nannofossils and amorphous iron oxides to claystone devoid of these components but bearing zeolites.

Units 1 and 2 are differentiated on the basis of induration, and the contact is assumed to occur at 266 meters just below Core 3. The sparse sampling and poor core recovery in the upper part of this hole make exact determination of the contact difficult; Core 3 contains soft claystone, but the coring rate decreases sharply below this core, and this criterion is used to establish the contact.

The contact between Unit 5 and basalt occurs in Core 18-6. The continuity of the core is broken at this

TABLE I  
Summary of Lithologic Units, Site 322

Unit	Lithology	Subbottom Depth (m)	Unit Thickness (m)	Age
1	Gray unconsolidated sand, silt, clay, and diatom ooze	0-295	295	Holocene to late Miocene
2	Gray consolidated claystone	295-466	171	Late Miocene to middle (?early) Miocene
3	Dark gray sandstone with minor siltstone and claystone	466-509	43	Middle (?early) Miocene to early Miocene
4	Brown pelagic claystone	509-513.3	4.3	Early Miocene to (?) Oligocene

point, however, and sediment from the actual contact is probably missing. Detailed description of each of the units is given below.

Unit 1 (0-266 m) consists largely of unconsolidated gray diatom-clays and diatom-oozes of late middle Miocene to Holocene age, and it correlates with relatively rapid drilling and coring rates. Subtle color changes in the clays are often sharp. Semi-indurated clays near the base of the unit are still pliable and appear to be transitional to the claystones of Unit 2. Silts and sands usually occur as distinct intervals 7-15 cm thick interbedded with clays. Sand stringers and pods 1-2 cm thick are common and appear to be beds disturbed by coring; their upper and lower contacts are normally sharp. No size grading was observed in any of these beds. Primary structures within the sand, silt, and clay units are virtually nonexistent; the few that may have been present have been destroyed by coring.

The sediments of Unit 1 are primarily composed of detrital quartz and clay minerals (Figure 5). Feldspar and heavy minerals comprise up to 10% of the silts and sands. One exceptional sample (3-3, 121 cm) is a quartz silty sand containing about 35% heavy minerals, which may indicate placering. Rock fragments appear sporadically in quantities usually less than 10%, as do opaque minerals, pyrite, and glauconite in trace quantities.

The biogenic fraction is dominated by fragmentary diatoms comprising up to 60% of the sediment, but the average is about 10%. Radiolarians and sponge spicules are much less common (3%-5%), but occasionally exceed 10%.

Unit 2 spans 240 meters of lower through middle Miocene sediment from just below Core 3 to Core 10-2. It is characterized by grayish claystones with common diatoms, radiolarians, and sponge spicules, and is distinguished from Unit 1 by the dominance of indurated claystones and by sharply reduced drilling and coring rates.

Sediment recovery was generally poor throughout Units 1 and 2, and it appears likely that thick sequences of unconsolidated or poorly consolidated silt and sand were penetrated but not trapped by the dog-type core-catchers used at this site (a similar situation was experienced at Site 322).

Core 4 (75 to 85 m) taken at the top of Unit 2 is atypical, consisting of: (1) a drilling slurry of claystone

fragments and (2) a well sorted, very coarse sand. The sand contains angular to subangular rock fragments with traces of abraded pelecypod fragments. Although the sand is totally disturbed by drilling, its size sorting is unlike that of drill cuttings, and it is probably representative of an unconsolidated sand layer.

The claystones down to Core 7 (370 m) have little internal structure or color variation. Yellowish-brown claystone galls were occasionally observed in drill slurry but never in distinct beds. Smear-slide mineralogy of these galls is similar to that of the gray claystones. Faint bedding, trace fossils (burrowing), and silty-sand pods were occasionally observed in Cores 7-10.

With the following two exceptions, the claystones of this interval are mineralogically similar to the clays of Unit 1: (1) occurrences of authigenic calcite (5-1, 135 and 7-1, 95) represent the only carbonate detected in either Unit 1 or 2, and (2) cherts are present in the lower part (Cores 8-10) of Unit 2.

The cherts are lithified claystones developed by precipitation of cryptocrystalline silica. They are generally dark gray (N3) in color and can be scratched easily or with difficulty with a knife, depending on the degree of lithification; the most strongly lithified samples have a subconchoidal fracture, but most are less well lithified and can be described as porcelanitic cherts (Lancelot, 1973). The siliceous cement is predominantly cristobalite, with lesser amounts of tridymite (Zemmel and Cook, this volume). Such cherts were encountered in the following locations: 8-1, 110-120 cm; 8, CC; 9-2, 117-140 cm; 10-1, 92-96 cm; 10-2, 4-6, 12-14 and 135-138 cm; 10-3, 62-63, 124-125 cm. The lithification of these claystones has not disturbed the fine faint bedding and trace fossils. Silicification is strongly localized, with the transition from unlithified claystone to chert usually occurring over a few centimeters and occasionally within a centimeter (notably at 9-2, 117 cm and 10-1 95 cm). Faint corroded relics of diatoms and radiolarians are observed in the aggregate of cryptocrystalline silica and clay minerals comprising the cherts. The cherts mark the deepest occurrence of biogenic or reprecipitated silica in other than trace quantities.

The 130.5 meters of sediment comprising Unit 3 (?Oligocene to lower Miocene) have the same megascopic lithology as the grayish claystones of Unit 2, although Unit 3 claystones are, on the whole, slightly

SMEAR SLIDE SUMMARY

SITE 322



CORE SECTION	INTERVAL cm	EXOGENIC										AUTHIGENIC-DIAGENETIC										BIOGENIC									
		DETRITAL QUARTZ	FELDSPARS	HEAVY MINERALS	ROCK FRAGMENTS	LIGHT GLASS	DARK GLASS	MAGNETITE	MICA	UNIDENTIFIED OPAQUES	GLAUCONITE	CLAY MINERALS	PALAGONITE	ZEOLITES	HEMATITE	AMORPHOUS IRON OXIDES	MICRO-NODULES	PYRITE	RECRYSTALL SILICA	RECRYSTALL CALCITE	FORAM-INIFERS	NANNO-FOSSILS	RADIO-LARIANS	DIATOMS	SILICO-FLAGELLATES	SPONGE SPICULES	FISH DEBRIS	OTHER			
1	1	52																													
1	1	121	*																												
1	2	29	*	*																											
1	2	53	*	*																											
1	2	73	*	*																											
1	2	87	*	*																											
1	2	130	*	*																											
1	3	62	*	*																											
1	3	68	*	*																											
1	3	85	*	*																	*										
1	4	47	*	*																											
1	4	72	*	*																											
1	6	125	*	*																											
1	6	139	*	*																											
1		CC	*	*																											
2	2	111	*	*																											
2	2	144	*	*																											
2		CC	*	*																											
3	1	50	*	*																											
3	1	61.5	*	*																											
3	1	63	*	*																											
4	1	31	*	*																											
4	1	32	*	*																											
4	1	38.5	*	*																											
4	1	106	*	*																											
4	1	122	*	*																	*										
4	1	127.5	*	*																											
4	2	36	*	*																											
4	2	77	*	*																											
5	1	67	*	*																											
6	1	18	*	*																											
6	1	32	*	*																											
6	1	80	*	*																											
6	1	145	*	*																											
6		CC	*	*																											
7		CC	*	*																											
7		CC S.S.	*	*																											
8		CC	*	*																											
9	2	75	*	*																											
9	2	78	*	*																											
9		CC S.S.	*	*																											
9		CC claystone	*	*																											
10	1	4	*	*																											
10	1	17	*	*																											
10	1	29	*	*																											
10	1	105	*	*																											
10	2	42	*	*																											
10	5	48	*	*																											
11	1	66	*	*																											
11	2	147	*	*																											
11	4	29	*	*																											
11	4	32	*	*																											
11	4	62	*	*																											
11	4	125	*	*																											
11	5	6	*	*																											
11	5	19	*	*																											
11	5	23	*	*																											

Figure 3. Smear-slide summary, Site 322.

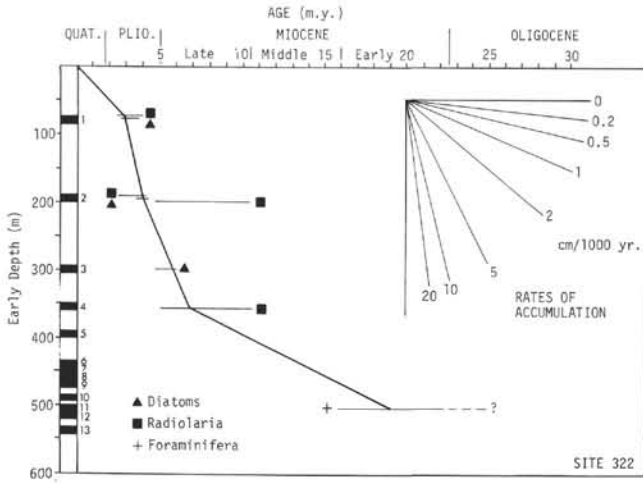


Figure 4. Sediment accumulation rates, Site 322.

siltier. The single most important distinction between the units is in the composition. Biogenic silica is absent from Unit 3, whereas recrystallized calcite and pyrite are commonly observed (Figure 5). Clay minerals dominate in the sediment, quartz varies from less than 5% to more than 75%, and feldspars occur sporadically in quantities less than 5%. Heavy minerals average less than 5% but are consistently observed throughout the unit, whereas only scattered occurrences were observed in the two overlying sedimentary units.

Recrystallized carbonate occurs most commonly in Core 13 (617-626.5 m), where two thin (3 mm) quartz-silt layers are enriched (50%) in authigenic calcite. No other calcite was noted in the smear slides, although severely corroded forams were observed in megascopic descriptions of Cores 11 through 13 (550-626 m). Cores 11 and 12 contain traces to more than 5% pyrite, and pyritized diatoms occur in Core 11-1.

The claystones of this unit also exhibit distinct internal structures including very fine laminae (bedding planes) which are often associated with sharp color changes between shades of gray and gray-brown. Bioturbation is uncommon but is distinct in Cores 12-2, 13-5, 13-6, 14-1, and 14-2. No sedimentary structures diagnostic of current reworking of the sediments were noted.

Units 4 and 5, in contrast to the overlying gray claystones, are composed almost entirely of brownish pelagic claystones. Clay minerals, amorphous iron and manganese oxides, nanofossils, and zeolites are the primary constituents of the sediments; traces of opaque minerals and manganese micronodules are found, but detrital quartz, feldspar, heavy minerals, and recrystallized calcite are conspicuously absent (Figure 5).

The 28.5-meter-thick Unit 4 consists of iron-rich dusky yellow-brown claystone of Danian to (?) Oligocene age. Bedding is very poorly defined, and the sediment is extensively mottled by burrowing. From Core 15-6 to 16-2 (55) the sediment is a yellow-brown nannoclaystone.

Below Core 16-2 (55), Unit 5 (upper Maestrichtian to Danian) is brownish zeolitic claystone. Zeolites are very common (10%-50%) immediately above the contact with basalt. Amorphous iron oxide is rare in this unit and nannoplankton are rare. The claystones are structureless and devoid of trace fossils except for a *Zoophycos* burrow at 110 cm in Core 18-4 and minor mottling in Core 18-5. Sharp color contrasts are developed around the *Zoophycos* burrow (yellow-gray, green-gray, brown), but no mineral differences were detected in these varicolored sediments. The lower half of Unit 5 also has numerous corroded foraminifera (*Cyclamina*) detected as tiny white specks in the brown claystone (see Rögl, this volume). Montmorillonite is the dominant mineral component in both Units 4 and 5 (Zemmels and Cook; Gorbunova, this volume).

The base of Unit 5, immediately overlying basalt at 701 meters, shows no effects of contact metamorphism. However, the continuity of the core is broken at the sediment-basalt contact, and metamorphosed sediments may have been lost.

Sedimentation rates at Site 323 average about 2.8 cm/1000 yr from the early Miocene (?Oligocene) to the Holocene and are therefore comparable to average rates for coeval sediments at Site 322. As at Site 322, there is also a suggestion of slightly decreased rates in middle to upper Miocene sediments, followed by higher rates (~8 cm/1000 yr) in the early Pliocene (Figure 6).

A disconformity may exist at the top of the brown pelagic claystones between Units 3 and 4. Judging from the probable rates of accumulation above and below

TABLE 2  
Summary of Lithologic Units, Site 323

Unit	Lithology	Subbottom Depth (m)	Unit Thickness (m)	Age
1	Gray unconsolidated sandy silt, diatom clay, diatom ooze	0-266	266	Holocene to middle Miocene
2	Gray diatom claystone and chert	266-507.5	241.5	Middle to early Miocene
3	Gray claystone devoid of biogenic silica	507.5-638	130.5	Early Miocene to (?) Oligocene
4	Fe-claystone, nannoclaystone	638-666.5	28.5	(?) Oligocene to Danian
5	Brown zeolitic claystone	666.5-701	34.5	Danian to late Maestrichtian

SMEAR SLIDE SUMMARY

SITE 323

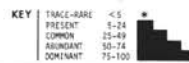


CORE SECTION	INTERVAL cm	EXOGENIC										AUTHGENIC-DIAGENETIC										BIOGENIC									
		DETRITAL QUARTZ	FELDSPARS	HEAVY MINERALS	ROCK FRAGMENTS	LIGHT GLASS	DARK GLASS	MAGNETITE	MICA	UNIDENTIFIED OPAQUES	GLAUCONITE	CLAY MINERALS	PALAGONITE	ZEOLITES	HEMATITE	AMORPHOUS IRON OXIDES	MICRO-NODULES	PYRITE	RECRYSTALL SILICA	RECRYSTALL CALCITE	FORAM-INFERS	MANNO-FOSSILS	RADIO-LARIANS	DIATOMS	SILICO-FLAGELLATES	SPONGE SPICULES	FISH DEBRIS	OTHER			
1	1 55	*								*																					
1	1 70	*				*				*																					
1	1 108	*		*						*	*													*	*						
1	1 131	*								*													*		*						
1	2 7																														
1	2 54	*								*	*														*						
1	2 119	*	*	*						*	*														*						
1	2 119	*	*	*						*	*														*						
1	2 148	*		*						*	*														*						
1	3 21	*		*						*	*						*														
1	3 34	*								*	*																				
1	3 54	*								*	*																				
1	3 87									*	*																				
1	3 103	*		*	*					*	*																				
1	3 137	*	*	*						*	*												*	*							
1	4 18	*								*	*											*	*								
1	4 51	*	*	*						*	*											*	*		*						
1	4 113	*								*	*											*	*		*						
1	5 80	*								*	*											*	*		*						
1	5 106	*								*	*											*	*		*						
1	CC	*	*	*						*	*											*	*		*						
2	1 75	*								*	*											*	*		*						
2	1 84	*								*	*											*	*		*						
2	1 112	*								*	*											*	*		*						
2	1 120	*								*	*											*	*		*						
2	1 137	*								*	*											*	*		*						
2	1 143	*								*	*											*	*		*						
2	CC	*	*	*						*	*											*	*		*						
3	1 87	*								*	*					*?						*	*		*						
3	1 117	*	*	*	*					*	*											*	*		*						
3	1 121	*								*	*											*	*		*						
3	1 138	*				*				*	*											*	*		*						
3	2 14	*	*	*	*					*	*											*	*		*						
3	2 22	*	*	*	*					*	*					*?						*	*		*						
3	2 57	*	*	*	*					*	*											*	*		*						
3	2 71	*	*	*	*					*	*											*	*		*						
3	2 121	*	*	*	*					*	*											*	*		*						
3	CC	*	*	*	*					*	*											*	*		*						
4	CC	*								*	*											*	*		*						
5	1 129	*		*						*	*											*	*		*						
5	1 135	*		*						*	*											*	*		*						
5	1 135	*		*						*	*											*	*		*						
5	1 141									*	*			*	*							*	*		*						
5	1 145	*	*			*				*	*											*	*		*						
5	CC 1									*	*										*	*		*							
5	CC 2									*	*										*	*		*							
5	CC 3									*	*										*	*		*							
5	CC 4	*	*			*				*	*										*	*		*							
6	1 76	*		*						*	*											*	*		*						
6	1 90	*				*				*	*											*	*		*						
6	1 105					*				*	*											*	*		*						
6	1 124	*		*						*	*											*	*		*						
6	1 140									*	*											*	*		*						
6	1 149									*	*											*	*		*						

Figure 5. Smear-slide summary, Site 323.

SMEAR SLIDE SUMMARY

SITE 323



CORE SECTION	INTERVAL cm	EXOGENIC										AUTHIGENIC-DIAGENETIC										BIOGENIC									
		DETRITAL QUARTZ	FELDSPARS	HEAVY MINERALS	ROCK FRAGMENTS	LIGHT GLASS	DARK GLASS	MAGNETITE	MICA	UNIDENTIFIED OPAQUES	GLAUCONITE	CLAY MINERALS	PALAGONITE	ZEOLITES	HEMATITE	AMORPHOUS IRON OXIDES	MICRO-NODULES	PYRITE	RECRYSTALL SILICA	RECRYSTALL CALCITE	FORAM-INIFERS	NANNO-FOSSILS	RADIO-LARIANS	DIATOMS	SILICO-FLAGELLATES	SPONGE SPICULES	FISH DEBRIS	OTHER			
7 1 78	*	*	*	*					*													*	*								
7 1 85		*	*	*					*													*	*								
7 1 95		*	*	*					*													*	*								
7 1 100					*																	*	*								
7 1 120				*					*							*						*	*								
7 1 130																						*	*								
7 1 143		*	*	*																		*	*								
7 1 145		*	*	*																		*	*								
7 2 70	*	*	*	*																		*	*								
7 2 80																						*	*								
7 2 90				*																		*	*								
7 2 105	*	*	*	*																		*	*								
7 3 4	*	*	*	*					*													*	*								
7 3 15	*	*	*	*					*													*	*								
7 3 29	*	*	*	*					*													*	*								
8 1 88																						*	*								
8 1 88																						*	*								
8 1 100	*	*	*	*					*							*						*	*								
8 1 100																						*	*								
8 1 130	*	*	*	*					*													*	*								
8 CC									*													*	*								
9 2 85																						*	*								
9 2 98																						*	*								
9 2 113																						*	*								
9 2 120									*													*	*								
10 1 98	*	*	*	*					*													*	*								
10 1 102	*	*	*	*					*													*	*								
10 1 103	*	*	*	*					*													*	*								
10 1 110	*	*	*	*					*													*	*								
10 1 120	*	*	*	*					*													*	*								
10 1 120	*	*	*	*					*													*	*								
10 1 148	*	*	*	*					*													*	*								
10 2 25	*	*	*	*					*													*	*								
10 2 85	*	*	*	*					*													*	*								
10 2 85	*	*	*	*					*													*	*								
10 2 103	*	*	*	*					*													*	*								
10 2 148	*	*	*	*					*							*						*	*								
10 3 15	*	*	*	*					*													*	*								
10 3 58	*	*	*	*					*													*	*								
10 3 122	*	*	*	*					*													*	*								
10 CC									*													*	*								
10 CC									*													*	*								
11 1 10	*	*	*	*					*													*	*								
11 1 43	*	*	*	*					*													*	*								
11 1 93	*	*	*	*					*													*	*								
11 1 116	*	*	*	*					*													*	*								
11 2 116	*	*	*	*					*													*	*								
11 CC	*	*	*	*					*													*	*								

Figure 5. (Continued).

SMEAR SLIDE SUMMARY

SITE 323



CORE SECTION	INTERVAL cm	EXOGENIC										AUTHIGENIC-DIAGENETIC										BIOGENIC									
		DETRITAL QUARTZ	FELDSPARS	HEAVY MINERALS	ROCK FRAGMENTS	LIGHT GLASS	DARK GLASS	MAGNETITE	MICA	UNIDENTIFIED OPAQUES	GLAUCONITE	CLAY MINERALS	PALAGONITE	ZEOLITES	HEMATITE	AMORPHOUS IRON OXIDES	MICRO-NODULES	PYRITE	RECRYSTALL SILICA	RECRYSTALL CALCITE	FORAM-IFIFERS	MANNO-FOSSILS	RADIO-LARIANS	DIATOMS	SILICO-FLAGELLATES	SPONGE SPICULES	FISH DEBRIS	OTHER			
12 1	100	*		*																											
12 1	107			*		*				*																					
12 2	3		*	*																											
12 2	59		*	*																											
12 2	66		*	*																											
12 2	80		*	*						*																					
12 2	84		*	*						*																					
12 2	90	*		*						*																					
12 2	105	*		*						*																					
12 2	114	*	*	*						*			*																		
12 2	119	*	*	*						*																					
12 2	148	*	*	*						*																					
13 1	8	*		*						*																					
13 1	20			*						*																					
13 3	140	*	*	*						*																					
13 3	140	*	*	*						*																					
13 3	145	*	*	*						*																					
13 5	77	*	*	*						*																					
13 5	142	*	*	*						*																					
13 5	149	*	*	*						*																					
13 6	5	*	*	*						*																					
13 6	36	*	*	*						*																					
13 6	46	*	*	*						*																					
13 6	51	*	*	*						*																					
13 6	56	*	*	*						*																					
13 6	125	*	*	*						*																					
13 CC	1	*	*	*						*																					
13 CC	2	*	*	*						*																					
14 1	139	*	*	*						*																					
14 2	13	*	*	*						*																					
14 2	74	*	*	*						*																					
14 2	143	*	*	*						*																					
14	CC	*	*	*						*																					
14	CC	*	*	*						*																					
15 1	70	*		*						*																					
15 2	13			*						*																					
15 3	102			*						*																					
15 5	11			*						*																					
15 5	13			*						*																					
15 6	12			*						*																					
15 6	65			*						*																					
15	CC			*						*																					
16 1	20			*						*																					
16 1	49			*						*																					
16 1	49			*						*																					
16 1	100			*						*																					
16 1	100			*						*																					
16 2	55			*						*																					
16 2	127			*						*																					
16 2	141			*						*																					
16 3	32			*						*																					
16 4	86			*						*																					
16	CC			*						*																					
17 6	133			*						*																					
18 1	147			*						*																					
18 2	100			*						*																					
18 3	143			*						*																					
18 4	109			*						*																					
18 4	112			*						*																					
18 4	130			*						*																					
18 5	50			*						*																					

Figure 5. (Continued).

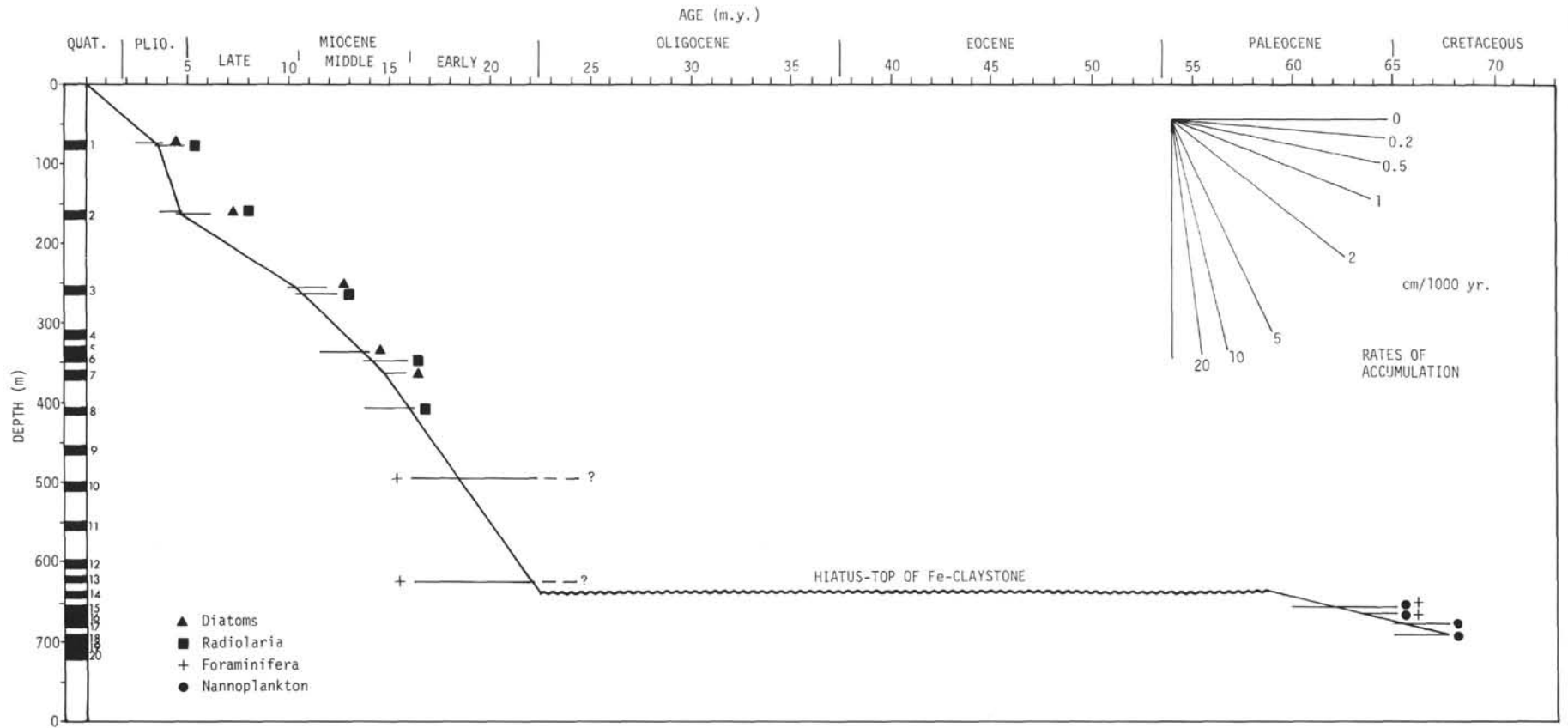


Figure 6. *Sediment accumulation rates, Site 323.*

this level, the gap spans about 35-40 m.y. from middle Paleocene to lower Miocene. If middle Paleocene to lower Miocene sediments are actually present in a compressed section, they must have accumulated at an unusually slow rate of less than 1 mm/1000 yr. The upper Maestrichtian to Danian iron claystones in Units 4 and 5 accumulated at rates of about 0.5 cm/1000 yr.

#### Site 324

Site 324 was drilled to 218 meters in acoustically non-laminated sediments on the lower continental rise, but the deepest sediment recovered was at 189.5 to 199 meters. The deepest, unsuccessful core (10) contained only traces of coarse sand, and the hole collapsed when this interval was penetrated; the combined evidence suggests that the drill string had penetrated coarse, unconsolidated sand underlying the nonlaminated sediments (see Tucholke et al., this volume).

The sediments recovered are remarkably uniform in lithology, and the entire sequence is discussed as one unit. Cores 1 through 9 recovered gray Pliocene to Pleistocene clays with scattered ice-rafted debris and well-sorted silt and sand in beds, stringers, and in pods created by drilling disturbance. Diatom clays and oozes were found only in Core 1; both diatoms and radiolarians are rare in deeper sediments (Figure 7).

Silt-sized quartz is ubiquitous in the clays, usually in amounts of 5%-10%. The clays are mostly structureless, although a few trace fossils are present. Color changes in the clays are normally subtle and gradational but are occasionally sharp. Very well sorted laminae and 0.5 to 1.0 cm thick beds of quartz silt were found in most cores. Their frequency appears to be inversely related to the amount of ice-rafted debris in the cores. In addition to quartz, the layers contain heavy and opaque minerals, feldspar, and mica. Rock fragments are sporadically observed. Even where core disturbance was not severe, primary structures were seldom observed in the silt layers. Occasionally, alternating light/dark, silt/clay laminae form the beds. Upper and lower contacts are invariably sharp.

The clays in Core 8-3 (174 m) show incipient induration to claystone, but are still pliable. A clay gall in Core 8-2 and silt and clay beds in Cores 9-1 and 9, CC are weakly silicified.

Sedimentation rates at Site 324 have averaged about 5.5 cm/1000 yr during the Pliocene to Holocene (Figure 8). Discrepancies in sediment ages indicated by diatoms and radiolarians are probably caused by: (1) reworking of microfossils by bottom currents, and (2) downhole contamination during drilling (see Weaver, and Schrader, both this volume).

#### Site 325

The sediment at this site is composed of terrigenous clays, silts, sands, and their consolidated analogs, but the recovered sediments represent only 4.8% of the hole. The sequence is divided into two lithologic units: (1) an upper silty clay, silty claystone, and claystone unit, and (2) a lower sandstone, siltstone, and claystone unit. The division is somewhat artificial because of the poor core control and because, like Sites 322 and 323, low core recovery at mid-depth in the hole suggests the

presence of significant amounts of unconsolidated sand.

**Unit 1:** The dominance of clay over occasional silts and sands distinguishes this middle Miocene to Holocene unit from the underlying unit where sandstones and siltstones predominate. The contact lies between Cores 7 and 8 (528-612 m).

Soft sticky clay extends to a depth of about 300 to 400 meters between Cores 4 and 5; Cores 5 through 7 (404-528 m) are claystones. The clays of Cores 1-4 are disturbed by coring and show no detectable primary structures. The claystones of Cores 5-7, however, are locally laminated and have common and well developed trace fossils. Core 7 contains about 5 cm of structureless nanofossil claystone. The clays contain silt both disseminated and as discrete layers, laminae, and pods. Silt layers show no internal structure except for occasional silt/clay laminae. The silt is primarily quartz, but rock fragments and heavy minerals are always found in amounts between 3% and 15% (Figure 9). Feldspars and opaque minerals are normally less than 5%, but the amount varies considerably. Unlike the silt beds at Site 324, most of these silts are not well sorted.

Ice-rafted cobbles, fine gravel, and sand dispersed in the clays are observed down through Core 7.

Diatoms are present in Cores 1-6; they are particularly abundant (up to 25%) in Core 4, and to a lesser extent in Core 5. In each case they are poorly preserved and fragmentary, suggesting they are largely detrital.

**Unit 2:** This unit (Cores 8-10; 612.5 to 718 m) has abundant lower Miocene sandstone and siltstone with minor claystone. The three lithologies are interbedded throughout the unit, and sedimentary structures are clearly preserved.

The interbedded claystones are gray to olive-black and vary from massive, though extensively mottled by trace fossils, to finely laminated. They are composed dominantly of detrital clays with auxiliary quartz, feldspar, and heavy minerals in trace quantities (Figure 9). Nanofossil claystone was recovered only in Core 8-2 (615 m). Lower contacts are usually gradational on siltstone, and upper contacts are marked by a sharp change to siltstone or sandstone.

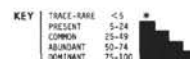
The silts occur as relatively thick (approximately 10 cm) clayey beds or as thin, clean, light gray laminae in claystone. Some silt laminae are barely discernible partings, yet they extend in a series of parallel lines across the entire core without disturbance. In thicker layers we observe foreset beds, interbedded clay laminae, and variations in layer thickness across the core. Graded bedding is uncommon and poorly developed where present. At the top of Core 9-2 (642.5 m), sandy silt beds are strongly distorted due to syndepositional deformation (Figure 27). Deeper in the same core, faulting is clearly evident in the lithified siltstone and sandstone (Figure 28).

Primary structures in the sandstones encompass the spectrum created by deposition from turbidity currents: size grading, parallel laminae, foreset and cross bedding.

The sandstones and siltstones have a similar mineralogy, consisting dominantly of quartz, although rock fragments comprise up to 50% of the rock. Rock

SMEAR SLIDE SUMMARY

SITE 324



CORE SECTION	INTERVAL cm	EXOGENIC										AUTHIGENIC-DIAGENETIC										BIOGENIC									
		DETRITAL QUARTZ	FELDSPARS	HEAVY MINERALS	ROCK FRAGMENTS	LIGHT GLASS	DARK GLASS	MAGNETITE	MICA	UNIDENTIFIED OPAQUES	GLAUCONITE	CLAY MINERALS	PALAGONITE	ZEOLITES	HEMATITE	AMORPHOUS IRON OXIDES	MICRO-NODULES	PYRITE	RECRYSTALL SILICA	RECRYSTALL CALCITE	FORAM-INIFERS	MANNO-FOSSILS	RADIO-LARIANS	DIATOMS	SILICO-FLAGELLATES	SPONGE SPICULES	FISH DEBRIS	OTHER			
1 1	146	*		*		*																*									
1 2	100			*		*																*									
1 3	76	*		*											*								*								
1 3	126			*		*																*									
1 4	13	*		*											*							*	*		*						
1 4	119	*		*		*																*	*		*						
1 5	49		*	*		*																*	*		*						
1 5	65		*	*		*																*	*		*						
1 5	99		*	*		*																*	*		*						
1 5	120	*		*		*																*	*		*						
1 6	14		*	*		*																*	*		*						
1 6	85	*		*		*																*	*		*						
1 6	127	*		*		*												*													
1 6	135	*		*		*												*													
1	CC	*	*	*		*											*?					*	*		*						
2 1	23		*	*		*																									
2 1	25	*		*		*									*																
2 2	145		*	*		*																									
2 3	42	*		*		*																									
2 4	20		*	*		*																									
2 5	20		*	*		*																									
2	CC		*	*		*									*								*	*		*					
3 1	21		*	*		*																									
3 1	71		*	*		*													*												
3 1	87		*	*		*													*												
3 1	116		*	*		*													*												
3 2	37		*	*		*																									
3 2	95	*		*		*																									
3 2	103	*		*		*																									
3 3	51		*	*		*																									
3 4	20		*	*		*													*												
3 4	31		*	*		*													*												
3 4	76		*	*		*													*												
3 5	87		*	*		*																									
3 5	137		*	*		*																									
3 6	121		*	*		*																									
3	CC	*	*	*		*																									
4 1	140	*		*		*																	*	*		*					
4 2	101		*	*		*																			*						
4 2	118		*	*		*																									
4 2	150		*	*		*																			*						
4 3	80		*	*		*																				*					
4 3	117		*	*		*																			*						
4 4	90		*	*		*																									
4 4	112		*	*		*																									
5 1	110		*	*		*																*	*		*						
5 2	110		*	*		*																									
5 2	121	*		*		*																									
5 3	40		*	*		*																			*						
5 3	95		*	*		*																									
5 3	103	*		*		*																									
5 3	132		*	*		*																									
5	CC	*	*	*		*													*												

Figure 7. Smear-slide summary, Site 324.

SMEAR SLIDE SUMMARY

SITE 324



CORE	SECTION	INTERVAL cm	EXOGENIC										AUTHIGENIC-DIAGENETIC										BIOGENIC									
			DETRITAL QUARTZ	FELDSPARS	HEAVY MINERALS	ROCK FRAGMENTS	LIGHT GLASS	DARK GLASS	MAGNETITE	MICA	UNIDENTIFIED OPAQUES	GLAUCONITE	CLAY MINERALS	PALAGONITE	ZEOLITES	HEMATITE	AMORPHOUS IRON OXIDES	MICRO-NODULES	PYRITE	RECRYSTALL SILICA	RECRYSTALL CALCITE	FORAM-IFERS	INIFERS	MANNO-FOSSILS	RADIO-LARIANS	DIATOMS	SILICO-FLAGELLATES	SPONGE	SPICULES	FISH DEBRIS	OTHER	
6	1	32	*																													
6	1	90	*																													
6	2	7																														
6	2	40																														
6	6	146	*	*	*														*						*		*					
6	6	148	*	*	*	*																										
6		CC	*	*	*																											
7	1	7	*	*	*																											
7	1	56	*	*	*															*												
7	1	80	*	*	*																											
7	2	119	*	*	*																											
7	3	125	*	*	*																											
7	4	125	*	*	*																											
7	5	50	*	*	*																											
7	6	125	*	*	*																											
7	6	133	*	*	*																											
8	1	78	*	*	*																											
8	2	70	*	*	*		*												*				*	*		*						
8	2	100	*	*	*		*												*				*	*		*						
8	2	130	*	*	*		*												*				*	*		*						
8	3	32	*	*	*														*				*	*		*						
8	3	92	*	*	*														*				*	*		*						
8		CC	*	*	*														*				*	*		*						
9	1	90	*	*	*														*	*			*	*		*						
9	1	126	*	*	*														*	*			*	*		*						
9	1	140	*	*	*														*	*			*	*		*						
9		CC	*	*	*														*	*			*	*		*						
9		CC	*	*	*														*	*			*	*		*						

Figure 7. (Continued).

fragments in sandstones are generally well rounded with medium sphericity. The quartz varies from sub-angular to subrounded. Heavy minerals, feldspars, and detrital clays are found in most sandstones and siltstones (Figure 9).

Several conglomerates were found in Core 10 (708.5-718 m). They contain common to abundant clay clasts which in some cases are preferentially oriented parallel to the bedding. The matrix is usually siliceous clay, but one sample in Core 10-3 is cemented with authigenic carbonate.

Authigenic cementation of sediments by silica and calcite is common below Core 4 at this site (Figures 9 and 29). Recognizable tests of diatoms and radio-

larians decrease in abundance below this level, and dissolution and reprecipitation of the biogenic silica apparently has caused the observed cementation. Nannoplankton were found in significant quantities only in the deeper part of the hole (Cores 7 and 8); however, dissolution and precipitation of biogenic calcite apparently does not account for the calcite cementation because carbon isotope compositions are different in the two carbonates (see Anderson and Lawrence, this volume).

The average accumulation rate for the 718 meters of sediment penetrated at Site 325 is about 4 cm/1000 yr. Available paleontologic control suggests rates two to three times greater in the early Miocene and late-Miocene to early Pliocene, and slower rates in the Pleistocene and mid to late Miocene (Figure 10). Thus the coarse clastics of Unit 2 have accumulated at about 8 cm/1000 yr which is commensurate with their textural characteristics.

ICE-RAFTED SEDIMENTS

One of the major goals of Leg 35 was to extend our knowledge of the glacial history of West Antarctica by recovering older Neogene and Paleogene sediments from the continental margin. Ice-rafted debris was encountered at all four sites drilled, and Sites 322, 323,

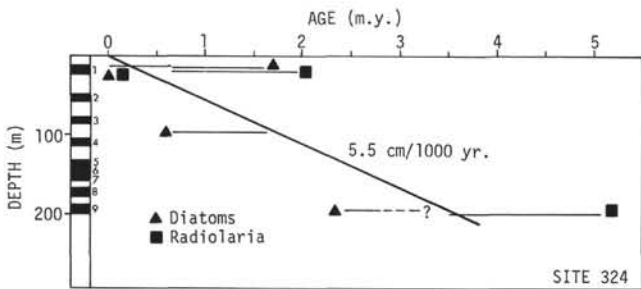


Figure 8. Sediment accumulation rates, Site 324.



CORE SECTION	INTERVAL cm	EXOGENIC										AUTHIGENIC-DIAGENETIC										BIOGENIC									
		DETRITAL QUARTZ	FELDSPARS	HEAVY MINERALS	ROCK FRAGMENTS	LIGHT GLASS	DARK GLASS	MAGNETITE	MICA	UNIDENTIFIED OPAQUES	GLAUCONITE	CLAY MINERALS	PALAGONITE	ZEOLITES	HEMATITE	AMORPHOUS IRON OXIDES	MICRO-NODULES	PYRITE	RECRYSTALL SILICA	RECRYSTALL CALCITE	FORAM-INIFERS	NANNO-FOSSILS	RADIO-LARIANS	DIATOMS	SILICO-FLAGELLATES	SPONGE SPICULES	FISH DEBRIS	OTHER			
1	1	17	*	*	*	*	*	*	*	*	*	*	*	*	*	*	*	*	*	*	*	*	*	*	*	*	*	*			
1	1	28	*	*	*	*	*	*	*	*	*	*	*	*	*	*	*	*	*	*	*	*	*	*	*	*	*	*			
1	1	31	*	*	*	*	*	*	*	*	*	*	*	*	*	*	*	*	*	*	*	*	*	*	*	*	*	*			
1	1	126	*	*	*	*	*	*	*	*	*	*	*	*	*	*	*	*	*	*	*	*	*	*	*	*	*	*			
1	2	21	*	*	*	*	*	*	*	*	*	*	*	*	*	*	*	*	*	*	*	*	*	*	*	*	*	*			
1	2	47	*	*	*	*	*	*	*	*	*	*	*	*	*	*	*	*	*	*	*	*	*	*	*	*	*	*			
1	2	59	*	*	*	*	*	*	*	*	*	*	*	*	*	*	*	*	*	*	*	*	*	*	*	*	*	*			
1	2	63	*	*	*	*	*	*	*	*	*	*	*	*	*	*	*	*	*	*	*	*	*	*	*	*	*	*			
1	2	91	*	*	*	*	*	*	*	*	*	*	*	*	*	*	*	*	*	*	*	*	*	*	*	*	*	*			
1	2	147	*	*	*	*	*	*	*	*	*	*	*	*	*	*	*	*	*	*	*	*	*	*	*	*	*	*			
1	3	5	*	*	*	*	*	*	*	*	*	*	*	*	*	*	*	*	*	*	*	*	*	*	*	*	*	*			
1	3	73	*	*	*	*	*	*	*	*	*	*	*	*	*	*	*	*	*	*	*	*	*	*	*	*	*	*			
1	3	99	*	*	*	*	*	*	*	*	*	*	*	*	*	*	*	*	*	*	*	*	*	*	*	*	*	*			
1	4	57	*	*	*	*	*	*	*	*	*	*	*	*	*	*	*	*	*	*	*	*	*	*	*	*	*	*			
1	4	104	*	*	*	*	*	*	*	*	*	*	*	*	*	*	*	*	*	*	*	*	*	*	*	*	*	*			
1	4	141	*	*	*	*	*	*	*	*	*	*	*	*	*	*	*	*	*	*	*	*	*	*	*	*	*	*			
1	4	143	*	*	*	*	*	*	*	*	*	*	*	*	*	*	*	*	*	*	*	*	*	*	*	*	*	*			
1	4	149	*	*	*	*	*	*	*	*	*	*	*	*	*	*	*	*	*	*	*	*	*	*	*	*	*	*			
1		CC	*	*	*	*	*	*	*	*	*	*	*	*	*	*	*	*	*	*	*	*	*	*	*	*	*	*			
2	2	44	*	*	*	*	*	*	*	*	*	*	*	*	*	*	*	*	*	*	*	*	*	*	*	*	*	*			
2	2	121	*	*	*	*	*	*	*	*	*	*	*	*	*	*	*	*	*	*	*	*	*	*	*	*	*	*			
2	2	133	*	*	*	*	*	*	*	*	*	*	*	*	*	*	*	*	*	*	*	*	*	*	*	*	*	*			
2		CC	*	*	*	*	*	*	*	*	*	*	*	*	*	*	*	*	*	*	*	*	*	*	*	*	*	*			
3	1	113	*	*	*	*	*	*	*	*	*	*	*	*	*	*	*	*	*	*	*	*	*	*	*	*	*	*			
3	1	121	*	*	*	*	*	*	*	*	*	*	*	*	*	*	*	*	*	*	*	*	*	*	*	*	*	*			
3	1	131	*	*	*	*	*	*	*	*	*	*	*	*	*	*	*	*	*	*	*	*	*	*	*	*	*	*			
3	1	146	*	*	*	*	*	*	*	*	*	*	*	*	*	*	*	*	*	*	*	*	*	*	*	*	*	*			
3	2	6	*	*	*	*	*	*	*	*	*	*	*	*	*	*	*	*	*	*	*	*	*	*	*	*	*	*			
3	2	41	*	*	*	*	*	*	*	*	*	*	*	*	*	*	*	*	*	*	*	*	*	*	*	*	*	*			
3	2	56	*	*	*	*	*	*	*	*	*	*	*	*	*	*	*	*	*	*	*	*	*	*	*	*	*	*			
3	2	140	*	*	*	*	*	*	*	*	*	*	*	*	*	*	*	*	*	*	*	*	*	*	*	*	*	*			
3	3	12	*	*	*	*	*	*	*	*	*	*	*	*	*	*	*	*	*	*	*	*	*	*	*	*	*	*			
3	3	71	*	*	*	*	*	*	*	*	*	*	*	*	*	*	*	*	*	*	*	*	*	*	*	*	*	*			
3	3	129	*	*	*	*	*	*	*	*	*	*	*	*	*	*	*	*	*	*	*	*	*	*	*	*	*	*			
3	4	76	*	*	*	*	*	*	*	*	*	*	*	*	*	*	*	*	*	*	*	*	*	*	*	*	*	*			
3		CC	*	*	*	*	*	*	*	*	*	*	*	*	*	*	*	*	*	*	*	*	*	*	*	*	*	*			
4	1	147	*	*	*	*	*	*	*	*	*	*	*	*	*	*	*	*	*	*	*	*	*	*	*	*	*	*			
4	2	25	*	*	*	*	*	*	*	*	*	*	*	*	*	*	*	*	*	*	*	*	*	*	*	*	*	*			
4	2	30	*	*	*	*	*	*	*	*	*	*	*	*	*	*	*	*	*	*	*	*	*	*	*	*	*	*			
4	3	91	*	*	*	*	*	*	*	*	*	*	*	*	*	*	*	*	*	*	*	*	*	*	*	*	*	*			
4	3	96	*	*	*	*	*	*	*	*	*	*	*	*	*	*	*	*	*	*	*	*	*	*	*	*	*	*			
5	1	82	*	*	*	*	*	*	*	*	*	*	*	*	*	*	*	*	*	*	*	*	*	*	*	*	*	*			
5	1	88	*	*	*	*	*	*	*	*	*	*	*	*	*	*	*	*	*	*	*	*	*	*	*	*	*	*			
5	1	148	*	*	*	*	*	*	*	*	*	*	*	*	*	*	*	*	*	*	*	*	*	*	*	*	*	*			
5	2	122	*	*	*	*	*	*	*	*	*	*	*	*	*	*	*	*	*	*	*	*	*	*	*	*	*	*			
5		CC	*	*	*	*	*	*	*	*	*	*	*	*	*	*	*	*	*	*	*	*	*	*	*	*	*	*			
5		CC	*	*	*	*	*	*	*	*	*	*	*	*	*	*	*	*	*	*	*	*	*	*	*	*	*	*			

Figure 9. Smear-slide summary, Site 325.

and 325 penetrated sediment older than Pliocene. Distribution of ice-rafted debris was examined in three ways: (1) megascopic identification of exotic pebbles and cobbles in all core material and of dispersed sands and granules in otherwise uniform, clay-size sediments, (2) grain-size analyses of clayey sediments, and (3) scanning-electron microscope (SEM) study of quartz surface textures on sand grains dispersed in clay (Table 3). In addition, the provenance of the detritus was investigated by petrographic examination of the pebbles and cobbles recovered at Sites 324 and 325. Because the

paucity of paleontologic data does not allow precise age control, no attempt has been made to determine rates of sedimentation for ice-rafted material other than by subjective description.

**Method of SEM Examination**

Forty-three 10-cc samples from Sites 322, 323, and 325 were studied using the scanning electron microscope. Each sample was washed over a 62 μm sieve, the residue dried, and the grains examined with a binocular microscope. Twenty quartz grains were randomly

SMEAR SLIDE SUMMARY

SITE 325



CORE SECTION	INTERVAL cm	EXOGENIC										AUTHIGENIC-DIAGENETIC										BIOGENIC									
		DETRITAL QUARTZ	FELDSPARS	HEAVY MINERALS	ROCK FRAGMENTS	LIGHT GLASS	DARK GLASS	MAGNETITE	MICA	UNIDENTIFIED OPAQUES	GLAUCONITE	CLAY MINERALS	PALAGONITE	ZEOLITES	HEMATITE	AMORPHOUS IRON OXIDES	MICRO-NODULES	PYRITE	RECRYSTALL SILICA	RECRYSTALL CALCITE	FORAM - INIFERS	NANNO-FOSSILS	RADIO-LARIANS	DIATOMS	SILICO-FLAGELLATES	SPONGE	SPICULES	FISH DEBRIS	OTHER		
6	1	148	*	*	*																										
6		CC	*	*	*									*								*	*			*					
7	1	123	*	*	*													*					*			*					
7	1	130	*	*	*													*					*		*						
7	1	143	*	*	*													*					*		*						
7	2	52	*	*	*													*				*		*							
7	2	77	*	*	*													*				*		*							
7	2	130	*	*	*													*				*		*							
7		CC	*	*	*													*				*		*							
7		CC	*	*	*													*				*		*							
8	1	76	*	*	*								*	*							*		*								
8	1	96	*	*	*							*	*							*		*						*			
8	1	121	*	*	*							*	*							*		*						*			
8	2	40	*	*	*							*	*		*	*				*		*									
8	2	95	*	*	*							*	*		*	*				*		*									
8	2	119	*	*	*							*	*		*	*				*		*									
8	3	31	*	*	*							*	*		*	*				*		*									
8	3	115	*	*	*							*	*		*	*				*		*									
8		CC	*	*	*							*	*		*	*				*		*									
8		CC	*	*	*							*	*		*	*				*		*									
9	1	122	*	*	*							*	*		*	*				*		*									
9	1	127	*	*	*							*	*		*	*				*		*									
9	2	6	*	*	*							*	*		*	*				*		*									
9	2	48	*	*	*							*	*		*	*				*		*									
9	2	140	*	*	*							*	*		*	*				*		*									
9	3	10	*	*	*							*	*		*	*				*		*									
9	3	55	*	*	*							*	*		*	*				*		*									
9	3	142	*	*	*							*	*		*	*				*		*									
10	1	11	*	*	*							*	*		*	*				*		*						*			
10	1	74	*	*	*							*	*		*	*				*		*						*			
10	1	120	*	*	*							*	*		*	*				*		*						*			
10	2	80	*	*	*							*	*		*	*				*		*						*			
10	2	125	*	*	*							*	*		*	*				*		*						*			
10	3	23	*	*	*							*	*		*	*				*		*						*			
10	3	56	*	*	*							*	*		*	*				*		*						*			
10	3	117	*	*	*							*	*		*	*				*		*						*			
10	3	136	*	*	*							*	*		*	*				*		*						*			
10		CC	*	*	*							*	*		*	*				*		*						*			
10		CC	*	*	*							*	*		*	*				*		*						*			

Figure 9. (Continued).

selected from each sample and mounted on a standard SEM stub, coated with a thin film of carbon and gold-palladium in a vacuum evaporator, and examined for diagnostic glacial surface microtextures on an International Scientific Instruments Super Mini-Scan. The criteria for the recognition of primary glacial microtextures on quartz grains as outlined by Margolis and Kennett (1971) was utilized in this investigation. It should be noted that the validity of their technique has been questioned by Setlow and Karpovich (1972) and by Brown (1973), and therefore the utilization of this method is best implemented for interpretation of paleoglacial history when other evidence, both sedimentological and paleontological, is simultaneously available.

**Distribution of Ice-Rafted Debris**

**Site 322 (Eastern Bellingshausen Abyssal Plain)**

Thirteen clay and claystone samples were examined by SEM from 31.2 meters of sediment recovered at this site. Although their abundance is low, the first appearance of quartz grains whose surface microtextures are indicative of a primary glacial origin, and thus of ice-rafting, occurs in upper Miocene sediments (322-2, CC) (Table 3). The abundance of ice-rafted quartz sand increases upward in the Pliocene sediments examined at this site, all of which fall within the Upsilon radiolarian Zone.

The only ice-rafted debris observed in megascopic descriptions consists of sand and fine gravel dispersed

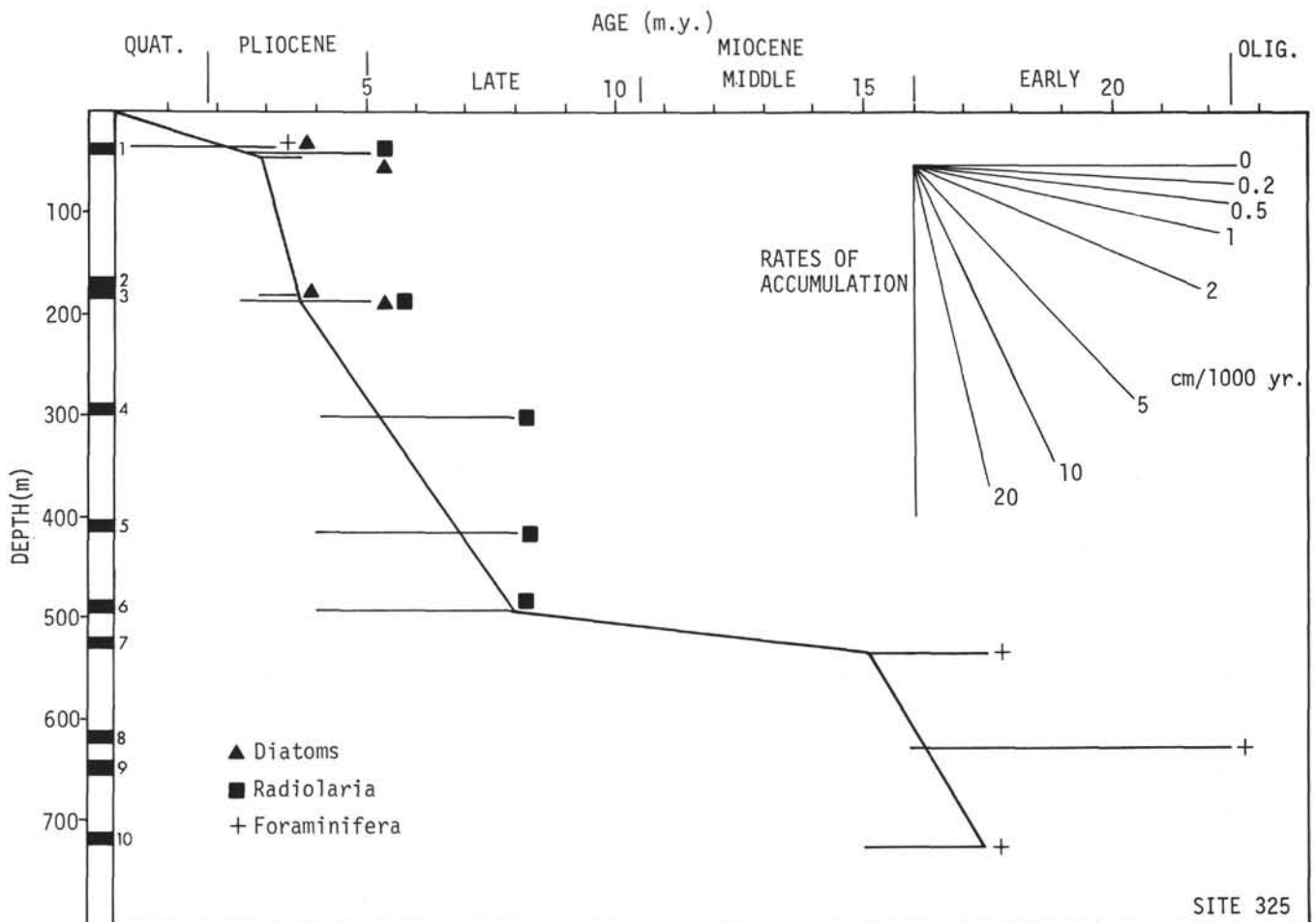


Figure 10. Sediment accumulation rates, Site 325.

in detrital-diatom silty clay in Core 1-2 at 79 meters. The clay is only slightly disturbed, and the coarse detritus appears to be in place rather than due to down-hole reworking. The sediment is dated as Pliocene.

Ice-rafted sediment could not be differentiated in grain-size analyses of sediment at this site.

#### Site 323 (Bellingshausen Abyssal Plain)

Sixteen pelagic clay, claystone, and mudstone samples were examined by SEM at this site for their ice-rafted quartz component. The earliest appearance of ice-rafted quartz is in the late middle Miocene (*Antarctissa conradae* radiolarian Zone of Chen, 1975), but this sample (323-3-2, 33-35 cm) contained only one quartz sand grain which exhibited primary glacial microtextures. Moderately abundant ice-rafted quartz was also found in several Pliocene samples. These samples fall within the Tau radiolarian Zone of Hays and Opdyke (1967) and the *Helotholus vema* radiolarian Zone of Chen (1975).

One ice-rafted pebble was found in drill slurry in Core 7-2 and minor amounts of gravel are dispersed in dark greenish-gray clay in Sample 7, CC. Although the pebble may be reworked from uphole, the clay which is middle Miocene in age does not appear to be severely disturbed. As at Site 322, ice-rafted detritus cannot be

distinguished in Site 323 sediments purely on the basis of grain-size analyses.

#### Site 324 (Lower Continental Rise)

Ice-rafted debris was recovered in most cores at this site (Table 3) and the oldest sediment recovered (9, CC) is Pliocene in age. The amount of ice-rafted debris observed in the sediment varies dramatically down-hole, and therefore, assuming constant rates of accumulation for nonice-rafted sediment, so does the rate of ice-rafting. The most concentrated ice-rafted debris observed visually occurs in Cores 1, 2, 4, and 9. Two features relating to ice-rafted debris at this site are noteworthy:

1) Concentrated ice-rafted debris and well-sorted silt/sand layers in the cores are mutually exclusive lithologic facies (Figure 11). Diffuse ice-rafted debris is absent or very rare in clay units which contain silt layers.

2) Most clay intervals which contain concentrated ice-rafted sand and gravel show increasing intensity of ice-rafting with time (upward in the core), followed by a rapid, often sharp, transition to clay free of ice-rafted debris and containing silt layers. Several cores also exhibit a bluish or greenish-gray coloration in the ice-

**TABLE 3**  
Distribution of Ice-Rafted Debris in Leg 35 Drill Sites (Core-Section)

Site 322				Site 323				Site 324				Site 325			
P/C	G/S	GZ	SEM	P/C	G/S	GZ	SEM	P/C	G/S	GZ	SEM	P/C	G/S	GZ	SEM
			1-1, 44-46				1-2, 107-109	1-1				1-1	1-1	1-1	
	1-2							1-2	1-2	1-2		1-4		1-4	
			1-4, 70-72				2-1, 65-67	1-3	1-3	1-3		2-1			2-2, 22-24
			2-2, 97-99				2-1, 132-134		1-4 1-5			2-2 2, CC	2-2	2-2	
			2, CC				3-2, 33-35	1-6 1, CC	1-6 1, CC	1-6		3-1 3-2	3-1 3-2		
				7-2								3-3 3-2	3-3 3-2		
					7, CC					2-1		3-3 3-3	3-3 3-3	3-3	3-3, 43-45
										2-2 2-3 3-6		3-4 3, CC	3-4 3-4	3-4	3-4, 106-108 3, CC
								4-2				4-1 4-2	4-1 4-2		
										5-3 7-1		4, CC 5-1			
								7-3		7-3		5-2			
								9-1		9-1		6, CC			6, CC
								9, CC		9, CC			7-1 7-2	7-1	
												8-1			

Note: P/C = pebbles and cobbles; G/S = gravel and sand; GZ = sand (>2%) in clay-size sediments from grain-size analysis; SEM = primary glacial surface textures on quartz grains (>62 μm) from clay-size sediments – scanning electron microscope.

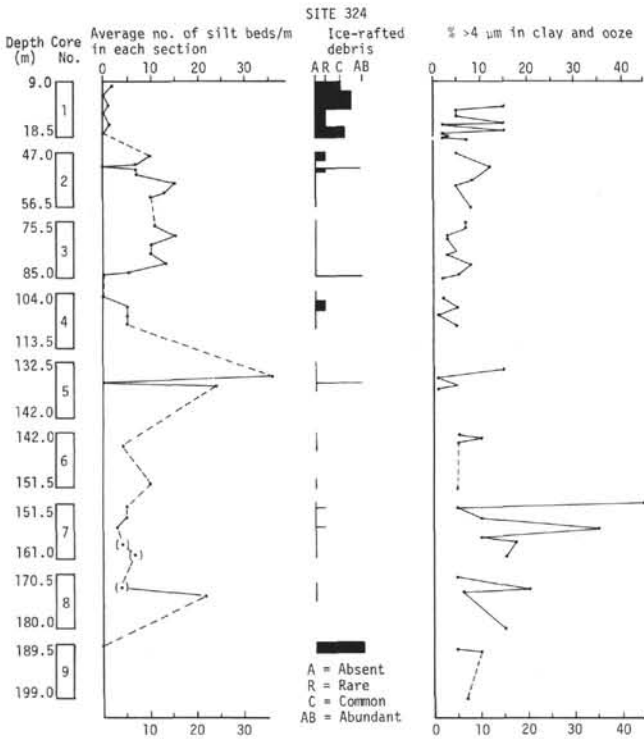


Figure 11. Silt-bed frequency, abundance of ice-rafted debris and percent >4 μm in clays and ooze in cores from Site 324.

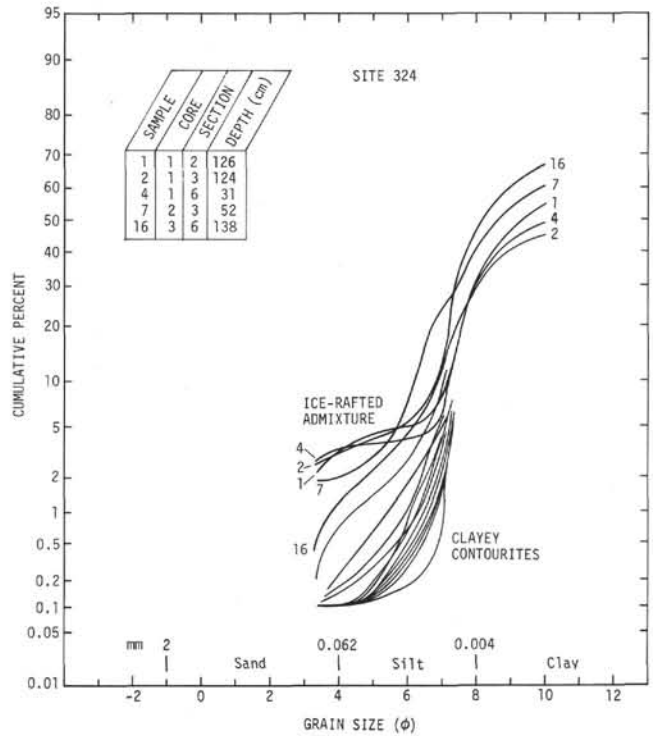


Figure 12. Cumulative curves for samples from Site 324.

rafted intervals with a sharp color transition to the overlying gray clay.

The grain size data, plotted as cumulative percent coarser (probability) versus grain size ( $\phi$ ), of all 23 samples from this site show a distinctive family of curves indicating an admixture of up to 5% coarse material into fine-grained, well-sorted clays with median grain size at approximately 8-10 $\phi$  (Figure 12). This characteristic is indicative of a bimodal grain-size distribution, and we infer that the coarse mode is ice-rafted material which has been dropped into the fine clays. The size sorting of these samples is correspondingly poorer; however, the grain size analyses (Bogdanov et al., this volume) do not extend beyond 10 $\phi$ ; material finer than this size accounts for about 50% of the total sample, and reliable sorting coefficients are therefore impossible to calculate.

**Site 325 (Upper Continental Rise)**

Fourteen clay and claystone samples were examined by SEM from sediment recovered at Site 325. The record of occurrence and abundance of ice-rafted quartz sand at Site 325 is similar to that at Site 322 in the eastern Bellingshausen Abyssal Plain. The first appearance of ice-rafted quartz sand is in the late Miocene within the *Theocalypta bicornis spongothorax* radiolarian Zone of Chen (1975) (325-6, CC). Pliocene ice-rafted quartz was also found in Site 325 samples corresponding to occurrences noted at Sites 322 and 323.

Cores 1 through 7 contain megascopically identified ice-rafted material indicating iceberg transport of terrigenous debris to this site no later than early to middle Miocene. Debris is contained within a claystone in Core 7, but Core 8 contained only a pyroxene-andesite cobble which could be downhole contamination. Megascopic identification of ice-rafting is very difficult below Core 7 because the sediments are predominantly sandstones, siltstones, and conglomerates emplaced by turbidity currents.

Grain-size analysis of fine siltstone and claystone shows the characteristic bimodal distribution of a coarse admixture in an otherwise fine-grained (8-10 $\phi$  median) material (Figure 13). Sediment containing the coarser admixture appears not to have a significantly larger median grain size; however, this inference is probably an artifact of the analytical procedure on material that is up to 50% finer than 10 $\phi$ . The coarse material (> 4 $\phi$ ) accounts for less than 20% of the total sample.

**Petrography of Ice-Rafted Pebbles and Cobbles**

**Site 324**

A suite of eight ice-rafted pebbles from this drill site was petrographically examined (Appendix I). Four of the samples are plutonic and the remainder are sedimentary or metasedimentary in origin. The plutonic pebbles include a remarkably fresh olivine gabbro, a biotite quartz diorite, a hornblende-biotite quartz diorite, and a single microcline crystal which is

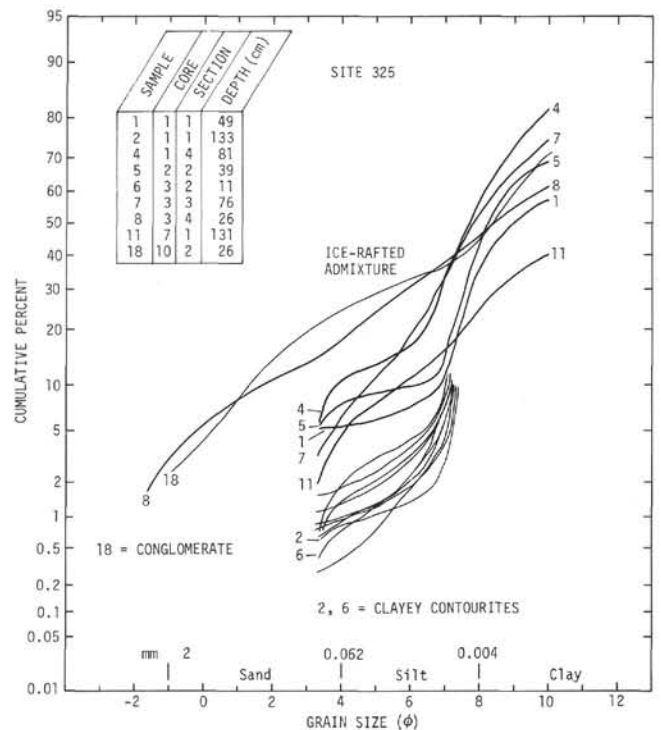


Figure 13. Cumulative curves for samples from Site 325.

probably pegmatitic in origin. The sedimentary rocks include a silty limestone and three arkosic sandstones, one of which contains metamorphic sericite and epidote. The plutonic rocks may have been derived from Thurston Island and/or the adjacent Eights Coast area, but the lithology of the sedimentary rocks demands a different source area.

The principal rock types described from the Thurston Island-Eights Coast area are quartz dioritic gneisses and quartz diorites of the Eights Coast batholith; gabbro phases are present in the batholith and are cut by the quartz diorite on Dustin Island (Drake et al., 1971). Drake's (1962) descriptions of the Eights Coast quartz diorite are very similar to two of the samples recovered from Site 324: a light gray, medium grained, and rather leucocratic rock containing variable amounts of biotite and hornblende. The gneissic quartz diorite contains abundant amphibolite layers on the eastern end of Thurston Island (Craddock et al., 1964), but sedimentary rock types similar to those recovered at Site 324 have not been reported from this sector of Antarctica, although coring and dredging close to the shore of Thurston Island has yielded quartzite fragments (Craddock and Hubbard, 1961).

The nearest plausible source areas for the sedimentary material are the (?) Carboniferous-aged Trinity Peninsula Series which outcrops extensively along both sides of the Antarctic Peninsula (Adie, 1969a, b) and the Lower Cretaceous sandstones and conglomerates of Alexander Island (Horne, 1968; Bell, 1973), more than 1200 km to the east. Elliott (1965) has described arkosic sandstones from the Trinity Peninsula Series identical to pebbles recovered at Site 324. The presence of abun-

dant quartz-mica schist rock fragments and metamorphic epidote in both the ice-rafted pebbles and the sandstones of the Trinity Peninsula Series is hardly conclusive proof, but is at least suggestive of a common origin. Arkosic sandstones also crop out in the Edsel Ford Ranges almost 1500 miles to the southwest, but here they are a minor part of the sedimentary sequence (Passel, 1945). Metamorphic effects described in these rocks (cleavage defined by micaceous minerals; Warner, 1945) do not appear in the ice-rafted pebbles. Adie (1957) has described calcareous shales and argillaceous limestones from the Trinity Peninsula Series, but these rocks are not common anywhere on the Antarctic Peninsula.

#### Site 325

Sixteen ice-rafted pebbles from this drill site were examined petrographically (Appendix I). They include four hornblende quartz diorites, three pyroxene andesites, two basalts, four siltstones, two sandstones, and a lapilli tuff. The proximity of this drill site to the west coast of the Antarctic Peninsula and the close similarity of the above-mentioned pebbles to the rock types exposed there leave little doubt of the general source area although it is difficult to ascertain the specific parts of the peninsula from which the pebbles might have been derived.

By far the most abundant rocks exposed on the Antarctic Peninsula are the various members of the Andean Intrusive Series, a Cretaceous to Tertiary aged series of calcalkaline intrusives which range in composition from gabbro to alkali granite (Adie 1955, 1969a, b). Quartz diorites are the most common intrusives in the northern part of the peninsula (Adie, 1955, p. 9), but American geologists working further to the south have found that granodiorites and quartz monzonites are more numerous near the base of the peninsula (Rowley and Williams, 1974). The hornblende quartz diorite pebbles recovered at Site 325 are also petrographically indistinguishable from rocks of the Thurston Island-Eights Coast area approximately 1300 km to the southwest (Drake et al., 1971), but in light of the associated sediments and volcanics, it is hardly necessary to invoke such a distant source area when an equally adequate one is considerably closer.

Volcanic rocks of several geologic ages are abundant both along the west coast of the Antarctic Peninsula and in the offshore islands, and the presence of these rock types as ice-rafted pebbles poses no problem other than trying to more sharply delineate the source area. Extensive outcrops of Late Jurassic volcanic rocks occur from the Danco Coast (61°S) to Marguerite Bay (69°S) and are assumed to extend even further south (Dalziel and Elliot, 1973). This assumption is supported by the occurrence of petrographically similar Jurassic volcanics in eastern Ellsworth Land (Laudon et al., 1969) and on the Lassiter Coast (Williams et al., 1972). This sequence is dominantly andesitic lava and pyroclastics, but also contains subordinate amounts of basaltic and rhyolitic flows, pyroclastics, and water-deposited tuffaceous sediments (Dalziel and Elliot, 1973). Jurassic, Tertiary, and Quaternary volcanic rocks occur extensively throughout the South Shetland

Islands (Adie, 1969a) and eruptions have continued into the 1970's on Deception Island (Baker and McReath, 1971). Andesites and olivine basalts are also abundant constituents of these units (Dalziel and Elliot, 1973). Adie (1954) has described propylitized porphyritic volcanics of questionable early Paleozoic age from Pourquoi Pas Island, Dalglish Bay, and adjacent offshore islands. These are the closest land masses to Site 325, and it is highly probable that one of the three pebbles examined from Core 7-2 (40 cm), a propylitized andesite, came from one of these localities.

The siltstones and sandstones are very similar to descriptions of the various sedimentary lithologies found by Elliot (1965) in the (?)Carboniferous Trinity Peninsula Series which outcrops extensively throughout the northern part of the peninsula (Adie, 1969a, b). In addition, some resemble the Lower Cretaceous sediments described from Alexander Island (Bell, 1973).

In summary, an easterly provenance is indicated for ice-rafted pebbles at both Sites 324 and 325. The pebbles are found in sediment dating back through the middle Miocene at Site 325 and into the Pliocene at Site 324. It appears that the East Wind Drift which flows westward along the coast of Antarctica (Gordon, 1971c) has been a significant agent in transporting sediment-laden berg ice during this period.

#### Synthesis of DSDP Evidence for Ice-rafting

Figure 14 summarizes the earliest documented occurrences of ice-rafted sediment in circum-Antarctic sites drilled on Legs 28, 29, and 35, together with the first significant occurrence of diatomaceous sediment (Piper and Brisco, 1975; Hayes, Frakes, et al., 1975; Margolis, 1975). Identification of ice-rafted debris is based on megascopic lithology, grain-size analysis, or SEM identification of glacial surface-textures on quartz sand.

Several features of this diagram are noteworthy: (1) There is clear latitudinal control on the first occurrence of significant ice-rafting. Superimposed on this trend are substantial variations which probably relate to proximity to berg source, availability of source rock, and surface current patterns. Piper and Brisco (1975) have suggested that proximity to berg source is a primary control, and that long-distance transport by surface currents may be unimportant. (2) Deposition of ice-rafted debris at a site is preceded by northward migration of the Antarctic polar front zone (indicated by diatomaceous sediments) across the area. (3) The earliest firm evidence for glaciation of Antarctica (i.e., ice-rafted debris) occurs in the early Miocene (ca 20 m.y.), although there are earlier suggestions of ice-rafting dating back through the late Oligocene at Sites 268 and 274 (Hayes, Frakes, et al., 1975).

Although early Paleogene sediments are not well represented in circum-Antarctic drill holes, those that have been recovered have provided no evidence of either diatomaceous sediment or ice-rafted debris that should accompany any extensive Antarctic glaciation. Thus the DSDP results do not agree with Margolis and Kennett's (1970) proposal of Antarctic continental glaciation in the Eocene; rather, the data suggest either

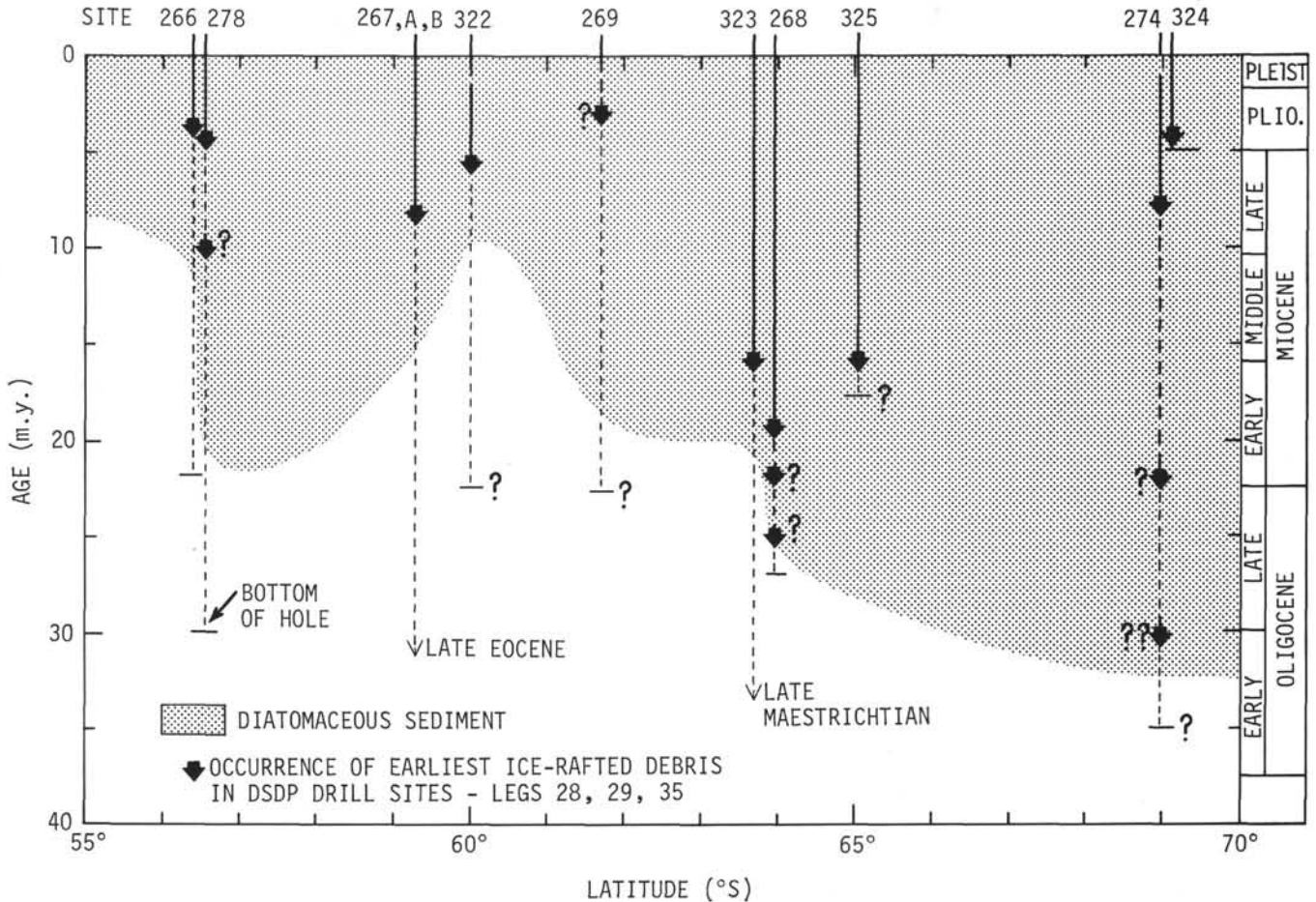


Figure 14. Occurrence of diatomaceous sediment and ice-rafted debris in circum-Antarctic sediments drilled on Legs 28, 29 and 35.

very slight glaciation in Antarctica or an extra-Antarctic source for early Paleogene glacially derived quartz grains.

### ABYSSAL-CURRENT-CONTROLLED SEDIMENTATION

#### Introduction

The modern abyssal circulation in the Bellingshausen Basin is not yet well documented, but studies to date suggest two opposing current systems which may affect abyssal sedimentation. The southernmost system is a contour-following current which flows westward along the Bellingshausen continental rise. The water appears to originate in the Weddell Sea, passes through a deep passage near 39°W into the Scotia Sea, and then flows westward as a deep current through the southern Drake Passage (Gordon, 1966). Reid and Nowlin (1971) found little evidence for the westward transport of Weddell Sea water through the Drake Passage, but their southernmost current measurement was 60 km north of the southern edge of the passage. Hollister and Heezen (1967) and Heezen et al. (1968) mapped potential temperature of the bottom water and traced the contour current along the Bellingshausen continental rise to about 130°W. Their bottom photographs indicate weak currents and rapid rates of sediment ac-

cumulation along the rise. The only direct current measurements on the rise suggest a general westward flow at speeds up to 12 cm/sec, but mostly less than 7 cm/sec (Jacobs et al., 1972). Indirect evidence for the contour current, in the form of hyperbolated sea floor and sediment dunes, is discussed by Schroeder, and by Tucholke and Houtz (both this volume).

To the north, the eastward-flowing Antarctic Circumpolar Current reaches the sea floor and has a dramatic effect on sediment covering the Bellingshausen Abyssal Plain and abyssal hills. Bottom photographs show strong current erosion and murky bottom water (Hollister and Heezen, 1967; Heezen et al., 1968). The effect of this current in eroding or preventing deposition of sediment is also indicated by a zone of anomalously thin sediment between about 55° and 60°S (Ewing et al., 1969).

Nephelometer measurements made on *Eltanin* Cruises 42 and 43 (Jacobs et al., 1972) indicate that both these current systems are transporting particulate matter. Based on an in situ nephelometer calibration made by Biscaye and Eitrem (1974), the concentrations of sediment in the currents probably approach 30 µg/l.

There were two primary controls on the development of these circumpolar currents during the Cenozoic. First was the existence of land barriers adjacent to Ant-

arctica, i.e., Australia against East Antarctica, and a land bridge between South America and the Antarctic Peninsula. Drilling on DSDP Leg 29 indicated that deep oceanic flow was established between Australia and Antarctica by the late Oligocene (ca. 30 m.y.) when the South Tasman Rise separated from Antarctica (Kennett et al., 1974). Geophysical evidence from the Drake Passage and Bellingshausen Basin suggests that the South America-Antarctic Peninsula link may not have been deeply breached until the latest Oligocene or early Miocene, 8-10 m.y. later (see Herron and Tucholke, and Tucholke and Houtz, this volume). It is likely, however, that initial fragmentation of this connection allowed shallow circumpolar flow well before the early Miocene.

A second agent, that of Antarctic glaciation, has undoubtedly had strong control on the intensity of circumpolar circulation by controlling thermohaline density contrasts responsible for the currents. One of the purposes in drilling in the Bellingshausen Basin was to differentiate between these controls and to determine their timing by examination of their inferred effect on the sedimentary record. The observed effects of abyssal currents in the Leg 35 drill sites are discussed below.

### Site 322

There is little evidence in the megascopic and microscopic lithology of the dominantly greenish-gray, terrigenous sediments at this site to indicate bottom current activity, although this is not surprising in view of the poor core recovery and strong coring disturbance in unconsolidated sediments (Cores 1-3). Intermittent current-reworking of detritus which was initially deposited by other mechanisms is inferred from the following data:

1) Thin unstructured layers (<1 cm) and partings of silt are present in silty clay and claystone units (Cores 1 and ?4). These features are not common, but they generally exhibit sharp top and bottom contacts. Compositionally, they are dominated by quartz, heavy minerals, feldspars, and diatoms, and they exhibit moderate to excellent sorting. This latter characteristic is interpreted to result from winnowing by bottom currents. It is debatable whether these placers result from winnowing of the adjacent silty clays or from winnowing of thin silty turbidites, because the silt fraction is compositionally similar for both. However, the intensity of reworking by currents does not appear to be strong because the mineral grains are mostly angular to subangular. Although the diatoms are generally fragmentary, the angularity of the mineral grains suggests the diatoms were broken mostly during the original depositional process rather than by current reworking.

2) Core 1 also contains short intervals (<5 cm) of laminated silt-clay interbeds of less than 2 mm thickness. The silts are texturally and compositionally similar to those described above, and the interbeds are therefore thought to result from winnowing by currents of variable intensity.

No erosional unconformities were detected visually in the cores recovered, but undetected hiatuses may well exist in the sparsely sampled sedimentary section.

The role that bottom currents may have played in the erosion, transportation, and deposition of clay-size material is open to question. Indirect evidence is provided by the scarcity of burrow mottling in the clays and claystones of Cores 1-9, in that sediment redistribution by bottom currents may have obscured trace fossils. Yellow-brown claystones with only minor terrigenous silt occur sporadically in these cores; they appear to represent dominantly pelagic deposition and offer additional evidence that bottom-current activity was intermittent. The basal, yellow-brown claystone unit immediately above basalt (Unit 4) also suggests dominantly pelagic deposition; however, the presence of chlorite and illite in the unit indicates probable transportation of terrigenous clays to the site by surface currents or weak bottom currents in the (?) Oligocene to early Miocene.

Grain-size analysis of the pelagic/hemipelagic sediment (i.e., nonbedded silty clays) shows a cluster of curves of similar shape that indicate more than 40% of the material is finer than  $10\phi$  (Figure 15). There is some evidence of coarse material, however, and it is interpreted to represent admixture of diatoms and radiolarians (Sample 2), and perhaps minor fine silt from distal turbidites (Samples 6 and 7). The samples from bedded sands and silts are interpreted as distal turbidites (left side of Figure 15, see discussion below) with a characteristic admixture of fine grained (< $5\phi$ ) matrix. It is noteworthy that two samples (1-Pliocene, 9-?) lower Miocene) are well-sorted siltstones with little fine matrix; they may be current-deposited contourites or placers (Hollister and Heezen, 1972).

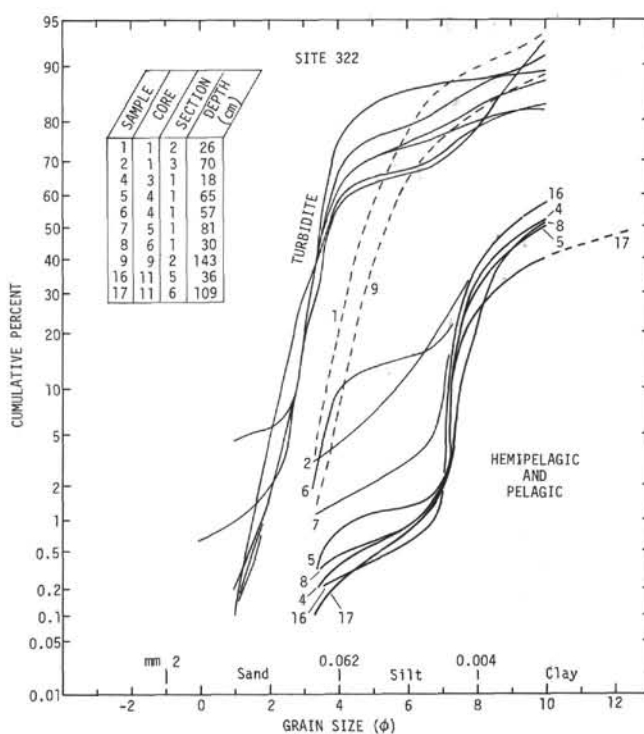


Figure 15. Cumulative curves for samples from Site 322.

Site 323

Obvious current-produced sedimentary structures or textures were not observed in the cores recovered at Site 323. Distorted layers and pods of silt and sandy silt with sharp upper and lower contacts were noted in Cores 1, 3, and 7; they show no grading or primary sedimentary structures and are poorly to moderately well sorted. Thin silt laminae and beds in deeper cores (10-13) are well preserved, and they are interbedded with bimodal, moderately sorted, quartz silty claystone of median size between 8 and 10 $\phi$  with an admixture of 2%-5% coarse silt and sand (Figures 16 and 17).

While data diagnostic of current activity are limited, other evidence may be used to infer the earliest possible occurrence of significant bottom-current activity. Iron-rich pelagic clays of middle Paleocene to Maestrichtian age in Cores 15-18 show no indication of disturbance by agents other than benthonic organisms. They are notably free of terrigenous silt (Figure 18) and terrigenous clays (chlorite and illite) which abyssal currents would surely transport. The overlying terrigenous sediments up through Core 10 (lower Miocene) may have accumulated in a relatively quiet environment interrupted only by the deposition of thin distal turbidites. Burrow mottling of these sediments is extensive in contrast to the limited evidence of trace fossils observed in shallower cores.

Pyrite is also common in Cores 10-14, both as small spherules and as replacement of diatoms, but it is rare in shallower cores. The upward loss of reducing conditions in the sediment could reflect the initiation of significant bottom circulation in the early Miocene. Although the change in conditions might result from a

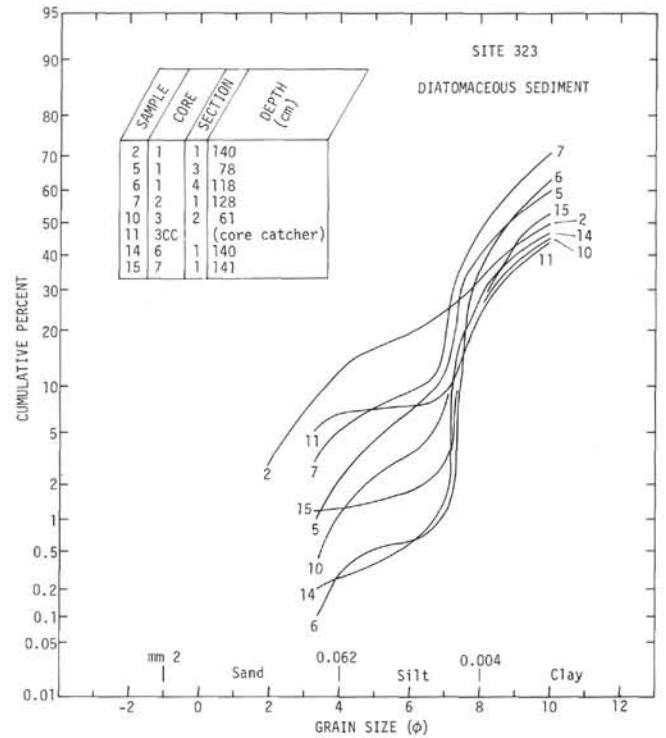


Figure 17. Cumulative curves for samples from Site 323.

difference in the amount of organic carbon within the sediment, the carbon content is nearly uniform (Cameron, this volume). However, recrystallized calcite is common below Core 10, and carbon isotope ratios suggest that its carbon source was organic carbon

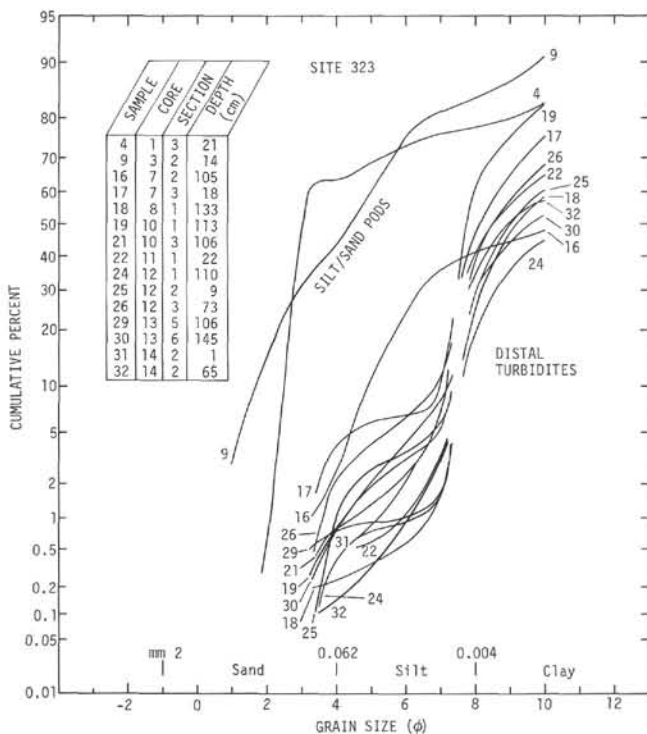


Figure 16. Cumulative curves for samples from Site 323.

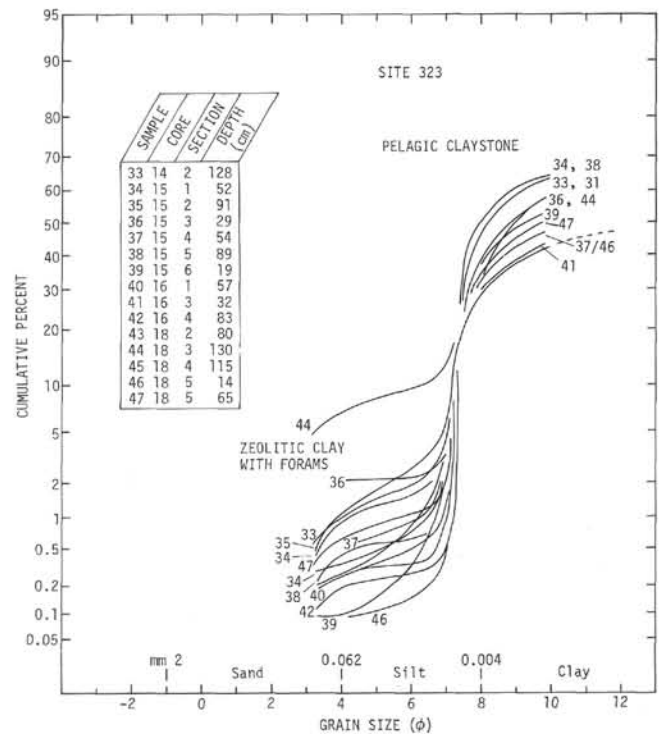


Figure 18. Cumulative curves for samples from Site 323.

rather than calcareous tests (Anderson and Lawrence, this volume); thus there may have been significantly more organic carbon than we presently observe, so that the change from reducing conditions could have been carbon controlled rather than current controlled.

The apparent disconformity between middle Paleocene and lower Miocene (?Oligocene) sediments at this site probably was caused by bottom current erosion. Because of the early Paleogene barriers to circum-Antarctic circulation noted earlier, it is unlikely that currents were strong enough to erode bottom sediment or prevent deposition until late in the Oligocene. However, by late Oligocene or early Miocene time, migration of the developing circumpolar current across the site could have eroded a substantial thickness of Paleocene-Oligocene pelagic clays deposited at the site. The remarkable capacity of bottom currents to erode seafloor sediment has been demonstrated in the equatorial Pacific (Johnson, 1972) where several tens to hundreds of meters of pelagic ooze were removed, probably just within the geologically short time span of the Pleistocene glacial stages. At Site 323, subsequent early Miocene to Holocene accumulation of terrigenous sediment at rates of 3-4 cm/1000 yr indicates that currents later played a lesser role in the depositional history. Currents may have become weaker, or more likely, the sedimentary record came to be dominated by rapid deposition of turbidites encroaching from Antarctica. Core recovery (and age control) is sparse in these younger sediments, and several current-generated hiatuses could exist undetected in our data (Figure 6).

#### Site 324

The Pliocene and Pleistocene sediments recovered at Site 324 exhibit the strongest evidence for bottom currents that was encountered on Leg 35. Nearly every core contains quartz-silt and sandy-silt layers (contourites) interbedded in terrigenous clay and ranging from a few millimeters to about one centimeter in thickness. The layers have sharp upper and lower contacts, generally show excellent sorting, but rarely exhibit internal structure. A few are faintly laminated because of thin, dark mineral placers or clayey laminae. Size grading was not observed in the beds, and heavy minerals are usually present in amounts of 5%-10%.

Site 324 lies beneath the westward-flowing counter-current on the continental rise and the cores were all recovered from a section of acoustically nonlaminated sediment. Sediments with this acoustic character on the rise appear to be confined to channel levees; the limited profiler data near this site do not show clear-cut evidence for an adjacent channel (Tucholke and Houtz, this volume), although a broad trough exhibiting highly reflective sediments east of the site may represent a primary path of turbidite dispersal.

Although the texture and structure of the silt layers appear to present strong evidence for their current-controlled origin, their mechanism of formation can be twofold. They may have been formed as placers by winnowing of fines from silty clay, or they may have been deposited from contour-following currents which pirated sediment placed in suspension by turbidity currents (Hollister and Heezen, 1972); when the current

is not competent to carry the material entrained, it deposits it as a laterally graded bed downstream from the channel. Ideally, slight vertical grading also would be present in the bed, with the finest material at the top representing the limit of competence of the bottom current.

If the silt beds were formed as placers by winnowing of silty clay, we would expect the frequency and thickness of the silt beds to increase in siltier sediment. However, as shown in Figure 11, there is no correlation between bed frequency and percent silt-in-clay, and bed thickness shows no correlative trend. In addition, the beds commonly contain a small fraction of sand ( $>62 \mu\text{m}$ ), whereas the interbedded clays contain no sand. One exception is the clays containing ice-rafted detritus, but silt beds are not observed in these intervals.

The alternative explanation, deposition of turbidity-current-derived sediment by contour currents, is more satisfactory. Variations in the intensity of contour-current flow and in the magnitude of turbidity currents can account for the variability in the silt-layer thickness, development of internal structure, and median grain size (fine to coarse silt). In this instance, each silt layer results from a discrete turbidity current traversing the continental rise upcurrent from the site. At the observed sedimentation rates (5.5 cm/1000 yr average), the frequency of silt beds suggests turbidity currents as often as one per 500 yr, but at a lower average rate of about one per 2000 yr during the Pliocene (Figure 11). These are minimum frequencies because all turbidity currents may not result in deposition of a recognizable contourite down-current from the turbidite channel.

Structures generally cannot be recognized in the clay-size sediment recovered, although faint color laminations and contacts occur locally. Trace fossils are very rare. It is likely that most of the clay was deposited from a current-maintained nepheloid layer during periods of less intense bottom current activity.

The grain size data for Site 324 clays show dramatic evidence for hydraulic sorting in the form of very symmetrical sigmoid curves typical of well-sorted material (Figure 19). This is the only site with sediment exhibiting this characteristic, and we interpret the data to represent clayey contourites. Unfortunately, no detailed grain size analyses were made on the coarser contourite silts; however, one sand-silt-clay determination made on a contourite silt in Core 7-6 (133 cm) showed that the size-class percentages are 0-86-14. This is a very well sorted silt (14% less than  $4 \mu\text{m}$ ) and is clean compared to matrix values for abyssal turbidites (Hollister and Heezen, 1964); the data thus support our contourite interpretation of the silt.

#### Site 325

Cores recovered at this site show very little evidence of bottom current activity. Cores 1 and 2 contain disturbed silt beds which are similar to those at Site 324, but which normally have gradational upper contacts. These beds also show poor to very poor sorting; only rarely are very well sorted beds observed. The deeper cores contain sedimentary structures diagnostic of turbidites with little indication of current reworking. A

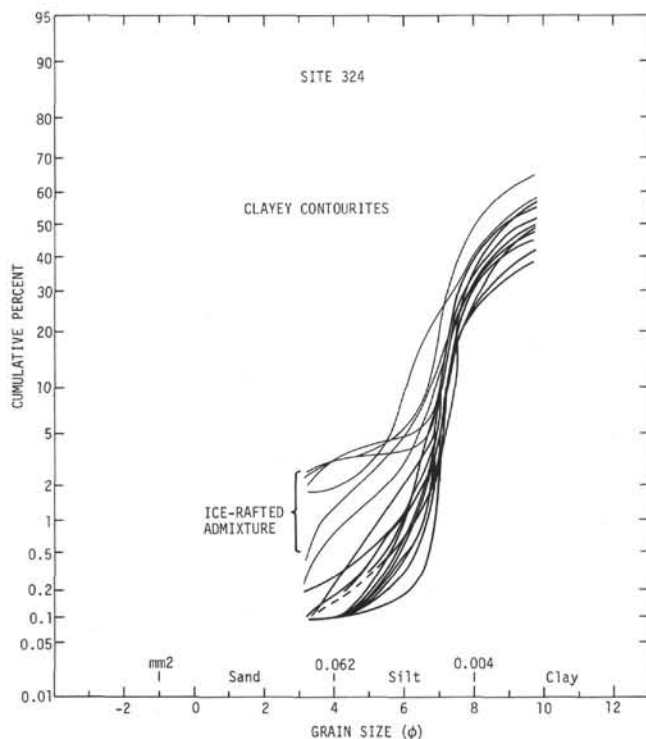


Figure 19. Cumulative curves for samples from Site 324.

few samples (for example, 2 and 6) analyzed for grain size and dating back to the Pliocene show the good sorting and sigmoid curves that we associate with a clayey contourite (Figure 13). However, it is apparent that turbidite deposition has dominated the area since the early Miocene.

### Summary

Analysis of sediments recovered at four drill sites in the Bellingshausen area suggests that significant bottom circulation did not develop in the southeast Pacific Basin until the latest Oligocene or early Miocene, perhaps in response to development of deep passages in the Drake Passage-Scotia Sea. A probable disconformity between middle Paleocene and lower Miocene (?Oligocene) sediments at Site 323 may represent an erosional surface created by these early currents. Lower Miocene sediments at Site 322 are brown pelagic claystones with a small admixture of terrigenous debris, grading upward into terrigenous sediments with some textural properties characteristic of current-controlled sedimentation; very little current evidence was detected in coeval terrigenous sediment at Site 323. Thus, after its initial development, the system of bottom currents over the Bellingshausen Abyssal Plain apparently had little effect on sea-floor sediments during the early Miocene. Turbidites which began to reach these sites in the early Miocene dominate the sedimentary record. There is increased evidence of bottom currents in middle Miocene to Holocene sediments (including possible hiatuses), but pelagic brown claystones interbedded in these sediments suggest that current activity was intermittent.

The appearance of diatomaceous sediments (taken to indicate migration of the polar front northward across the drill sites) postdates the initiation of bottom current activity at Sites 322 and 323 and suggests that the surface-water expression of the Antarctic Circumpolar Current reached Site 323 in the early to middle Miocene and Site 322 in the late Miocene (Figure 14).

Evidence for the contour-following countercurrent along the Bellingshausen continental rise is well preserved in the Pliocene-Pleistocene sediments cored at Site 324. At Site 325, current-produced sediment textures are poorly documented in the turbidite-dominated sediments, but there is some evidence for the countercurrent back through the Pliocene.

## TURBIDITE DEPOSITION

### Introduction

Sedimentary structures indicative of turbidites are well represented at Sites 322, 323, and 325, and they indicate that turbidity currents have played a major role in the development of the continental rise and abyssal plain. Regional patterns and effects of turbidity currents are discussed by Tucholke and Houtz (this volume).

Recent turbidity-current activity has apparently occurred throughout the Bellingshausen Basin. Three piston cores taken from R/V *Conrad* in the eastern basin and cores taken from *Eltanin* in the western basin (Frakes, 1971) contain sharp-based sand layers which are interpreted as turbidites. Grain-size data, especially from samples of the turbidite layers at Site 322 (Figure 20), clearly show the characteristic moderately sorted sand and silt with an admixture of clayey matrix typical of modern deep-sea graywacke-type sediment (Hollister and Heezen, 1964).

### Site 322

Turbidites first reached this site in the early Miocene. Core 11-4 at 509 meters contains a graded turbidite exhibiting several intervals of the Bouma sequence (basal graded sand, parallel laminae, and convolute laminae; Bouma, 1962). It is truncated by a thick (>4 m), dark gray, silty sandstone bed composed of rock fragments, quartz, feldspars, and heavy minerals. The bed is massive and of nearly uniform grain size (~3.5φ, Figure 20), has approximately 20% matrix finer than 8φ, and exhibits only slight grading in the basal 5 cm. It is noteworthy that the clayey matrix is composed of montmorillonite to the exclusion of illite, kaolinite, and chlorite (Gorbunova, this volume). The absence of more typically terrigenous clays in this otherwise terrigenous interval suggests that the montmorillonite may be the alteration product of volcanic ashes originally deposited with the sandstone. Portions of probably similar, massive sandstone beds were recovered in Cores 9 and 10. The beds locally show very faint bedding and cross-bedding but are mostly structureless.

Silty and sandy turbidites recovered commonly show a sharp, irregular basal contact on clay. The irregularity results both from erosion by turbidity currents

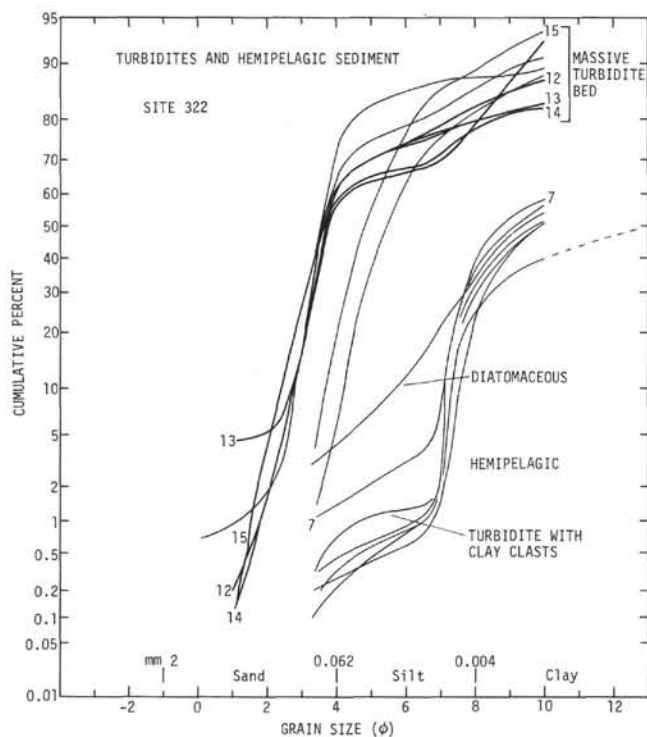


Figure 20. Cumulative curves for samples from Site 322.

and from post-depositional deformation (load casts). The basal parts of the turbidites contain clasts of the underlying clay which are angular to subrounded and often are deformed, indicating their original plasticity. In Cores 4-1, 4-2, and 10-1 the size of the clasts exceeds the diameter of the core; in Core 4 the structure suggests deposition of a thick bed of fluid silts which subsequently penetrated and disturbed the underlying soft clays. Strong, irregular deformation of bedding in the silts is apparent in these instances.

Core 5 (390-399.5 m) contains a remarkable bed of silty claystone which is heavily peppered with tiny (1-2 mm) clay clasts. These clasts are angular to (mostly) rounded and are oriented with their long axes horizontal, apparently being flattened by postdepositional compaction. They comprise an average of 50% of the sediment and form several weakly graded rhythmic sets. This unit was analyzed for grain size (Sample 7, Figure 20). It has a median grain size of  $8.7\phi$  and a prominent bimodal frequency indicative of an admixture of fine silt with clay. However, these results do not represent true grain-size distribution in the layer, because the tiny clay clasts were disaggregated before analysis. Occasional larger and irregular clay clasts (several cm) are scattered in this matrix. The original softness of the tiny clay clasts (indicated by their rounding during transport and by postdepositional flattening) and the presence of erratic larger clasts suggests that they were transported only a short distance; longer transport in a turbidity current would have destroyed the small clasts and cannot account for the scattered appearance of the larger clasts. It is likely that this sedimentary sequence represents deposition from a

slump which originated on one of the adjacent (now buried) basement peaks.

The grain size data for this site (Figures 15 and 20) illustrate the expected strong contrast in textural characteristics of coarse turbidites and hemipelagic sediments which represent two of the more extreme end members of textures measured on Leg 35.

#### Site 323

The earliest influx of terrigenous material at Site 323 occurs in Core 14 (638 m) in the ?Oligocene or early Miocene, but we cannot determine conclusively whether it represents distal turbidites or current-deposited sediment. Unlike the presumed clayey contourite samples at Site 324 (Figure 19), the grain-size curves of Site 323 show a bimodal silt admixture which may represent distal turbidites (Figure 16). Megascopically identified distal turbidites appear in Core 13-6 in the ?Oligocene to early Miocene. They consist of thin (3 mm) basal layers of about 50% quartz silt in clay and grade upward through finely laminated clay and silty clay interbeds to structureless clay, locally burrowed at the top. The basal silts are cemented by authigenic  $\text{CaCO}_3$ . Similar laminated and burrowed clays continue upward through Core 8. Cores 8 through 11 contain displaced neritic and shallow-water benthonic diatoms, and the fossil assemblage in Core 8 includes displaced fresh-water diatoms (Schrader, this volume).

Disturbed coarse silt and sand pods were recovered in Core 7 (lower to middle Miocene), at about the same chronostratigraphic level as the sand influx at Site 322. Textural analyses of these and shallower pods are shown in Figure 16 (Samples 4, 9, 16); they are poorly sorted in comparison to silt pods at Site 322 (Figure 15) and are more representative of turbidites than contourites. Massive unconsolidated sands were recovered only in Core 4 (middle Miocene), but the low core recovery ratio over the interval 100-600 meters suggests the presence of large quantities of unconsolidated sand which were not recovered (see Tucholke, et al., this volume).

#### Site 324

No turbidites were observed at this site. The sediment is interbedded silt and clay which was probably pirated from turbidity currents by bottom currents, transported parallel to the contours, and ultimately deposited as contourites. This injection mechanism best explains the textures and structures observed in sediment recovered from the site.

#### Site 325

Site 325 was drilled in the central continental rise near the upper boundary of braided channel development (see Schroeder, this volume). All the cores recovered contain some record of turbidity current activity, and there is a general upward progression in the hole from deposition of very coarse to fine detritus. Tucholke and Houtz (this volume) have correlated this with changes in the depositional style as the area evolved from an abyssal plain to a central continental rise.

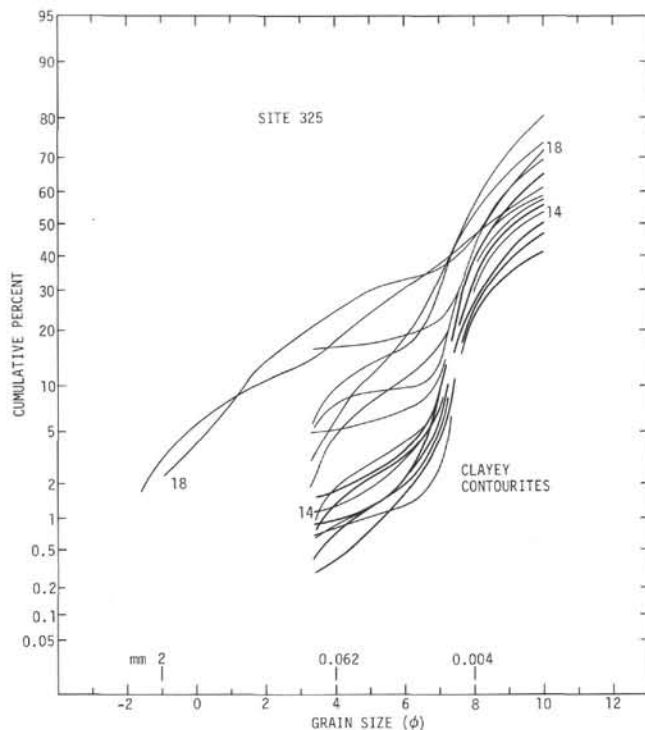


Figure 21. Cumulative curves for samples from Site 325.

Grain size analyses from this site (Figure 21) show a series of curves that may be grouped into: (1) sediment that is influenced by ice-rafting (see above), (2) sediment that may be deposited by turbidity currents (compare with Figure 16), and (3) possible clay contourite material deposited from nepheloid layers (highlighted in Figure 21). These latter curves have the sigmoid shape of probable clayey contourites at Site 324 (Figure 19), but they also have a few percent more silt and are less well sorted; thus they may reflect influences of both turbidite and contourite deposition.

One of the claystone conglomerates was sampled for detailed grain size (Sample 18, Figure 13); however, its fine median size ( $8\phi$ ) indicates destruction of clay clasts during the analysis.

A variety of depositional and postdepositional structures are well preserved in Cores 8 through 10 (Figures 22-29). Three conglomerates were observed, all in Core 10 (Figures 22 and 23). They contain angular to rounded clay clasts of a variety of colors and lithologies. Clast plasticity at the time of deposition is often indicated by deformation and interpenetrative structures; for such plastic clasts to have maintained their integrity during transportation, they must have been derived close to the depositional site. Thus they may indicate nearby slumping or may have been ripped up from the adjacent sea floor by a major flow.

Sharp, irregular basal contacts of turbidites are common, and the irregularity results both from erosion (Figures 24 and 25) and loading (Figure 23). Intervals of the Bouma sequence (Bouma, 1962) are commonly observed (Figures 23-26, 28), in some places showing almost a complete sequence.

Syn depositional and postdepositional structures are common. The fluidity of sandy silt turbidites has

resulted in flow and disruption of initially level bedding (Figure 27). Faulting of lithified sediment is also observed (Figure 28).

### SUMMARY OF BIOGENIC SEDIMENTS

Sediment recovered from the four sites is predominantly terrigenous debris with variable admixtures of diatom and radiolarian ooze. A total of less than 4 meters of calcareous sediment was recovered.

Grain-size analyses of biogenic sediment show that: (1) admixtures of siliceous organisms (diatoms, radiolarians) into claystone increase the fine silt mode of bimodal clay-silt samples (Figure 17), (2) foraminifera admixtures into Fe-rich pelagic clays create dramatic coarse modes in otherwise unimodal clayey samples (Figure 18, Sample 44), and (3) nannofossil chalk has the same textural characteristics as the fine-grained clayey contourites (Figure 21, Sample 14).

### Distribution — Siliceous Sediment

At Site 322 diatoms are common down through Core 4 (upper Miocene) and occur only rarely below that depth. Radiolaria are similarly distributed but are much less frequent. At Site 323 diatoms are common down through Core 9 (lower to middle Miocene); radiolarians are again less common but similarly distributed. Cherts appear in Cores 7-10, but become less consolidated downhole as biogenic silica decreases. At Site 324 diatoms are common only in Core 1 and occur in trace quantities to the bottom of the hole at Core 9 (Pliocene). Only traces of radiolarians occur in Cores 1 through 9. At Site 325 diatoms are common in Cores 1 through 6 (through upper Miocene) and are moderately common to the bottom of the sequence penetrated (lower Miocene in Core 10).

### Distribution — Calcareous Sediment

Only a few meters of calcareous nannofossil-rich sediment were recovered at Sites 323 and 325 (see Haq, this volume). Nannofossils were rarely observed at Site 322, but at Site 323 about 3 meters of nannoplankton chalk were recovered. This sediment contained a Danian assemblage of fragmented and partially dissolved and recrystallized coccoliths; a late Maestrichtian assemblage was identified in the oldest sediment recovered just above the basalt contact in Core 18. No calcareous material was recovered at Site 324. However, at Site 325 a few very thin layers of lower to middle Miocene nannofossil chalk were recovered from Cores 7 and 8. Preservation was fair to poor in these cores, and below this depth (622 m subbottom) nannofossils are extremely rare.

### Causes of Distribution

The primary control on the distribution of siliceous sediments is inferred to be the position of the polar front. Although diatoms occur throughout the lower Miocene to Pleistocene sediments cored at Site 325, the thin layers of nannofossil claystone recovered in Cores 7 and 8 suggest either southerly excursions of the polar front or upwelling of warmer water in the early to middle Miocene.

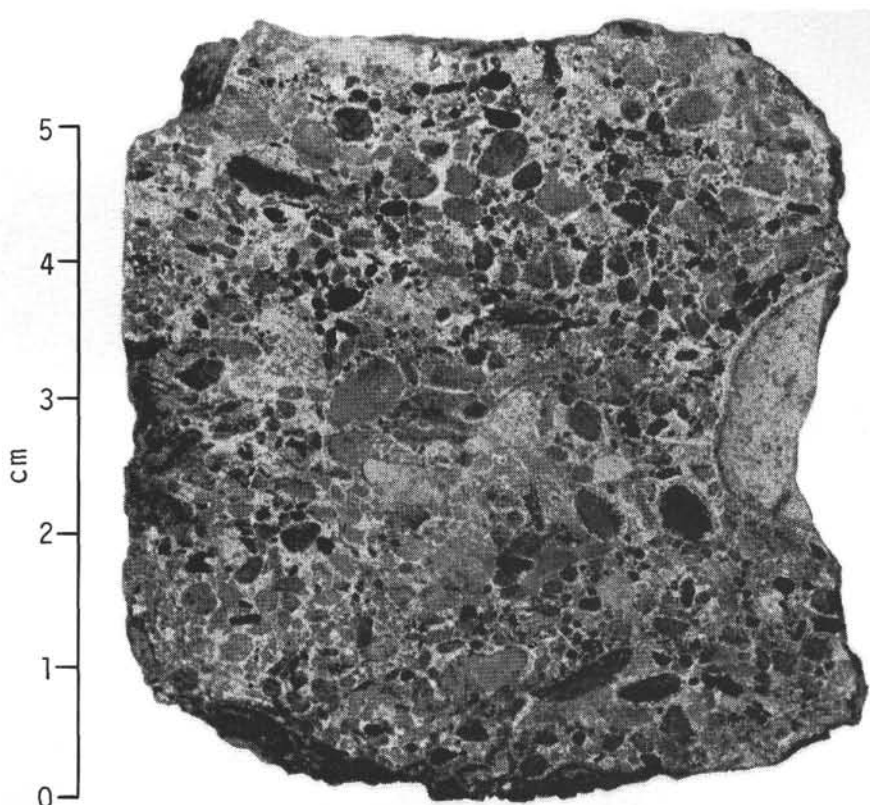


Figure 22. Clay-clast conglomerate in Sample 325-10-3, 145-151 cm.

The initial influx of diatoms in Core 4, Site 322, indicates migration of the polar front across the area in the late Miocene. The absence of calcareous nanofossils and planktonic foraminifera in the deeper sediments at Site 322 also indicates that the sea floor has been well below any fluctuations in the carbonate compensation depth (CCD) throughout the Neogene.

Fluctuations in the CCD are clearly indicated in the sediment recovered from Site 323. Both paleontologic data (Haq, this volume) and magnetic data (Herron and Tucholke, this volume) show that crust at this site originated at a spreading-ridge crest in the Maestrichtian. As the crust cooled, it subsided from a probable initial depth between 2000 and 3000 meters to its present depth of 5700 meters. A sparse nannoplankton assemblage in the upper Maestrichtian indicates deposition near the CCD, and well-preserved calcareous fossils suggest CCD depression during the Danian. Barren pelagic clays at the Cretaceous-Tertiary boundary and above the Danian sediments are thought to result from a shoaling CCD, supplementing the effect of the subsiding crust. Although the shallow CCD indicated at the Cretaceous/Tertiary boundary agrees with CCD fluctuations inferred elsewhere in the world's oceans (Hay, 1970; Worsely, 1974), the Paleocene fluctuations are nearly opposite.

The crustal plate on which the Leg 35 sites were drilled is thought to have remained in a nearly fixed position relative to Antarctica throughout the Cenozoic (Herron and Tucholke, this volume). Thus we need not consider possible horizontal movement of sedimentary facies in reconstructing paleoceanographic conditions.

#### BROWN PELAGIC CLAYSTONE FROM SITES 322 AND 323

Approximately 4 meters of ?Oligocene/early Miocene yellowish-brown (10YR 5/4) pelagic claystone were recovered just above the basalt contact in Core 11 at Site 322 (509 to 513 m subbottom). It is bedded with blebs (5-10 mm) of moderate yellowish-brown (10YR 4/2) clay that resemble burrows and fecal casts. Calcium carbonate content is nil. Grain size analysis shows approximately 65% clay-size material and 34% very fine (<10  $\mu\text{m}$ ) silt (Sample 16, Figure 15). Curiously, the X-ray mineralogy analysis indicates nearly the same quantities (75%-25%) for montmorillonite and (probably terrigenous) illite. This sediment is also enriched in iron and manganese and is depleted with respect to silica, aluminum, and titanium which suggests little terrigenous contribution. Detailed geochemical analyses of this material and the effects of diagenesis and hydrothermal alteration are presented in separate chapters (see Geochemistry Section, this volume).

Approximately 17 meters of brown, late Cretaceous-Paleocene pelagic claystone, interbedded with nanofossil claystone, were recovered between 638 and 701 meters in Units 4 and 5 at Site 323. The sediment is generally a dusky yellowish-brown (10YR 2/2) with varicolored brown burrow mottles and fecal casts. Some of the burrows are very well developed. Calcium carbonate is absent (Cameron, this volume). Like the basal clays at Site 322, these sediments are enriched in iron and manganese typical of abyssal clays. However, they differ in that zeolites become predominant near the basalt contact whereas amorphous iron-oxide de-

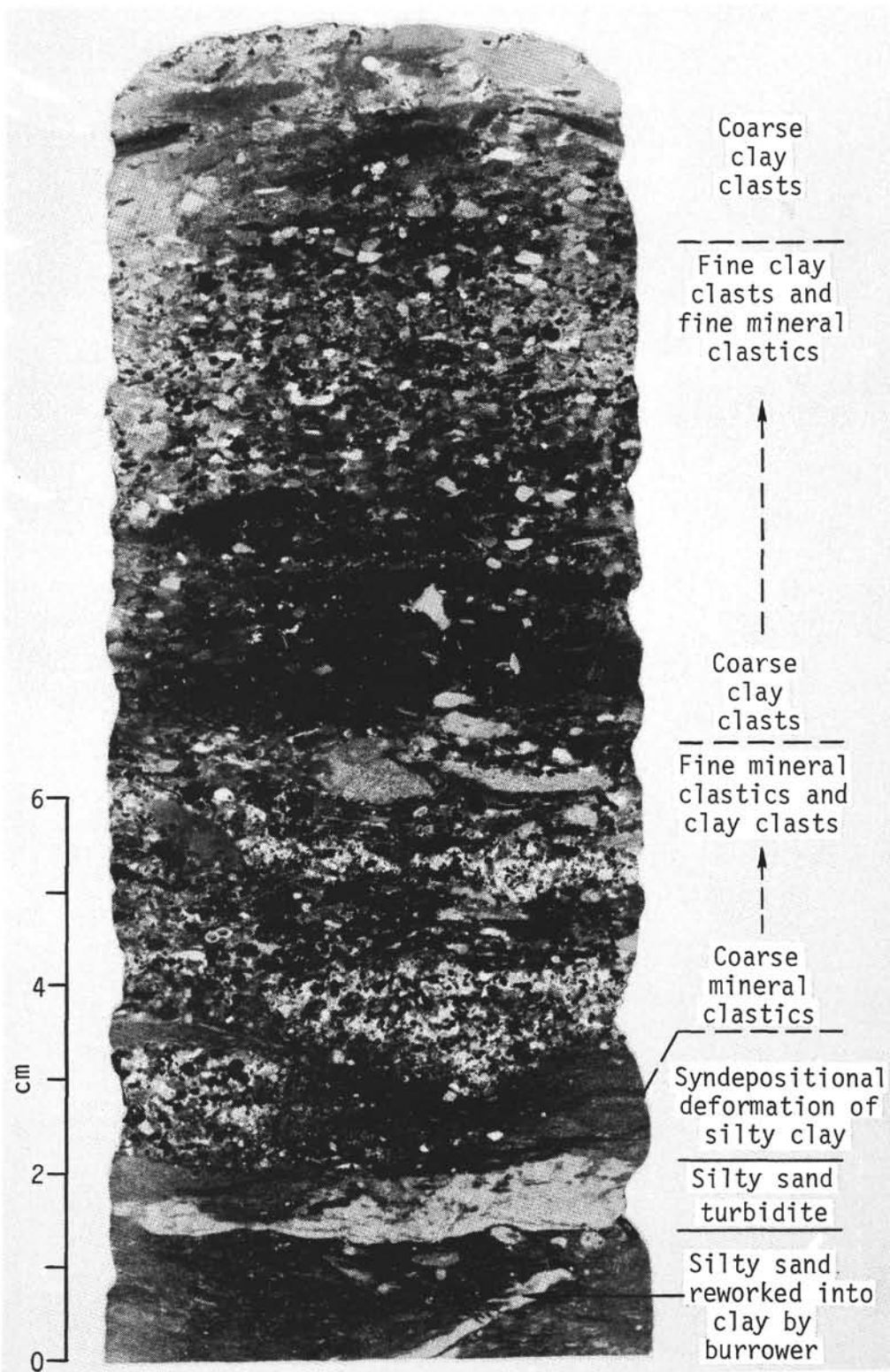


Figure 23. Clay-clast conglomerate in Sample 325-10-2, 62-76 cm. The central part of this core section may contain two hydrodynamically sorted sequences.

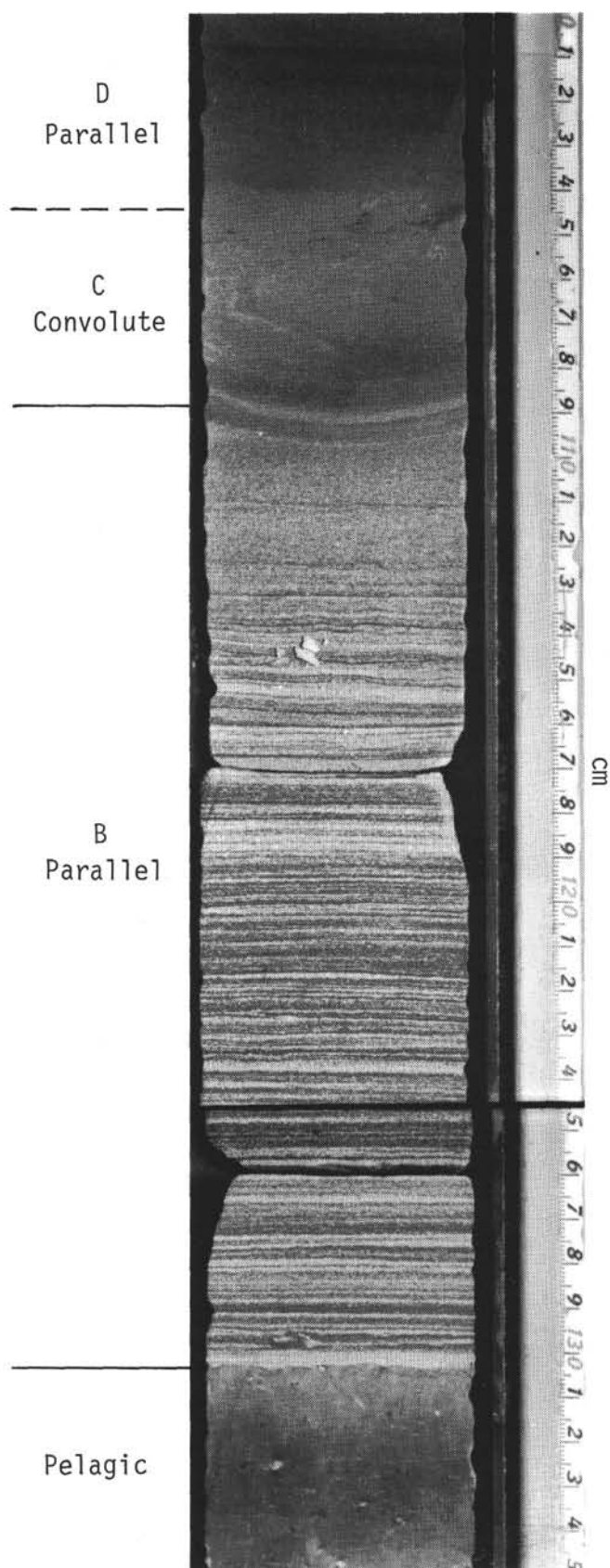


Figure 24. Turbidite on claystone in Sample 325-9-3, 100-135 cm showing intervals of the Bouma sequence.

creases. The grain size (Figure 18) is similar to Unit 4 at Site 322, with approximately 80% finer than  $6 \mu\text{m}$ . X-ray analysis shows a preponderance of montmorillonite and only traces of illite and chlorite. This claystone unit has been hydrothermally altered, and a detailed discussion of effects is given in the chapters noted above.

The Fe-Mn rich, brown claystone units at the bottom of Site 322 and especially Site 323 represent dominantly pelagic deposition of sediment in a tranquil but oxidizing environment, which was relatively free of continental debris. The units strongly resemble the Line Islands Oceanic Formation described by Cook (1972) in the equatorial Pacific Ocean. Sediments of this type, thought to be enriched in metallic oxides by precipitation from hydrothermal exhalations near spreading centers, have also been described from the East Pacific Rise by Böstrom and Peterson (1966).

### MODEL OF CIRCUM-ANTARCTIC SEDIMENTATION

#### Introduction

Circum-Antarctic deep-sea sediments offer an unparalleled opportunity to study the glacial history of Antarctica and probably the only opportunity to examine a continuous record of its climatic variations. To date, most efforts in climatic investigation have been directed toward analysis of planktonic organisms and ice-rafted debris contained in the sediment. In the latter instance, maximum ice-rafting often has been equated with maximum glaciation, but as Denton et al. (1971), Anderson (1972), and Watkins et al. (1974), among others, have pointed out, the relationship is not that simplistic. By themselves these methods can be fruitful in interpretation of Antarctic glaciation, but they make no use of a wealth of other valuable sediment data. In our study of circum-Antarctic sedimentation on Leg 35, it became increasingly obvious that an attempt should be made to consider all parameters which ultimately might affect sediment distribution. In this section we outline a preliminary model for circum-Antarctic deep-sea sedimentation which incorporates most aspects of the sedimentary record, and we evaluate it in terms of the data obtained on Leg 35. Although our core recovery and paleontological control in this instance are adequate only for qualitative comparisons, we hope that the model will provide impetus for quantitative examination of the full spectrum of sedimentological parameters in future studies.

#### The Model

Figure 30 shows schematically a model of the Antarctic margin, progressing from weakly glaciated to fully glaciated conditions. Conditions affecting sedimentation patterns are summarized below for each stage, and the relative influence of each is outlined for several sites on the deep sea floor. Site A is comparable to Sites 324 and 325 drilled on Leg 35, and Site B is similar to Sites 322 and 323. The model incorporates data on surface water productivity from El-Sayed (1970) and on probable wind and current patterns (Gordon, 1971a).

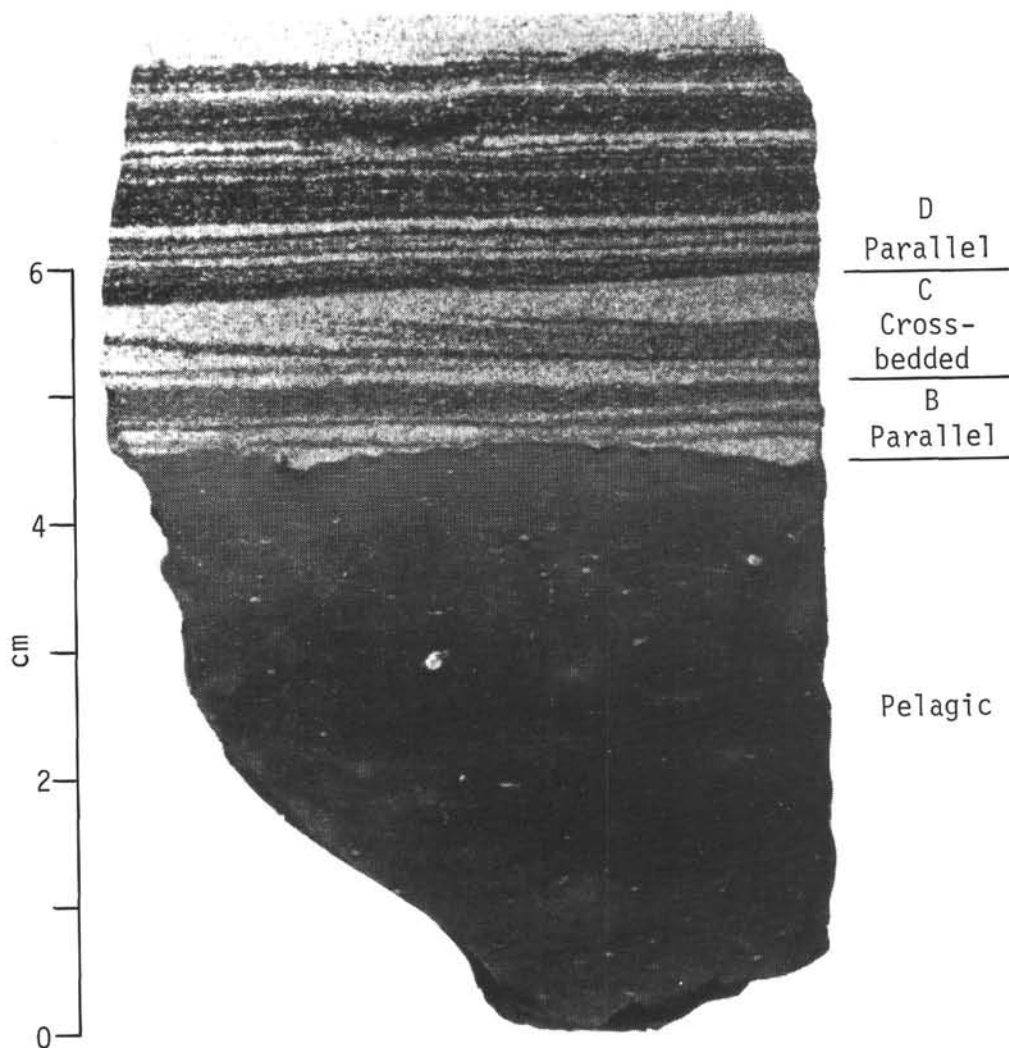


Figure 25. Turbidite on claystone in Sample 325-9-2, 65-73 cm showing intervals of the Bouma sequence.

**Stage 1: Weakly Glaciated Antarctica**

The Antarctic polar front zone is just north of Site A so that diatoms (used as an index of biogenic silica production) propagate in the surface waters, but their level of productivity is low. Slight southward excursions of the convergence result in nannoplankton production over the site and deposition of calcareous sediment. Seasonally averaged, easterly offshore winds around the Antarctic high-pressure cell cause moderate upwelling in coastal waters and consequent diatom production. Diatoms and sediment reworked from the shelf onto the slope generate minor turbidity currents. Very minor ice-rafted debris is contributed from a few bergs calving in fjords. Deep thermohaline circulation is poorly developed so that only a small amount of fine particulate matter is transported and deposited, and contourites are very rare. Minimal production of Antarctic bottom water results in a relatively deep CCD. Although diatom productivity is low, sediment derived from other sources also accumulates slowly at Site A, and diatoms thus are abundant in the sediment.

**Stage 2: Moderately Glaciated Antarctica**

The polar front moves north, and diatom productivity increases slightly in the surface water above Site A.

Productivity is much higher in the neritic environment of the continental shelf where the offshore easterly winds create intense upwelling. Cold, dense water generated near the ice reworks diatomaceous sediments from the shelf onto the slope and into the nepheloid layer over the continental rise. Debris-laden glaciers undergo extensive calving near the coastline and deposit large amounts of ice-rafted sediment around the perimeter of Antarctica. Turbidity currents are generated more frequently because of increased sediment supply to the continental slope. Increased thermohaline contrasts in the water cause stronger bottom circulation which transports and deposits fine-grained sediment. Current velocities are not high enough to erode bottom sediments, but scattered silt beds (contourites) are formed downstream from channels by contour currents depositing sediment entrained from turbidity currents. At Site A, the relative effect of these factors results in deposition of clayey sediment enriched in diatoms and ice-rafted debris.

**Stage 3: Extensively Glaciated Antarctica**

With further climatic deterioration, extensive ice shelves are formed around Antarctica. Ablation by melting at the bottom and snow accumulation at the

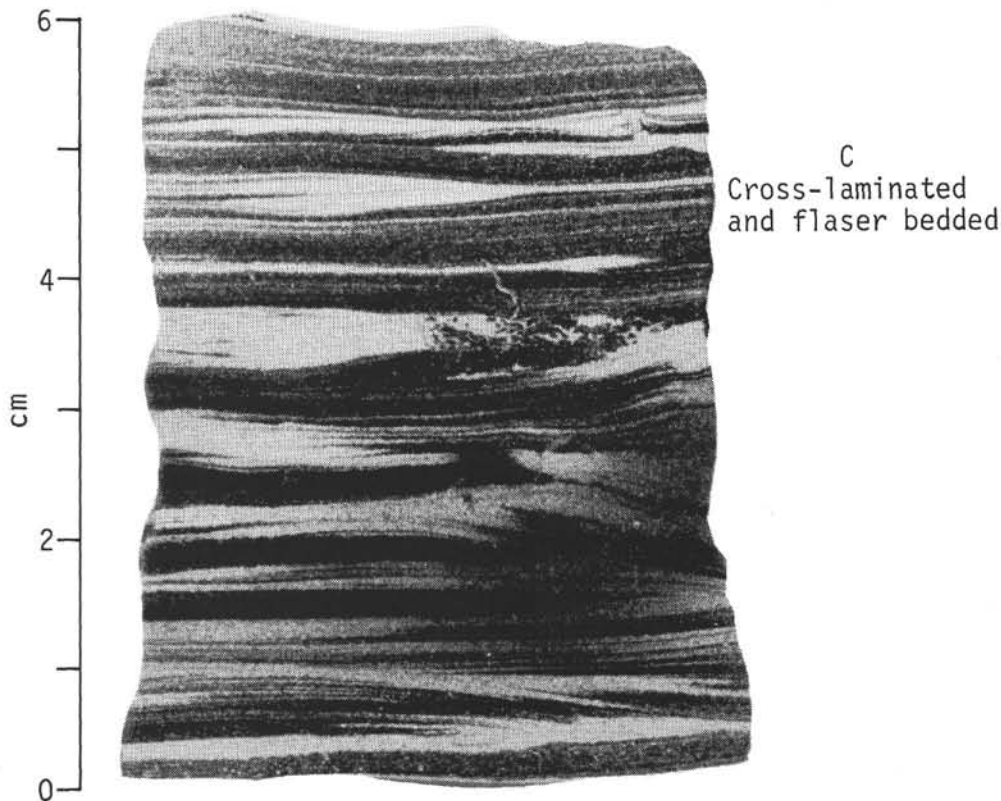


Figure 26. Turbidite section in Sample 325-9-2, 80-86 cm showing cross-bedding and flaser bedding in Bouma interval C.

top result in essentially sediment-free ice calving at the margin (Denton et al., 1971); thus there is very little ice-rafted detritus deposited in deep-water sediments. Off-shelf thermohaline circulation and turbidity current activity increase slightly, contributing more sediment to the current-maintained nepheloid layer. Although bottom circulation is more intense, it causes only local erosion, serving mainly to distribute and deposit large quantities of clay-size sediment. At Site A, surface productivity is probably increased because of more intense upwelling, but diatoms are not common in the bottom sediment because they are masked by sediment deposited from the nepheloid layer and from turbidity currents.

#### Stage 4: Fully Glaciated Antarctica

At this stage, thick grounded ice extends across most of the continental shelf, and debris-laden ice calves near the edge of the shelf. The polar front and isotherms of the cold Antarctic surface water are at their northernmost position. Thus the zone of most rapid iceberg melting (i.e., fastest deposition of ice-rafted debris) is shifted northward with respect to Stage 2. It is also skewed toward slightly warmer waters than in Stage 2 for two reasons: (a) the thicker (and possibly more sediment-laden) bergs survive longer, carrying more detritus into warm waters, and (b) provided the vertical temperature structure of the surface waters is similar to that observed today (see fig. 8 of Gordon, 1971b), the basal, sediment-bearing portion of these thick bergs would survive farther north in the cooler waters at several hundred meters depth. Arguing again on the basis of present-day water structure, the base of the

thick bergs would also begin to melt farther south with respect to the surface water isotherms than in Stage 2, because of deeper water temperatures (below the temperature minimum) warmer than the surface water. These factors tend to smear out the zone of most rapid deposition of ice-rafted debris.

Grounded ice on the continental shelf has a dramatic effect on other aspects of deep basin sedimentation. Unconsolidated sediment deposited at earlier stages is bulldozed off the shelf, generating massive turbidity currents which inundate the deep basin. At Site A, deposition of turbidites masks most sediment deposited from floating ice, bottom currents, and surface phytoplankton production. Ice erosion on the shelf creates U-shaped valleys and truncates dipping beds (see Tucholke and Houtz, this volume).

Bottom currents are strongly developed, eroding sediment in many areas and only locally depositing clay-sized detritus. Coarse sediment pirated from frequent turbidity currents by contour-following currents is deposited as well-sorted silt and sand beds, while the fine fraction remains in suspension except in areas of slack water. Local erosion of silty and sandy sediment creates placer deposits of coarse detritus.

#### Discussion

Two important conclusions can be drawn from the model when we compare the sedimentary record at several places on the sea floor (Sites A, B, and C; Figure 30).

First, it is apparent that the *rate* of production of a textural or compositional parameter at a given location on the sea floor need not vary linearly with intensity of

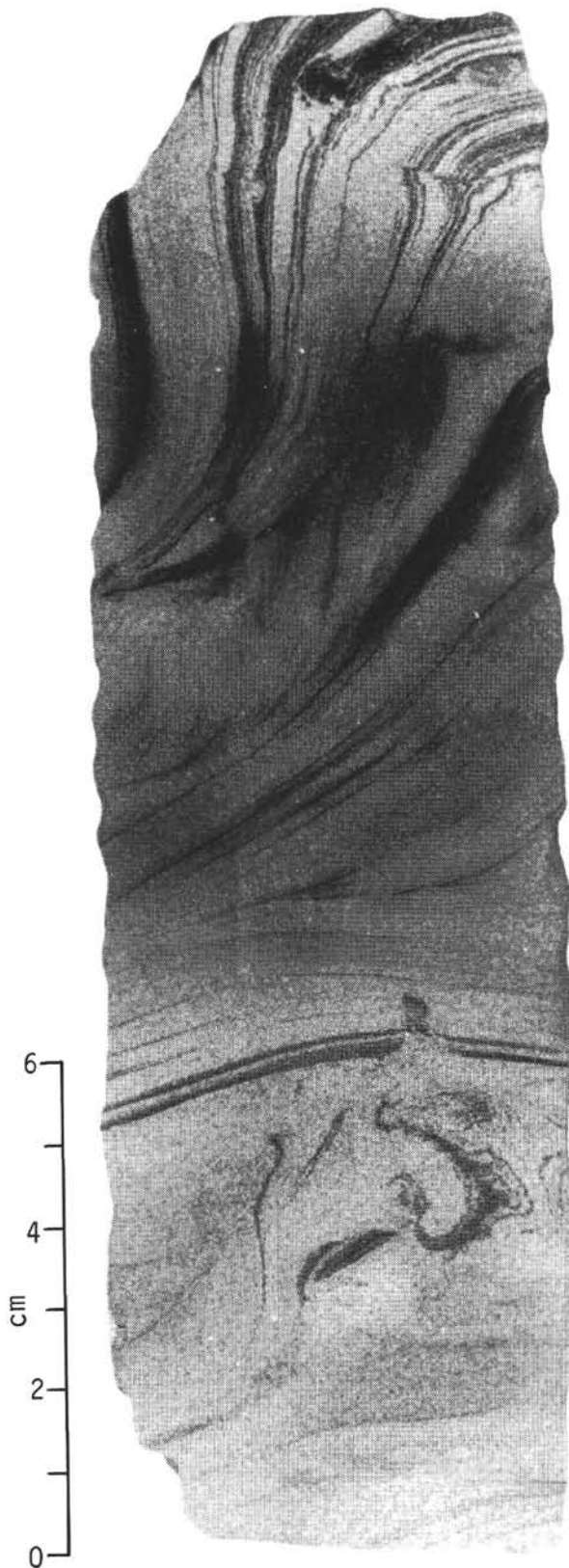


Figure 27. Turbidite in Sample 325-9-2, 1-20 cm with syndepositional deformation of silt beds.

glaciation, and when the effect of other processes is considered, its *relative* abundance in the sediment almost certainly will appear to be independent of inten-

sity of glaciation. For example, while diatom production may increase regularly in surface waters, the increase is masked in the sediment wherever terrigenous detritus can reach the site. In another instance, although the intensity of bottom circulation is modeled to vary directly with increasing glaciation, its manifestation in the sediments (clay contourites, silt beds, etc.) does not. The manifestation is affected by other source mechanisms which contribute sediment to the flow, as well as by the flow itself, which creates different textural and compositional changes at varying threshold velocities. The rates of production of other components (ice-rafted debris, turbidites) do not vary directly with intensity of glaciation, nor does their relative abundance in the sediment.

Secondly, at any given chronostratigraphic level, there is strong lateral variation in the sedimentary record, and it is dependent upon latitude and distance from Antarctica (not necessarily one and the same). Although this conclusion is obvious, the actual magnitudes of the variations are less clear, except perhaps for turbidites which generally decrease in importance with distance from the source area. In the cases of ice-rafted debris, diatom productivity, and bottom-current circulation, all are dependent on the thermohaline characteristics of circum-Antarctic waters, and, in the instance of ice-rafted debris, on the mass and sediment load of icebergs as well; consequently, their effects can only be estimated in a general way.

The variations in time and space described above combine to provide a complex sedimentary record which, as a first approximation, can be studied by evaluating relative contributions of the various textural and compositional parameters. When good age control is available, the study can be refined to determine rates on the parameters.

The model described is no panacea, but it does serve to show general sedimentary relationships. Complexities superimposed by local variations in thermohaline characteristics, productivity, and bottom topography are averaged out in the model but several complexities and qualifications should be pointed out.

It is apparent that we cannot equate intensity of ice-rafting with intensity of glaciation. Intense ice-rafting will be observed far north of Antarctica when it is fully glaciated (Stage 4), but also in a proximal band around the continent when it is only moderately glaciated (Stage 2; Weaver, 1973; Watkins et al., 1974). Furthermore, if the peak glaciation in a cycle reaches only advanced shelf-ice conditions (Stage 3), intense ice-rafting would not be observed at any latitude unless the ice was dry based (i.e., freezing) and the debris ice-rafted beyond the shelf (Anderson, 1972). Unfortunately, we cannot as yet predict the state of the Antarctic ice sheet merely by the surface-water temperature in the paleo-Antarctic Ocean; it is unlikely that there is a one-to-one relationship. We envision modern ice conditions in Antarctica as intermediate between Stages 2 and 3. Thus, even though Antarctica is extensively glaciated, there is very little ice-rafting of sediment at present (Warnke, 1970).

The uncertainty in the relationship between the thermohaline structure of the ocean and ice-sheet conditions presents additional problems. Although we have

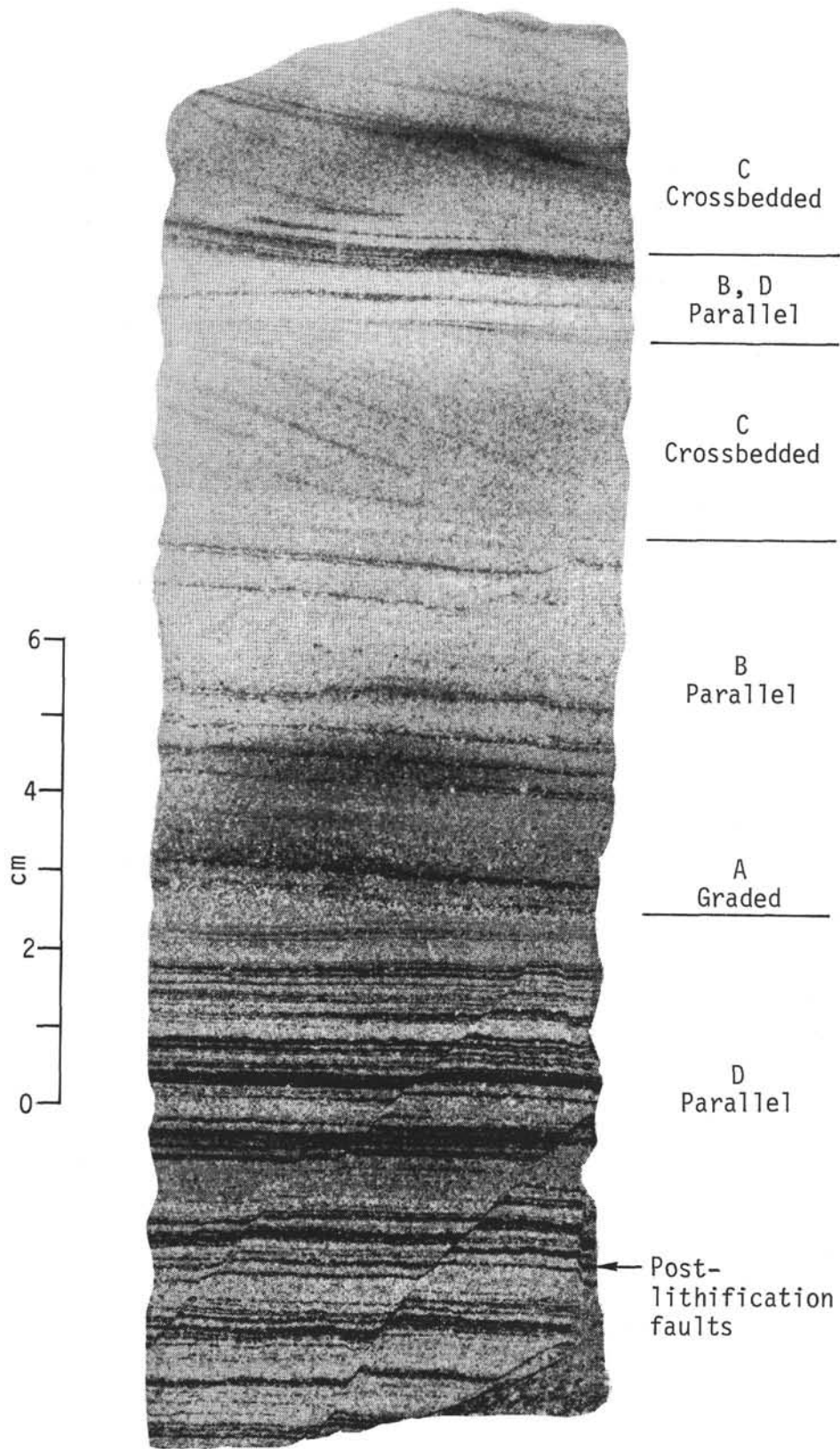


Figure 28. Turbidite in Sample 325-9-2, 24-42 cm.

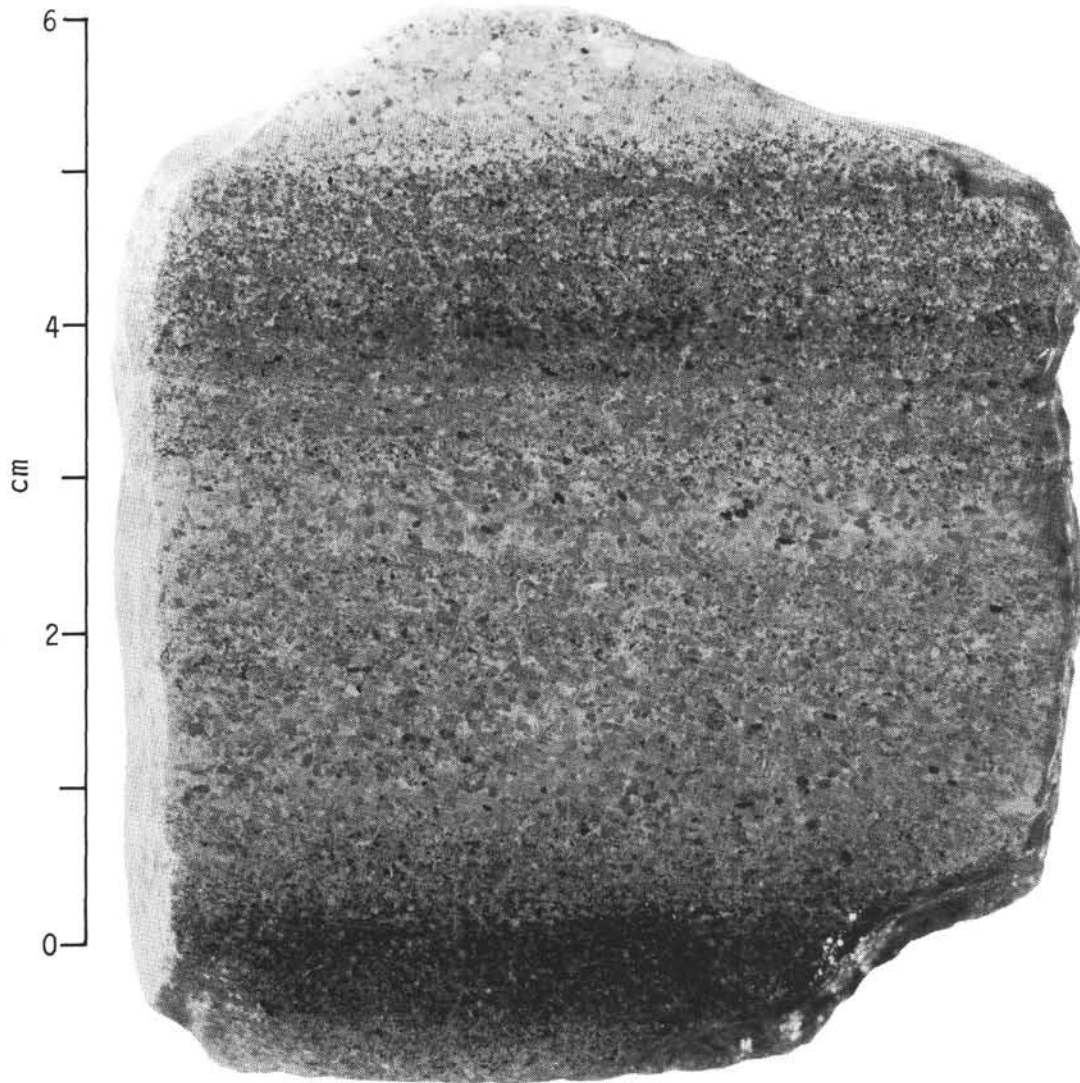


Figure 29. *Calcite-cemented sandstone from Sample 325-10, CC.*

assumed a linear relationship between intensity of bottom currents and intensity of climatic deterioration in Antarctica, the fine-scale picture may be much more complex, and the circulation of the surface waters, which affects the productivity of planktonic organisms, also may vary from a direct relationship. Variations in the level of the CCD, which probably are closely related to the extent of Antarctic Bottom Water production, are undoubtedly very complex during a glacial cycle. AABW is produced by (1) formation of sea ice during winter months, (2) freezing of seawater to, or melting from, the bottom of large ice shelves, and (3) intense cooling and evaporation of the surface water by katabatic winds (Gordon, 1971c). Thus, both the mass and the thermohaline characteristics of AABW produced at various times in a glacial cycle may be highly variable. For this reason, we have incorporated very few inferences about CCD fluctuations in our model.

The model predicts sedimentary environments through the first half of a glacial cycle, but we can expect asymmetrical distribution of several parameters

over a full cycle. For example, turbidity currents will be more important during Stage 3 deglaciation than during Stage 3 glaciation, because of the large volume of sediment deposited on the continental slope during peak glaciation. Furthermore, deep-sea sedimentation, particularly the distribution of ice-rafted debris, within a glacial cycle and during subsequent cycles will be affected by the intensity of erosion of continental source rock.

#### Comparison of Leg 35 Drilling Results with Model

It is not possible to make any kind of complete interpretation of Antarctic glacial history on the 180 meters (8.5% of sequence drilled) of sediment recovered on Leg 35. However, several basic trends seem to be defined, and they can be used as an initial test of the model described.

#### Paleocene to Oligocene

Sediments of this age were recovered at Site 323 and possibly Site 322 (Figure 2); they consist predom-

inantly of pelagic claystones with rare diatoms and sporadic occurrences of nannoplankton. At Site 323, their rate of accumulation probably decreased with time as the sea floor subsided below the range of CCD fluctuations and moved away from volcanogenic sources near the ridge crest. The absence of terrigenous detritus suggests that deep circumpolar flow was not established until the latest Oligocene or early Miocene, although shallow circumpolar flow may have existed earlier. Cool-water species of nannoplankton flourished in the surface water (Bukry, this volume), but most nannos were severely corroded or dissolved before reaching the sea floor.

### Miocene

Bottom currents probably became active near the beginning of the Miocene, presumably because the Scotia Arc was breached to deep circumpolar flow and/or because thermohaline contrasts in the deep water increased as climate deteriorated in Antarctica. During their development, these currents may have eroded many tens of meters of soft Paleocene to Oligocene pelagic clay in the Bellingshausen basin. Current-transported terrigenous detritus was subsequently deposited at Sites 322 and 323, but current activity was mostly masked by deposition from turbidity currents, especially at Site 325. Significant quantities of siliceous organisms appear in the oldest sediments corer at Site 325 (lower Miocene), but they fluctuate in abundance, and interspersed nannoplankton were recovered locally into the upper lower Miocene.

Depositional conditions in the earliest Miocene are interpreted to correspond to late Stage 1 in the model; however, deposition at Site 325 (Site A) is dominated by turbidites. Farther north, Sites 322 and 323 are similar to Stage 1, Site B, in that they contain rare diatoms, no detectable ice-rafted debris, and clays which may be current deposited. Nannoplankton are very rare and were apparently dissolved before reaching the sea floor because of the shoaling CCD. Fine distal turbidites are present at Site 323, but extensive turbidity currents at Site 322 are suggested by massive sandstones. The frequent turbidites at the two eastern drill sites (Sites 322 and 325) appear to be related to early Miocene tectonism along the eastern sector of the continental margin (Tucholke and Houtz, this volume).

Northward migration of the polar front is suggested by the appearance of common diatoms in the lower Miocene at Site 323 (63°41'S) and in the lower upper Miocene at Site 322 (60°01'S). Fluctuations in this general northward migration are suggested by the interspersed diatoms and nannoplankton at Site 325, but unfortunately our core control is inadequate to define the variations. The fact that the nannoplankton are a cold-water assemblage (Haq, this volume) also suggests an alternate explanation that the productivity is due to local upwelling of warmer, carbonate-rich subsurface water (see Anderson, 1972). Similar interbedded nannoplankton and diatomaceous sediments were found off East Antarctica on Leg 28 in the Miocene to lowermost Pliocene (Site 266), upper lower Miocene (Site 268), and middle Miocene (Site 269) (Hayes, Frakes, et al., 1975).

Stage 2 conditions appear to have been reached by middle Miocene time. Ice-rafted debris is found in lower to middle Miocene sediments at Site 325, and in middle Miocene sediments at Site 323, but only uppermost Miocene ice-rafting was detected farther north at Site 322. By this time, the tectonic activity along the eastern continental margin appears to have decreased because only fine-grained turbidites are found at Sites 322 and 325. Silt beds indicative of current activity are not observed at Sites 322, 323, and 325, but much of the abundant clay-sized sediment present may have been deposited from abyssal currents.

The transition through Stage 3 may have occurred in the latter part of the middle Miocene and into the late Miocene, but the interpretation is ambiguous. Middle Miocene sediments (? Cores 4, 5, 6) are well represented only at Site 323. They show an absence of ice-rafting (Table 3) and common claystones interrupted by some turbidites in the latter part of the middle Miocene (compare with Stage 3, Site B, in Figure 30).

The best evidence for a fully glaciated Antarctica (Stage 4) is found in uppermost Miocene and lower Pliocene sediments, which contain varying amounts of ice-rafted debris and accumulated at rapid rates of about 6 to 20 cm/1000 yr (Figures 4, 6, 10). Although sediment deposited from turbidity and bottom currents dominates in this interval, a substantial quantity of diatoms is also present (Figure 2). Diatom productivity must have been extremely high, probably because of increased upwelling in the region of the Antarctic divergence, for diatoms not to be overwhelmed in the sedimentary record as predicted by the model (Figure 30b, Stage 4).

The latest Miocene to early Pliocene glacial maximum suggested by the sedimentary record agrees closely with independent evidence from DSDP Leg 28 drilling results (Hayes, Frakes, et al., 1975) and with interpretations of profiler data from the West Antarctic continental shelf and rise (Tucholke and Houtz, this volume).

### Pliocene—Pleistocene

The Pliocene and Pleistocene sedimentary record is best represented by cores from Sites 324 and 325. Site 324 appears to be on a channel levee and in a position comparable to Site A in Figure 30a. Comparison of Figures 11 and 30b shows a marked correlation between the Plio-Pleistocene sediments and Stages 2 and 3 of the model. In Cores 1 and 9, ice-rafted sediments are common, silt beds are infrequent or absent, and diatoms show their greatest abundance (oozes in Core 1; <2% in Core 9). The model would suggest Stage 2 glacial conditions for these cores.

Stage 3 conditions of extensive shelf ice are indicated throughout most of Cores 2 through 8. In these sediments, silt beds and clay (current deposited) are abundant, and ice-rafted debris and diatoms are virtually absent. Although the model predicts extensive dilution of diatoms by deposition from bottom currents, the virtual absence of diatoms is suspicious. It may well be that diatom productivity, rather than being moderately high as postulated, is quite low because of permanent sea-ice cover.

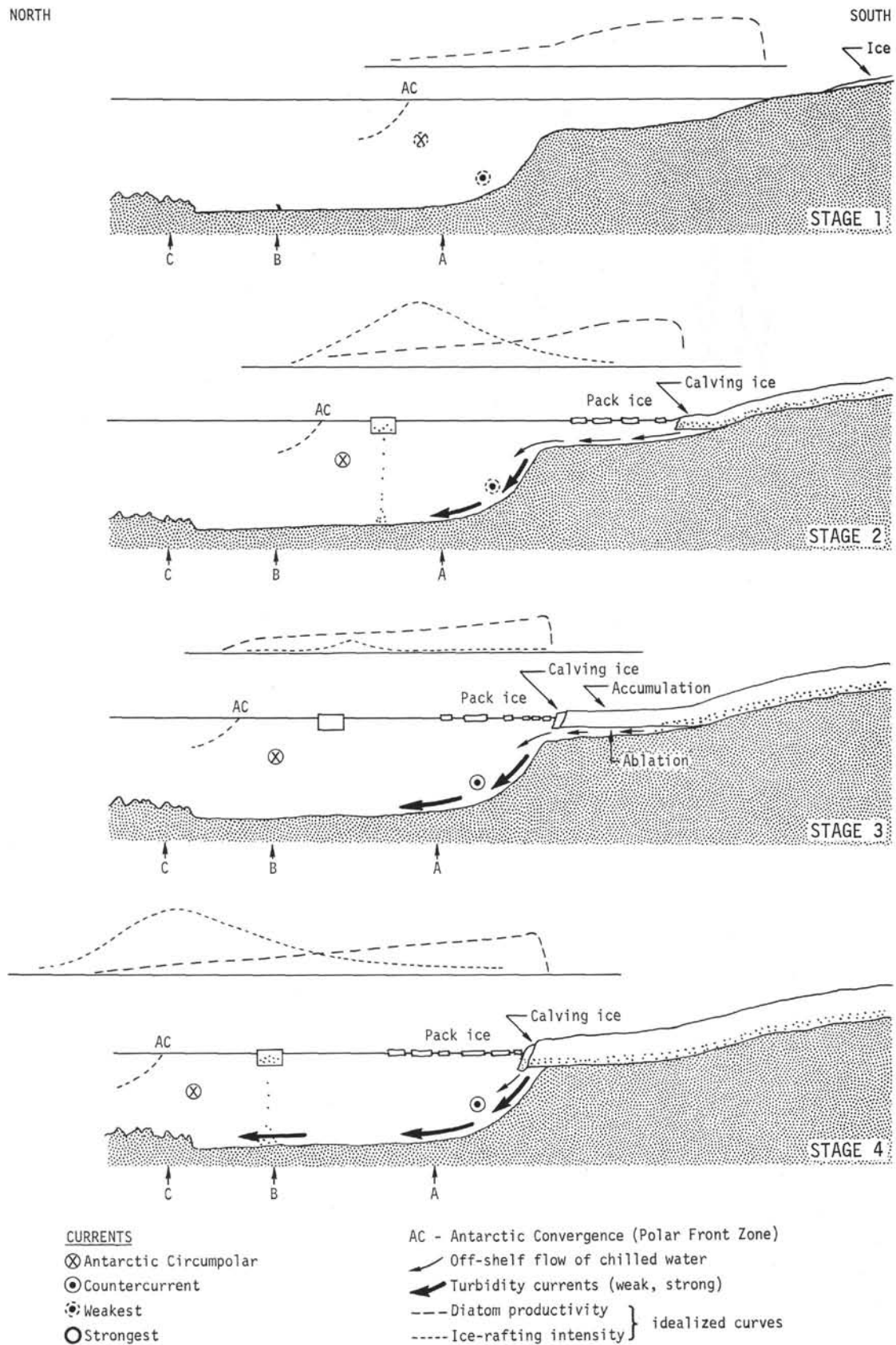


Figure 30a. Schematic representation of the Antarctic margin during the first half of a glacial cycle.

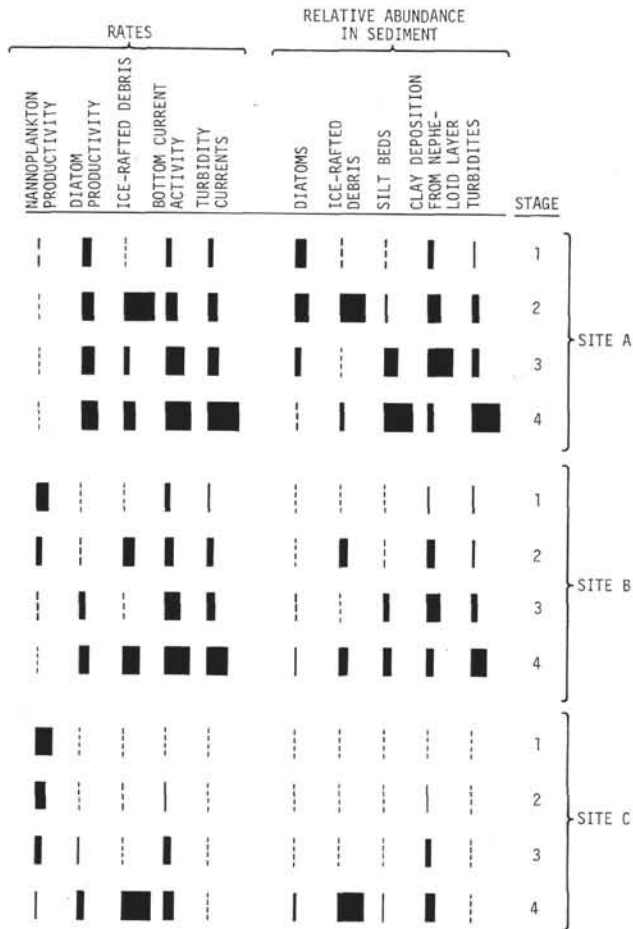


Figure 30b. *Qualitative estimates of parameters affecting sedimentary record at Site A, B and C during glacial stages shown in (a).*

If our assumption is correct that the frequency of silt beds is directly related to intensity of bottom circulation and frequency of turbidity currents, then the distribution of silt beds in the cores (Figure 11) shows variations in intensity of bottom circulation. If we equate intensity of circulation directly to extent of the ice-sheet, then we might suspect that the short influxes of ice-rafted debris in Cores 2, 3, and 5 represent brief intervals of Stage 4 grounded ice. However, the clayey sediments at these levels do not contain diatoms which would certainly be reworked off the shelf by ice. An alternate explanation is that during Stage 4 and the latter part of Stage 3, thermohaline contrasts in the water over the continental slope and upper rise are actually weaker than in less glaciated conditions, so that the most intense bottom circulation (i.e., best developed silt layers) occurs early in Stage 3. The short intervals of ice-rafting could then represent brief periods of ice-shelf deterioration and ice-rafting during Stage 2. In either case it is probable that strict one-to-one relationships do not exist between intensity of glaciation, intensity of circulation, and silt bed frequency.

Site 325, located a distance from Antarctica similar to Site 324, presently lies in an area of braided turbidite

channels, and it probably has done so during most of its depositional history. Thus the Plio-Pleistocene record there is dominated by turbidites, and most of the silt and sand layers are poorly sorted and unaffected by currents. However, as at Site 324, there is a general inverse relationship between the frequency of silt beds (turbidites) and intensity of ice-rafting, again suggesting fluctuation between Stages 2 and 3.

The two Pliocene cores from Site 322 and from Site 323 contain minor ice-rafted sand (Table 3). These conditions again represent fluctuations between moderately glaciated (Stage 2) and extensively glaciated conditions (Stage 3) on Antarctica.

The limited paleontologic control makes it impossible to refine the chronology of glacial fluctuations in the Plio-Pleistocene sediments. Until further deep-sea drilling can be undertaken in Antarctic waters, the late Tertiary and Quaternary fluctuations in the Antarctic ice sheet will best be studied in latitudinal transects of long piston cores along the deep-water continental margin. We hope that these studies will include interpretation of the full spectrum of depositional processes which are critical to a complete understanding of Antarctic glacial history.

#### REFERENCES

- Adie, R.J., 1954. The petrology of Graham Land, 1. The basement complex: early Paleozoic plutonic and volcanic rocks: Falkland Islands Dependencies Surv. Sci. Rept., No. 11, p. 1-22.
- , 1955. The petrology of Graham Land, 2. The Andean granite-gabbro intrusive suite: Falkland Islands Dependencies Surv. Sci. Rept., no. 12, p. 1-39.
- , 1957. The petrology of Graham Land; metamorphic rocks of the Trinity Peninsula series: Falkland Islands Dependencies Surv. Sci. Rept., no. 20, p. 1-26.
- , 1969a. Geology of the northern Antarctic Peninsula: Antarctic Map Folio Series 12, pl. 1, Am. Geogr. Soc.
- , 1969b. Geology of the Southern Antarctic Peninsula: Antarctic Map Folio Series 12, pl. 2, Am. Geogr. Soc.
- Anderson, J.B., 1972. Nearshore glacial-marine deposition from modern sediments of the Weddell Sea: *Nature Phys. Sci.*, v. 240, p. 189-192.
- Baker, P.E. and McReath, I., 1971. 1970 Volcanic eruption at Deception Island: *Nature*, v. 231, p. 5-9.
- Bell, C.M., 1973. The Geology of southern Alexander Island: *British Antarctic Surv. Bull.*, no. 33, p. 1-16.
- Berggren, W.A., 1973. A Cenozoic time scale: some implications for regional geology and paleobiogeography: *Lethaia*, v. 5, p. 195-215.
- Biscaye, P.E. and Eitrem, S.L., 1974. Temporal variations in benthic boundary layer phenomena: nepheloid layer, North American Basin. In Gibbs, R. (Ed.), *Suspended solids in water*: New York (Plenum Press), p. 227-260.
- Böstrom, K. and Peterson, M.N.A., 1966. Precipitates from hydrothermal exhalations on the East Pacific Rise: *Econ. Geol.*, v. 61, p. 1258.
- Bouma, A.H., 1962. *Sedimentology of some flysch deposits*: Amsterdam (Elsevier).
- Brown, J.E., 1973. Depositional histories of sand grains from surface textures: *Nature*, v. 242, p. 396-398.
- Chen, P.-H., 1975. Antarctic Radiolaria. In Hayes, D.E., Frakes, L.A., et al., *Initial Reports of the Deep Sea Drill-*

- ing Project, Volume 28: Washington (U.S. Government Printing Office), p. 437-514.
- Cook, H.E., 1972. Stratigraphy and sedimentation. *In* Hays, J.D., et al., Initial Reports of the Deep Sea Drilling Project, Volume 9: Washington (U.S. Government Printing Office), p. 933-943.
- Craddock, C. and Hubbard, H., 1961. Preliminary geologic reports on the 1960 U.S. Expedition to Bellingshausen Sea, Antarctica: *Science*, v. 133, p. 886-887.
- Craddock, C., Gast, P., Hanson, G., and Linder, H., 1964. Rubidium-strontium ages from Antarctica: *Geol. Soc. Am. Bull.*, v. 75, p. 237-240.
- Dalziel, I.W.D. and Elliot, D.H., 1973. The Scotia Arc and Antarctic Margin. *In* Nairn, A.E.M. and Stehli, F.G. (Eds.), *The ocean basins and margins*, vol 1: New York (Plenum Pub. Corp.), Ch. 5, p. 171-246.
- Denton, G.H., Armstrong, R.L., and Stuiver, M., 1971. The late Cenozoic glacial history of Antarctica. *In* Turekian, K.K. (Ed.), *The late Cenozoic glacial ages*: New Haven (Yale University Press), p. 267-306.
- Drake, A., 1962. Preliminary geologic report on the 1961 U.S. Expedition to Bellingshausen Sea, Antarctica: *Science*, v. 135, p. 671-672.
- Drake, A., Marvin, R., Stern, T., and Hubbard, H., 1971. The landfall peak adamellite and regional comparison of petrochemical and age data from the Thurston Island-Eights Coast Area, West Antarctica: U.S. Geol. Surv. Prof. Paper 750B, p. B62-B73.
- Elliot, D.H., 1965. Geology of northwest Trinity Peninsula, Graham Land: *British Antarctic Surv. Bull.*, no. 7, p. 1-24.
- El-Sayed, S.Z., 1970. On the productivity of the Southern Ocean. *In* Holdgate, M.W. (Ed.), *Antarctic ecology*, v. 1: New York (Academic Press), p. 119-135.
- Ewing, M., Houtz, R., and Ewing, J., 1969. South Pacific sediment distribution: *J. Geophys. Res.*, v. 74, p. 2477-2493.
- Frakes, L.A., 1971. USNS *Eltanin* core descriptions, cruises 32 to 45 (unpublished report): Antarctic Core Facility, Department of Geology, Florida State University.
- Goodell, H.G. and Watkins, N.D., 1968. The paleomagnetic stratigraphy of the Southern Ocean: 20° west to 160° east longitude: *Deep-Sea Res.*, v. 15, p. 89-112.
- Goodell, H.G., Watkins, N.D., Mather, T., and Koster, S., 1968. The Antarctic glacial history recorded in sediments of the Southern Ocean: *Paleogeog., Paleoclim., Paleocol.*, v. 5, p. 41-62.
- Gordon, A., 1966. Potential temperature, oxygen and circulation of bottom water in the Southern Ocean: *Deep-Sea Res.*, v. 13, p. 1125-1138.
- \_\_\_\_\_, 1971a. Antarctic polar front zone. *In* Reid, J.L. (Ed.), *Antarctic Oceanology I*, Antarctic Res. Series, v. 15: Washington (Am. Geophys. Union), p. 205-221.
- \_\_\_\_\_, 1971b. Oceanography of Antarctic waters. *In* Reid, J.L. (Ed.), *Antarctic Oceanology I*, Antarctic Res. Series, v. 15: Washington (Am. Geophys. Union), p. 169-203.
- \_\_\_\_\_, 1971c. Recent physical oceanographic studies of Antarctic waters. *In* Quam, L. (Ed.), *Research in the Antarctic*: Washington (Am. Assoc. for the Advancement of Sci.), p. 609-629.
- Hay, W.W., 1970. Calcium carbonate compensation. *In* Bader, R.G., et al., Initial Reports of the Deep Sea Drilling Project, Volume 4: Washington (U.S. Government Printing Office), p. 672.
- Hayes, D.E., Frakes, L., et al., 1975. Initial Reports of the Deep Sea Drilling Project, Volume 28: Washington (U.S. Government Printing Office).
- Hays, J.D. and Opdyke N.D., 1967. Antarctic Radiolaria, magnetic reversals, and climatic change: *Science*, v. 158, p. 1001.
- Heezen, B.C., Tharp, M., and Hollister, C.D., 1968. Illustrations of the marine geology of the Southern Ocean. *Symp. on Antarctic Oceanography*, Santiago 1966: Cambridge (Scott Polar Res. Inst.), p. 101-109.
- Hollister, C.D. and Heezen, B.C., 1964. Modern graywacke type sands: *Science*, v. 146, p. 1573-1574.
- \_\_\_\_\_, 1967. The floor of the Bellingshausen Sea. *In* Hersey, J.B. (Ed.), *Deep-sea photography*: Baltimore (Johns Hopkins Press), p. 177-189.
- \_\_\_\_\_, 1972. Geologic effects of ocean bottom currents. *In* Gordon, A.L. (Ed.), *Studies in physical oceanography*, v. 12: New York (Gordon & Breach), p. 37-66.
- Horne, R.R., 1968. Authigenic prehnite, laumontite and chlorite in the lower Cretaceous sediments of southeastern Alexander Island: *British Antarctic Surv. Bull.*, no. 18, p. 1-10.
- \_\_\_\_\_, 1969. Morphology, petrology, and provenance of pebbles from lower Cretaceous conglomerates of southeastern Alexander Island: *British Antarctic Surv. Bull.*, no. 21., p. 51-60.
- Jacobs, S.S., Bruchhausen, P.M., Rosselot, F.L., Gordon, A.L., Amos, A.F., and Belliard, M., 1972. *Eltanin* reports: Cruises 37-39, 1969; 42-46, 1970; Lamont-Doherty Geological Observatory Tech. Rept. 1-CU-1-72.
- Johnson, D.A., 1972. Ocean-floor erosion in the Equatorial Pacific: *Geol. Soc. Am. Bull.*, v. 83, p. 3121-3144.
- Kennett, J.P., Houtz, R.E., Andrews, P.B., Edwards, A.R., Gostin, V.A., Hajos, M., Hampton, M.A., Jenkins, D.G., Margolis, S.V., Ovenshine, A.T., and Perch-Nielsen, K., 1974. Development of the Circum-Antarctic current: *Science*, v. 186, p. 144-147.
- Lancelot, Y., 1973. Chert and silica diagenesis in sediments from the Central Pacific. *In* Winterer, E.L., Ewing, J.I., et al., Initial Reports of the Deep Sea Drilling Project, Volume 17: Washington (U.S. Government Printing Office), p. 377-405.
- Laudon, T.S., Lackey, L.L., Quilty, P.G., and Otway, P.M., 1969. Geology of eastern Ellsworth Land: Antarctic Map Folio Series 12, pl. 3, Am. Geogr. Soc.
- Margolis, S.V., 1975. Paleoglacial history of Antarctica inferred from Analysis of Leg 29 sediments by scanning-electron microscopy. *In* Kennett, J.P., Houtz, R.E., et al., Initial Reports of the Deep Sea Drilling Project, Volume 29: Washington (U.S. Government Printing Office), p. 1039-1048.
- Margolis, S.V. and Kennett, J.P., 1970. Antarctic glaciation during the Tertiary recorded in sub-Antarctic deep-sea cores: *Science*, v. 170, p. 1085-1087.
- \_\_\_\_\_, 1971. Cenozoic paleoglacial history of Antarctica recorded in Subantarctic deep-sea cores: *Am. J. Sci.*, v. 271, p. 1-36.
- Passel, C., 1945. Sedimentary rocks of the Southern Edsel Ford Ranges, Marie Byrd Land, Antarctica: *Am. Phil. Soc. Proc.*, v. 89, p. 123-131.
- Piper, D.J.W. and Brisco, C.D., 1975. Deep-water continental margin sedimentation, DSDP Leg 28, Antarctica. *In* Hayes, D.E., Frakes, L., et al., Initial Reports of the Deep Sea Drilling Project, Volume 28: Washington (U.S. Government Printing Office), p. 727-755.
- Reid, J.L. and Nowlin, W.D., 1971. Transport of water through the Drake Passage: *Deep-Sea Res.*, v. 18, p. 51-64.
- Rowley, P. and Williams, P., 1974. Plutonic rocks of the Lassiter Coast area: *Antarctic J. U.S.*, v. 9, p. 225-226.
- Setlow, L.W. and Karpovich, R.P., 1972. "Glacial" microtextures on quartz and heavy mineral sand grains from the littoral environment: *J. Sediment Petrol.*, v. 42, p. 864-875.

- Warner, W., 1945. Structure and petrography of the southern Edsel Ford Ranges, Antarctica: *Am. Phil. Soc. Proc.*, v. 89, p. 78-122.
- Warnke, D.A., 1970. Glacial erosion, ice rafting, and glacial-marine sediments: Antarctica and the Southern Ocean: *Am. J. Sci.*, v. 269, p. 276-294.
- Watkins, N.D., Keany, J., Ledbetter, M.T., and Huang, T., 1974. Antarctic glacial history from analyses of ice-rafted deposits in marine sediments: new model and initial tests: *Science*, v. 186, p. 533-536.
- Weaver, F.M., 1973. Pliocene paleoclimatic and paleoglacial history of East Antarctica recorded in deep-sea piston cores; *Sedimentological Res. Lab. Florida State University, Contrib.* 36.
- Williams, P., Schneider, D., Plummer, C., and Brown, L., 1972. Geology of the Lassiter Coast Area, Antarctic Peninsula: Preliminary Report. In Adie, R.J. (Ed.), *Antarctic geology and geophysics*: Oslo (Universitetsforlaget), p. 143-148.
- Worsley, T., 1974. The Cretaceous-Tertiary boundary event in the ocean. In Hay, W.W. (Ed.), *Studies in paleo-oceanography*, SEPM Spec. Publ. no. 20, p. 94-175.

#### APPENDIX I PETROGRAPHIC DESCRIPTIONS OF ICE-RAFTED PEBBLES

##### 35-324-1-2, 32 Biotite Quartz Diorite

This sample is only approximately 1 cm in diameter, a seriate-textured rock with a color index less than five. Quartz shows strong undulose extinction and a few of the grains appear to have been granulated. Plagioclase (andesine?) occurs in subhedral to anhedral grains that display strongly developed normal zonation and have slightly sausseritized cores. Mymerkite is developed along the margins of many of the grains, and in a few instances it rims at least half the grain. Biotite, the only mafic, is partially chloritized. There are trace amounts of apatite.

##### 35-324-1-6, 41 Olivine Gabbro

This sample is a rather fresh, fine-grained gabbro consisting of approximately 60% labradorite, 35% clinopyroxene, and 5% olivine and accessory minerals.

The plagioclase almost invariably occurs in euhedral laths, is profusely twinned on the albite law and occasionally on the Carlsbad law, occasionally shows slight normal zonation, and is inclusion-free and nonsausseritized.

Clinopyroxene (diplage) is always anhedral and is either interstitial to the plagioclase or partially surrounds it in a subophitic relationship. Optical properties are  $2V = 60^\circ$ ,  $Z_c C = 36^\circ$ ,  $\delta = 0.25$ ,  $R1\gamma = 1.695 \pm 0.005$ . Orthopyroxene exsolution lamelli are absent and the grains are fresh.

Olivine occurs as euhedral to subhedral prisms that are always jacketed, usually completely, by clinopyroxene. It is amazingly fresh although some marginal alteration to iddingsite, serpentine, and calcite has occurred. A high negative  $2V$  indicates a composition in the range  $F_{80-85}$ .

Titaniferous magnetite, sometimes marginally altered to hematite, is scattered throughout the rock as are trace amounts of red-brown biotite and weakly pleochroic green hornblende. Mymerkite is common along the borders of the plagioclase grains.

##### 35-324-9-1, 95 Three Pebbles Examined

a) Hornblende-biotite Quartz Diorite—This sample is only approximately 1 cm in diameter. It differs from the biotite quartz diorite above only by the presence of a few hornblende grains which have been almost completely replaced by chlorite, by a lack of mymerkite, and by sausseritization extensive enough to produce coarse-grained epidote in the cores of some of the plagioclase grains.

b) This sample consists of a single crystal of microcline approximately 1/2 cm in diameter. It displays extremely well developed tartan twinning and contains a few plagioclase inclusions all of which are sausseritized extensively enough to contain large amounts of coarse-grained epidote.

c) Arkosic Sandstone—a fine-grained sandstone containing abundant quartz, plagioclase, and rock fragments (quartz-sericite schist) set in a matrix of quartz and sericite. The detrital grains are all angular and the sample is notably lacking in heavy minerals. Diameter of the sample is slightly over 1 cm.

##### 35-324-1-1, 117 Meta-arkose

A fine-grained arkosic sandstone composed largely of angular quartz grains and quartz-sericite schist rock fragments with subordinate amounts of plagioclase and microcline set in a matrix of sericite and quartz. A few small rounded zircon grains are present along with abundant metamorphic epidote.

##### 35-324-4-2, 130 Arkosic Sandstone

A poorly sorted, angular sandstone composed dominantly of quartz and rock fragments (quartz-sericite schist) and lesser amounts of plagioclase and microcline. Calcite cement comprises a very small percentage of the rock, and a few minute grains of sphene and pyrite also occur.

##### 35-324-7-3, 45 Silty Limestone

An extremely fine grained almost micritic limestone with approximately 15% subangular quartz grains. Heavy minerals include titaniferous magnetite, hematite, zircon, hornblende, and (?) rutile.

##### 35-325-6, CC Hornblende Quartz Diorite

This sample is a fine-grained, somewhat altered quartz diorite with a color index of approximately 20. The major portion of the rock is composed of subhedral grains of andesine. Approximately 25% of the plagioclase is strongly zoned, both normally and oscillatorily from cores of sodic labradorite to rims of calcic oligoclase. Most of the grains show some signs of sausseritization, but the alteration is generally more strongly developed in the more sodic grain borders, many of which contain rounded inclusions of quartz. Micrographic intergrowths of quartz and sodic plagioclase are common in the groundmass.

The principal mafic mineral is green hornblende which occurs in subhedral to anhedral prisms. Fresh red-brown biotite, titaniferous magnetite, and apatite are abundant accessories. The biotite often occurs as inclusions in the hornblende, but the opposite relationship was not observed. The remaining three quartz diorites differ only slightly from this one.

##### 35-325-1-1, 10 Hornblende Quartz Diorite

This sample differs from the sample above as follows: slightly higher quartz content, biotite is slightly chloritized, sausseritization of the plagioclase has been extensive enough to produce coarse-grained epidote in the grain cores, hornblende displays a higher incidence of twinning, and the accessory mineral suite includes abundant zircons and traces of sphene.

##### 35-325-3-1, 107 Hornblende Quartz Diorite

This sample is one of three pebbles examined from this interval; it is  $5 \times 15$  mm in size. Plagioclase (sodic andesine) is only slightly zoned, occurs in subhedral tablets, and is fresh or only very slightly sausseritized. Micrographic intergrowths of quartz and sodic plagioclase do not occur nor are rounded quartz inclusions present in the margins of the plagioclase grains. Hornblende, the only mafic mineral, is generally fresh, but is sometimes marginally altered to epidote and/or chlorite. Zircons are present as accessory minerals.

##### 35-325-5-1, 67 Hornblende Quartz Diorite

This sample differs from sample 325-6, CC as follows: marginal sausseritization more highly developed and the cores of some plagioclase grains also contain rather coarse-grained epidote, biotite is absent, zircon is present as an accessory mineral, a few of the plagioclase grains occur as euhedral microporphyritic laths that are often twinned on the Carlsbad law.

##### 35-325-5-1, 112 Pyroxene (?) Andesite

This sample is a black aphyric lava of rather unusual composition. Approximately 85% of the rock is composed of strongly aligned slightly zoned laths of sodic andesine. Minute grains of titaniferous magnetite are interstitial to the plagioclase and comprise 10% of the thin section. A few highly sausseritized microphenocrysts of plagioclase

clase and several quartz-filled amygdules also occur. Mafic microphenocrysts have been completely replaced by chlorite and calcite; their stumpy habit suggests they were originally pyroxenes. Traces of chlorite and epidote and smectite occur in the groundmass.

**35-325-5-2, 112 Olivine Basalt**

A very fine grained dark gray-green lava with a hyaloophitic to microporphyritic texture. Labradorite laths and subhedral clinopyroxene grains are set in a matrix of palagonitized glass that is peppered with minute grains of titanomagnetite. Euhedral olivine microphenocrysts comprise 5%-7% of the thin section but are completely pseudomorphed by carbonate. One quartz-filled amygdale is present.

**35-325-7-2, 40 Prophyllitized Andesite**

This sample is one of three pebbles examined from this interval; it is only 10 × 15 mm in size. This rock is an aphyric pilotaxitic andesite consisting largely of fresh euhedral slightly zoned laths of sodic andesine. Anhedral clinopyroxene grains occasionally attain the size of the laths, but this mineral is essentially confined to the groundmass along with lesser amounts of titaniferous magnetite, epidote, calcite, and a few grains of quartz. Smectite is confined to the groundmass, but comprises 20% of the thin section.

**35-325-7-2, 40 Microporphyritic Basalt**

This sample is one of three pebbles examined from this interval; it is only 12 × 15 mm in size. Microphenocrysts, all but a very few of which are calcic labradorite, comprise approximately 20% of the thin section. The plagioclase grains are quite variable in shape, from subhedral to anhedral and some appear to have been broken, but the scalloped borders present on resorbed crystals in volcanic rocks are not present. Oscillatory zoning is evident only in the margins of some of the larger crystals and the remaining grains show only slight normal zonation. The remaining phenocrysts are clinopyroxene. The groundmass is exceedingly fine grained and consists of a granular intergrowth of plagioclase laths and anhedral clinopyroxene and titaniferous magnetite. The rock is very fresh.

**35-325-8-1, 37 Pyroxene Andesite**

This sample is a black lava that differs from Sample 325-5-1, 112 as follows: groundmass plagioclase slightly finer grained; phenocrysts reach 3 mm, a few are highly sausseritized plagioclase. The remainder are clinopyroxene which have been almost completely replaced by epidote and chlorite; smectite is absent from the groundmass.

**35-325-1-4, 80 Siltstone**

A dark black thinly laminated siltstone. The sample is only 15 mm across. Silt-sized grains of quartz and subordinate plagioclase are set

in a matrix of chlorite, sericite, and unidentified clay minerals. The lamination is defined by lenses of small opaque grains most of which appear to have been flattened. Small amounts of calcite cement and abundant detrital zircon are present.

**35-325-2-1, 146 Altered Lapilli Tuff**

A fine to medium grained poorly sorted crystal-lithic tuff. The fragments are largely andesitic in composition although an appreciable amount of more felsic material also occurs. Most of the fragments appear to be pieces of preexisting flows, but some recycled pyroclastic detritus is also present. A few of the fragments are fresh, but most are highly altered to masses of epidote and chlorite. Broken crystals of altered plagioclase are rather common and a few grains of quartz are also found. All of the fragments are set in a matrix of epidote and chlorite extensively enough developed to obscure the original texture and composition of the groundmass. The rock is cut by small veinlets of chlorite.

**35-325-3-1, 107 and 35-325-7-2, 40 Siltstones**

Both of these samples are dark black thinly laminated siltstones virtually identical to that described above. The latter sample (7-2) is cut by several thin intersecting stringers of quartz.

**35-325-3-1, 107 Sandstone**

This sample is one of three pebbles examined from this interval; it is less than 1 cm in diameter. It is a dark gray fine grained poorly sorted sandstone consisting of angular grains of quartz and minor plagioclase set in a matrix of very fine grained sericite, epidote, and clay minerals.

**35-325-3-2, 148 Siltstone**

A dark black thinly laminated siltstone identical to Sample 325-1-4, 80 except for its heavy mineral assemblage which includes epidote and traces of biotite in addition to zircon. Some of the opaque grains are altered to leucoxene. The sample is 25 mm in diameter.

**35-325-4-2, 3 Lithic Crystal Tuff or Tuffaceous Sandstone**

A fine to medium grained poorly sorted lithic crystal tuff or tuffaceous sandstone. About two-thirds of the large fragments are angular to subangular crystals of plagioclase and quartz, the two minerals being present in roughly subequal amounts. The remaining identifiable fragments are intermediate volcanics, some of which are so extensively stained with hematite that they are essentially opaque. The highly altered nature of the matrix renders its constituents unidentifiable; thus the uncertainty in the rock's origin. The presence of several clasts of graphic granite suggests a sedimentary history. Three fragments which appear to be broken spherulites were seen along with trace amounts of zircon and muscovite (detrital?).